



UNIVERSITY OF LEEDS

School of Chemical and Process Engineering

**Using Molecular Mechanics to understand
the stability of the different polymorphs of
ibuprofen**

Full Name	Abinaash Thirukkumar
Module Name	Research Project (MEng)
Supervisor	Dr A.J. Scott

Acknowledgements

Firstly, I would like to thank Dr A. Scott, from whom I received a great deal of support throughout the course of this project and across the entire year and for providing key insights in the wider scope of the topic of crystallography in the pharmaceutical industry.

I would also like to thank Dr R. B. Hammond for his aid in developing a greater understanding of VisualHabit

Finally, I would like to thank Dr F. Esat for her help in carrying out the experimental portion of this report.

Abstract

In this report, the stability of the two different polymorphs of ibuprofen were examined. The molecules that were used for this report were imported from the CCDC's CSD. The stability was measured using the lattice energy of the crystals, calculated using VisualHabit, using molecular mechanics. VisualHabit was an add-on for Materials Mercury, Materials Mercury was developed by the CCDC. Polymorph one, with lattice energy of -115.8kJ/mol, was more stable than polymorph two, which had lattice energy of -87.5kJ/mol; both lattice energies were determined using the Dreiding II Mod forcefield. The lattice energy obtained for polymorph one was consistent with sublimation enthalpy obtained from literature. There were, however, discrepancies when the lattice energies were calculated from the different forcefields; which lead to the analysis of the forcefields present in the VisualHabit software. The Dreiding II Mod, Momany and Gavezzotti forcefields were comparable, since they produced similar lattice energies, whilst the other force fields produced vastly different lattice energies. The CSD had 18 different molecules for the first polymorph of ibuprofen, all of which were obtained under different circumstances, temperature and pressure, and through different methods, neutron and X-ray diffraction of crystals and powders. Analysis was carried out to determine the best circumstances for a molecule to determine the most accurate lattice energy. This was concluded that the best molecule would be obtained at the coldest temperature in a vacuum using the neutron diffraction of a single crystal. The unit cells of both polymorphs were optimised to obtain a new position of the atoms in the unit cell which gave the minimum value for the unit cell. These optimised unit cells confirmed that polymorph one was more stable than polymorph two. In certain forcefields there was a large deviation between the lattice energies of the original molecule and the optimised molecule; this deviation was found to be due to the estimation of the Van der Waals energy, in particular the Van der Waals repulsive force. The Dreiding II Mod and Gavezzotti fields were the most consistent throughout.

Contents

Abstract.....	iii
Contents	iv
List of tables.....	vi
List of Figures	viii
List of Abbreviations	x
1. Introduction.....	1
1.1 Ibuprofen.....	1
1.2 Polymorphism	2
1.3 Molecular mechanics	3
1.4 Crystal morphology	5
1.4a BFDH	5
1.4b Attachment Energy	6
1.5 Packing patterns	6
1.5a Hydrogen bonds	6
1.5b Short contacts.....	7
1.5c Packing structure	10
1.5 Mercury and VisualHabit.....	13
1.6 Density Functional Theory.....	14
1.7 Impact on society	14
1.8 Project progress.....	15
2. Literature review	16
2.1 History of molecular mechanics	16
2.2 Limitations of molecular mechanics	16
2.3 Molecular mechanics with solvents	17
3. Aims and Objectives	18
4. Methodology	20
4.1 Lattice energy comparison of polymorphs.....	20
4.2 Comparison of Forcefields.....	21
4.3 Crystal shape	21
4.4 Identifying ideal conditions for cif file	21
4.4a Cell parameters and temperature.....	21
4.4b Cell Parameters and pressure	21
4.4c Short Contacts	21
4.4d The effect of chirality on lattice energy	22
4.5 DFT	22

4.5a Cell parameter comparison.....	23
4.5b Molecular overlay	23
4.5c DFT Lattice energy comparison.....	23
4.5d Bond analysis	23
4.6 X-Ray diffraction	23
5. Results and Analysis	24
5.1 Lattice energy comparison	24
Accuracy comparison.....	24
5.2 Comparison of Forcefields.....	26
5.3 Crystal Shape	29
5.3a Comparison of BFDH models for the two polymorphs	29
5.3b Comparison of VisualHabit models	30
5.4 Identifying ideal conditions for cif file	33
5.4a Cell parameters and temperature.....	33
5.4b Cell parameters and pressure	34
5.4c Short contacts	34
5.4d The effect of chirality on lattice energy	41
5.5 DFT analysis	42
5.5a Cell parameter comparison.....	42
5.5b Molecular overlay of polymorphs.....	43
5.5c Bond analysis	44
5.5d DFT Lattice energy comparison	46
5.5e Polymorph comparison for DFT molecules	58
5.6 X-Ray Diffraction	59
5.6a Evaluating Mercury XRD	59
5.6b XRD analysis of polymorph 1	59
5.6c XRD analysis of polymorph 2.....	59
6. Conclusion	65
Future work.....	66
References.....	67
Appendix.....	71
Atom energies	Error! Bookmark not defined.
Appendix A: Atom energies for a single molecule of IBPRAC04 and DFT2 Mod in the Dreiding II field (Hydrogen bonding atoms shown in red).....	71
Appendix B: Atom energies for a single molecule of IBPRAC04 and DFT2 Mod in the Momany field (Hydrogen bonding atoms shown in red)	72

Appendix C: Atom energies for a single molecule of IBPRAC04 and DFT2 Mod in the Tripos 5.2 field (Hydrogen bonding atoms shown in red)	73
--	----

List of Tables

Table 1.1a: Physical properties of Ibuprofen	1
Table 1.2a: Cell parameters of the two polymorphs	2
Table 1.5a: Parameters for each forcefield and the elements considered	13
Table 3a: Parameters for all .cif files of polymorph one	19
Table 4a: Geometry optimisation convergence parameters	22
Table 5.1a: Cell parameters, R factor and lattice energies for all available molecules of ibuprofen	25
Table 5.2a: Atom energies for Dreiding II and Dreiding II Mod for a molecule of IBPRAC01	27
Table 5.2a: Breakdown of Dreiding II Field	28
Table 5.2b: Breakdown of Dreiding II Mod and Tripos 5.2 fields	28
Table 5.2c: Break down of Momany and Gavezzotti fields	28
Table 5.3a: The three most significant indices for IBPRAC01	29
Table 5.3b: Crystal shapes produced from VisualHabit	31,32
Table 5.4a: Cell parameters for ibuprofen at different temperatures	33
Table 5.4b: Changes to lattice energy with varying temperature	33
Table 5.4c: Change in cell parameters with pressure, with the R factor for each molecule.	34
Table 5.4d: Lattice energies of both enantiomers of Form I	41
Table 5.4e: Averaged lattice energy of each enantiomer compared with Form II	41
Table 5.5a: Various cell parameters of Form I with percentage differences of DFT with other parameters	42
Table 5.5b: Original cell parameters of Form II with DFT2 cell parameters.	42
Table 5.5c: RMS of the two polymorphs	43
Table 5.5d: Bond lengths of Form I, with % differences (right)	45
Table 5.5e: Various lattice energies of molecules of Form I	46
Table 5.5f: Lattice energies of molecules of Form II	48

Table 5.5g: Break down of the Dreiding II field for IBPRAC01 and DFT1	50
Table 5.5h: Break down of the Dreiding II Mod field for IBPRAC01 and DFT1	50
Table 5.5i: Break down of the Momany field for IBPRAC01 and DFT1	50
Table 5.5j: Break down of the Gavezzotti field for IBPRAC01 and DFT1	51
Table 5.5k: Break down of the Tripos 5.2 field for IBPRAC01 and DFT1	51
Table 5.5l: Break down of the Dreiding II field for IBPRAC04 and DFT2	52
Table 5.5m: Break down of the Dreiding II Mod field for IBPRAC04 and DFT2	52
Table 5.5n: Break down of the Momany field for IBPRAC04 and DFT2	53
Table 5.5p: Break down of the Gavezzotti field for IBPRAC04 and DFT2	53
Table 5.5q: Break down of the Tripos field for IBPRAC04 and DFT2	53
Table 5.5r: Crystal shapes of IBPRAC01 and DFT1	54,55
Table 5.5s: Crystal shapes of IBPRAC04 and DFT2	56,57
Table 5.5t: Lattice energies for the two DFT molecules and the difference	58
Table5.5u: Lattice energies for the two original molecules and the difference	58

List of Figures

Figure 1.2a: Gibbs free energy graph for polymorphs one and two	2
Figure 1.3a: Comparison between Morse potential and Harmonic bond potential	4
Figure 1.4a: The method for calculating attachment energy	6
Figure 1.5a: Length of dimers for the polymorphs. Form I left, Form II right	7
Figure 1.5b: Carbon-Hydrogen short contact in Form I	7
Figure 1.5c: Oxygen-Hydrogen short contacts in Form I	8
Figure 1.5d: Hydrogen-Hydrogen Short Contacts in Form I	8
Figure 1.5e: Hydrogen-Hydrogen Short Contacts in Form II	9
Figure 1.5f: Slice through the {100} plane in Form I	10
Figure 1.5g: {01-1} plane in Form I	10
Figure 1.5h: {110} Plane in Form I	11
Figure 1.5i: {100} Plane in Form II	11
Figure 1.5j: {002} Plane in Form II	12
Figure 1.5k: {011} Plane in Form II	12
Figure 2.2a: Scanning electron micrograph recrystallised ibuprofen from different solvents	17
Figure 4.1a: Lattice energy convergence up to 60Å for ibuprofen in a Dreiding II Mod forcefield	20
Figure 4.4a: Ibuprofen molecule with chiral centre (blue)	22
Figure 5.3a: BFDH model for polymorph one	29
Figure 5.3b: BFDH model for polymorph two	29
Figure 5.4a: Effect of temperature on cell parameter a	36
Figure 5.4b: Effect of temperature on cell parameter b	36
Figure 5.4c: Effect of temperature on cell parameter c	36
Figure 5.4d: Effect of temperature on cell parameter β	36
Figure 5.4e: Change in lattice energy with temperature	37
Figure 5.4f: Effect of pressure on cell parameter a	38
Figure 5.4g: Effect of pressure on cell parameter b	38
Figure 5.4h: Effect of pressure on cell parameter c	38
Figure 5.4i: Effect of pressure on cell parameter β	38

Figure 5.4j: Number of short contacts with pressure	39
Figure 5.4k: Change in lattice energy with pressure	39
Figure 5.5a: Atom overlay of original molecules with DFT molecule	43
Figure 5.5b: Form I with atoms labelled.	44
Figure 5.6a: XRD spectrum for Tesco ibuprofen tablet	60
Figure 5.6b: Comparison of Mercury XRD function with raw data from report	61
Figure 5.6c: XRD patterns of IBPRAC01 and DFT1 (Obtained from Mercury)	62
Figure 5.6d: XRD patterns of IBPRAC01 and DFT1 (Obtained from Mercury) and Experimental XRD plots	63
Figure 5.6e: Comparison of XRD plots for form II	64

List of Abbreviations

API	Active Pharmaceutical Ingredient
BFDH	Bravais, Friedel, Donnay and Harker
CASTEP	Cambridge Serial Total Energy Package
COX enzyme	Cyclooxygenase enzyme
CSD	Cambridge Structural database
DFT	Density Functional Theory
EMA	European Medicines Agency
FDA	Food and Drug Administration
H Bond	Hydrogen Bond
ICDD	International Centre for Diffraction Data
IUPAC	International Union of Pure and Applied Chemistry
NICE	The National Institute for Health and Care Excellence
NSAID	Nonsteroidal anti-inflammatory drugs
QALY	Quality-adjusted life year
RMS	Root Mean Square
UFF	Universal Forcefield
VdW	Van der Waals
XRD	X-ray Diffraction

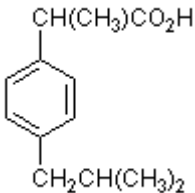
1. Introduction

1.1 Ibuprofen

Ibuprofen, a common over the counter pharmaceutical, has commonly been used as an anti-inflammatory and analgesic agent. The ibuprofen molecule inhibits the use of the cyclooxygenase enzyme (COX), preventing the formation of the inflammatory compounds in the body. The ibuprofen molecule is chiral, as such is available in the form of two enantiomers, R and S ibuprofen (Evans, 2001). Chirality is key to pharmaceuticals as different forms of the same molecule can have different effects, one notable example was thalidomide; one enantiomer helped morning sickness, whilst the other lead to birth defects (Franks et al., 2004). The S form is the better active pharmaceutical ingredient; the R form does not directly inhibit the enzyme reaction. A fraction of the R form can be converted to the S form; however, this varies upon the individual and the degree of pain (Evans, 2001).

The physical properties of ibuprofen are shown in table 1.1a. The most important characteristics are the melting point and solubility.

Table 1.1a: Physical properties of Ibuprofen (O' Neil, 2001; Osol, 1980; Yalkowsky, 1992; Gangolli, 2005)

Molecular formula	C ₁₃ H ₁₈ O ₂
Molecular weight (g/mol)	206.28
Diagram	
IUPAC name	a-methyl-4-(2-methylpropyl)benzeneacetic acid
Melting point (polymorph 1)	75-77°C
Boiling point	157°C
t_{1/2} in the body	1-2 hours
Colour and form	Colourless crystalline solid
Solubility in water @25°C	21mg/L
Solubility in alcohol	Very soluble
Solubility in organics	Readily soluble
Space Group (Number)	P21/c (14)
Crystal System	Monoclinic

The solubility of ibuprofen is considerably greater than aspirin, another NSAID, which is also a COX inhibitor (NTP, 1992). The tableability of ibuprofen is greatly affected by the solvent that was used, with ethanol being the best solvent (Hooper et al, 2017).

1.2 Polymorphism

Polymorphism is the ability of a compound to exist in multiple crystal structures. These different crystal structures will have different parameters for the unit cell and different crystal morphologies. Ibuprofen has two polymorphs, each with its own unit cell parameters, shown in table 1.2a, obtained from the CCDC (Shankland et al, 1996; Derollez et al, 2010). Both polymorphs are monoclinic but differ greatly in cell parameters.

Table 1.2a: Cell parameters of the two polymorphs

CCDC code	IBPRAC01	IBPRAC04
Cell parameter	Polymorph I	Polymorph II
a (Å)	14.667	12.3794
b (Å)	7.886	5.8723
c (Å)	10.730	17.5615
V (Å ³)	1182.511	1276.643
α (°)	90	90
β (°)	99.632	94.873
γ (°)	90	90

Polymorphism is significant in process engineering, as different polymorphs have different physical properties, such as melting point, solubility or the ability to be made into a tablet. The solid-state of the crystal can also affect the drug availability for the active pharmaceutical (API) (Zimmermann and Baranovic, 2011). Polymorph 2 is metastable and has a much lower melting point of 17°C, shown in figure 1.2a. These polymorphs also have different lattice energies as well as different melting enthalpies (Dudognon et al., 2008).

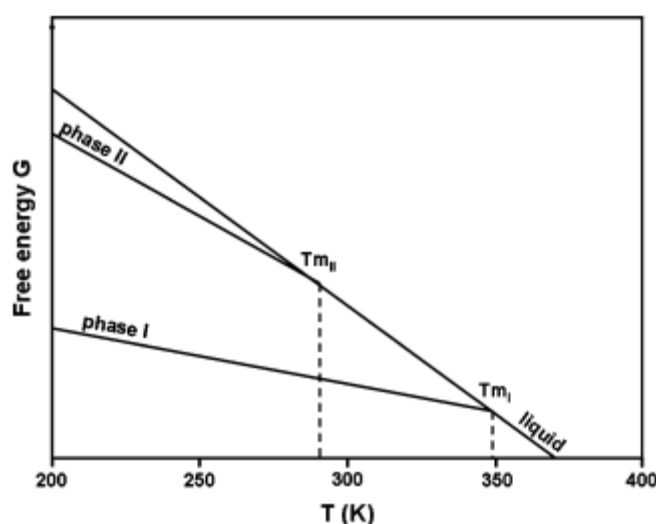


Figure 1.2a: Gibbs free energy graph for polymorphs one and two (Dudognon et al, 2008)

1.3 Molecular mechanics

Molecular mechanics is a method used to model the interactions between atoms and in turn molecules, which can then be used to determine the total energy of the system. The model treats the system as purely mechanical and disregards the position of the electrons, instead focusing on the atomic nuclei, where all the mass is concentrated. The bonds are thought to be springs and obey Hooke's law. The total energy of the system is broken down to four components: bond energy, bond angle potential energy, bond angle torsion energy and the non-bonded potential (Hammond, 2017). The three bonded potentials are due to the energy change when there is a deviation from the equilibrium parameter.

The bond energy is determined using the bond length and can be calculated using either the harmonic bond potential or the Morse potential, equations 1.3a and 1.3b respectively. When two atoms are covalently bonded there are both attractive and repulsive forces acting on the atoms. These forces are equal when the atoms are the optimum distance apart, resulting in the harmonic bond potential equalling zero and the Morse potential reaching its minimum value. This optimum distance varies depending on the atoms (Hammond, 2017).

The Morse potential represents 'real' behaviour more accurately and is used for larger displacements.

$$E_{Bond} = \frac{1}{2}k_{ab}(r_{ab} - r_{0ab})^2 \quad (1.3a)$$

Where k_{ab} force constant associated with a particular bond involving atoms a and b (energy/ \AA^2), r_{ab} actual distance between atoms a and b (\AA) and r_{0ab} is the equilibrium distance between atoms a and b (\AA)

$$E_{Morse} = E_{0ab}[\{1 - \exp(-k_{ab}(r_{ab} - r_{0ab}))\} - 1] \quad (1.3b)$$

Where E_{0ab} is the dissociation energy of a bond between atoms a and b, k_{ab} an asymmetry parameter for the bond a-b.

When the atoms are close together the repulsive forces dominate, when the displacement between the atoms is large the attractive forces demonstrate. Once a certain distance is passed the attractive forces will also decrease, demonstrated in figure 1.3a.

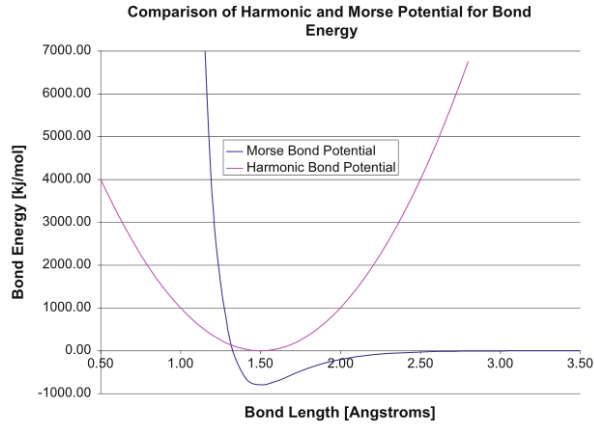


Figure 1.3a: Comparison between Morse potential and Harmonic bond potential. (Hammond, 2017)

The bond angle potential energy is calculated in a similar manner to the bond energy; three atoms have an ideal bond angle; at this angle, the bond angle potential is zero. The H—C—H bond angle in methane is 109.5° . When this bond angle flexes, the energy change follows the relationship stated in equation 1.3c.

$$E_{Angle} = \frac{1}{2} k_{abc} (\theta_{abc} - \theta_{0abc})^2 \quad (1.3c)$$

Where k_{abc} is the force constant for a particular bond angle with atoms a, b and c (energy/radian²), θ_{abc} is the actual bond angle between the three atoms a,b and c and θ_{0abc} is the equilibrium bond angle (radians).

The torsion energy is dependent on four atoms; A, B, C and D bonded as such A-B-C-D. B and C are the proximal atoms whilst A and D are the dihedral atoms. When the atoms are in equilibrium the angle between the AB plane and the BD plane is a specific value. When there is a change to this angle an energy change occurs, T_{orsion} , calculated using equation 1.3d (Hammond, 2017).

$$E_{Torsion} = \frac{1}{2} \sum_j V_j (1 - \cos(j\theta_{tor})) \quad (1.3d)$$

Where θ_{tor} is the torsion angle between the distal and proximal atoms around a covalent bond and V_j are atom energies.

There are two significant non bonded interactions, Van der Waals forces (VdW forces) and the electrostatic attraction. VdW can be calculated either using the Buckingham potential or Lennard-Jones 12-6 potential, equations 1.3e and f respectively.

$$E_{Buckingham} = A_{ij} \exp\left(-\frac{r_{ij}}{\rho_{ij}}\right) - \frac{C_{ij}}{r_{ij}^6} \quad (1.3e)$$

$$E_{12-6} = \frac{A_{ij}}{r_{ij}^{12}} - \frac{B_{ij}}{r_{ij}^6} \quad (1.3f)$$

Where r_{ij} represents the distance between the atoms (\AA), A_{ij} , B_{ij} , C_{ij} and p_{ij} all represent energy parameters. The first term in both equations represents the repulsive force between the atoms, whereas the second term represents the attractive force.

The electrostatic/ coulombic force is generated when there is a difference in electronegativity between the atoms in a covalent bond, resulting in a polarised bond. The energy for this interaction is generated by applying point charges to the nuclei of the atoms and using equation 1.3g.

$$E_{Coulombic} = \frac{1}{4\pi\epsilon_o} \frac{q_i q_j}{r_{ij}} \quad (1.3g)$$

Where ϵ_o is the permittivity of free space ($8.85 \times 10^{-12} \text{F/m}$), q_i and q_j are charges on atoms I and j and r_{ij} is the distance between the atoms (\AA).

These energies are combined to give the total energy of the system, equation 1.3h (Hammond, 2017).

$$E_{Total} = \sum_{n_{bonds}} E_{bond} + \sum_{n_{angles}} E_{angle} + \sum_{n_{torsion}} E_{torsion} + \sum_{n_{nonbond}} E_{nonbond} \quad (1.3h)$$

1.4 Crystal morphology

Crystal morphology is an important consideration in process engineering since this can affect how a crystal behaves in downstream processes such as filtration or milling. The crystal morphology is susceptible to change with changes in the solvent, due to the different intermolecular interactions that will occur between the solute and the solvent (Rosbottom and Roberts, 2017).

1.4a BFDH

The BFDH approach was one of the earliest methods for predicting crystal morphology. Developed by Bravais then later Freidel then Donnay and Harker, this model is one of the simplest and fastest methods of predicting crystal morphology. The foundation for this model is the interplanar spacing between different Miller planes. The rate of growth is inversely proportional to the d spacing. This approach is quick but not as accurate as other methods, such as attachment energy, when compared to experimental data (Hammond, 2017). This is owed to the fact that this approach does not consider intermolecular forces, and since the ordering of crystals is dependent on this, the method is not always accurate (Bladon et al., 2012).

1.4b Attachment Energy

The attachment energy is another method for calculating the crystal morphology but has a different foundation. Unlike the BFDH approach, in attachment energy, the rate of growth perpendicular to a crystal surface is proportional to the attachment energy of the crystal. The attachment energy is calculated by considering the lattice planes as slices, figure 1.4a, P represents an atom outside the slice whilst S is an atom inside the slice. There are interactions between atoms in different slices. The attachment energy is calculated from a single atom, C. There are interactions between atom C and other atoms in different slices. The sum of all these interactions is the attachment energy, it is also the energy change when a new slice is added or removed, shown by growth in the N^+ direction, or loss in the N^- direction. Whilst attachment energy represents the energy between slices, the slice energy is the sum of all the interactions within the same slice (Hammond, 2017).

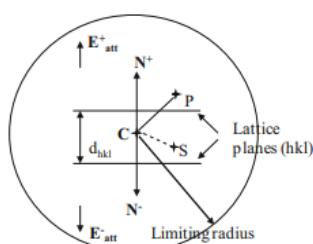


Figure 1.4a: The method for calculating attachment energy (Hammond, 2017)

The crystals generated by attachment energy have been much closer to experimental results than those predicted by the BFDH approach. However, both share a flaw as they do not consider the effect of the solvent; instead assuming a vacuum with no outside interaction (Balton et al., 2012).

1.5 Packing patterns

Although, there are two polymorphs of ibuprofen they share similarities in the intermolecular forces present. Each molecule would form short contacts between different molecules and hydrogen bonds where possible. The analysis was focused on IBPRAC01 and IBPRAC04 since these represented the two polymorphs and were obtained under circumstances where there no other factors, such as external pressure, contributed to the number of short contacts present in the molecule.

1.5a Hydrogen bonds

Each molecule of ibuprofen had a carboxylic acid group, which was capable of forming hydrogen bonds (H bond); since each molecule only had one such group. As such dimers would form around the carboxylic acid group, figure 1.5a. The oxygen bonded to the hydrogen would become the hydrogen donor and the lone oxygen, double-bonded to the carbon, was the acceptor. This was true for both polymorphs, however, they differed in the distance of the hydrogen bond, this was taken to be the distance from the donor oxygen to the accepting oxygen since the hydrogen atom was not in line with the oxygen atoms in Form II. Polymorph one had an H bond length of 2.570Å, whilst polymorph 2 was 2.701Å, these H bonds also differed in the angle of the hydrogen in the H bond. In polymorph one, the hydrogen lay on the H bond, drawn between the two oxygen atoms; whereas the hydrogen in polymorph two was askew, as it did not lay on the line, shown figure 1.5a.

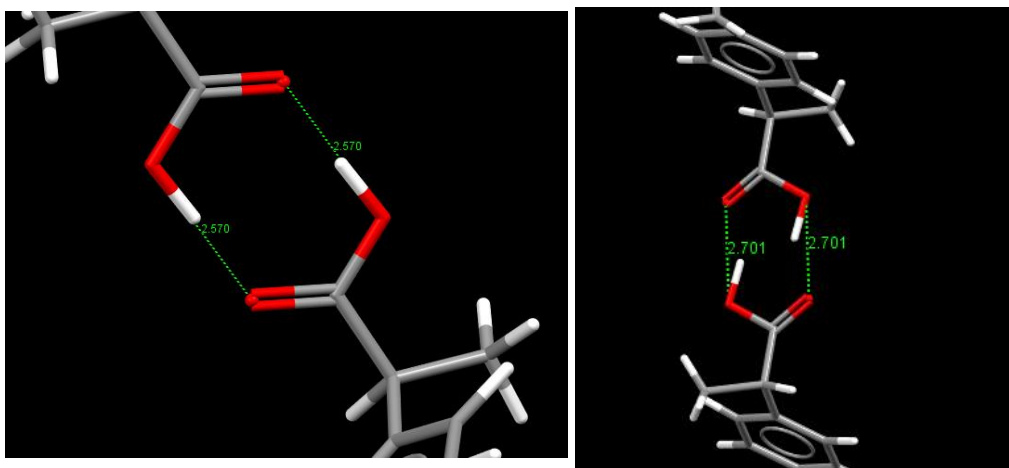


Figure 1.5a: Length of dimers for the polymorphs. Form I left, Form II right

1.5b Short contacts

Short contacts were any intermolecular interactions other than the hydrogen bond (H bond). These can be either coulombic or Van der Waals interactions (VdW), but for ibuprofen, these were solely Van der Waals forces, since there were no charges present.

Polymorph 1

The short contacts for polymorph one were broken down into three main categories, depending on the atoms involved. The most common was the carbon-hydrogen interactions; there were seven such short contacts for each ibuprofen molecule. These occurred within both the phenyl ring and the branched chains, Figure 1.5b. These contacts connected one orientation of the molecule to the other; as seen in the figure all the connected molecules have a different orientation from the central molecule but have the same orientation with each other.

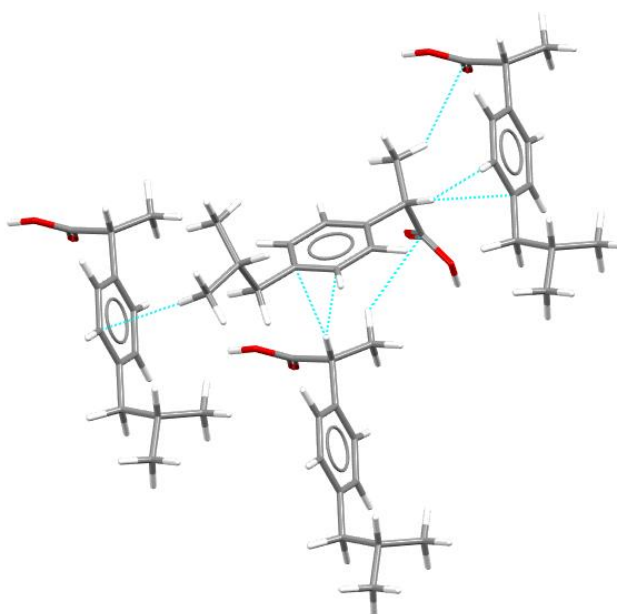


Figure 1.5b: Carbon-Hydrogen short contact in Form I

The next most frequent short contact was the oxygen-hydrogen interactions, these occurred solely around the double-bonded oxygen atom, Figure 1.5c. The hydrogen atoms in the phenyl ring, which have a small positive charge, were attracted to the lone pair of electrons on the oxygen atom. The phenyl rings of the molecules were in the same plane.

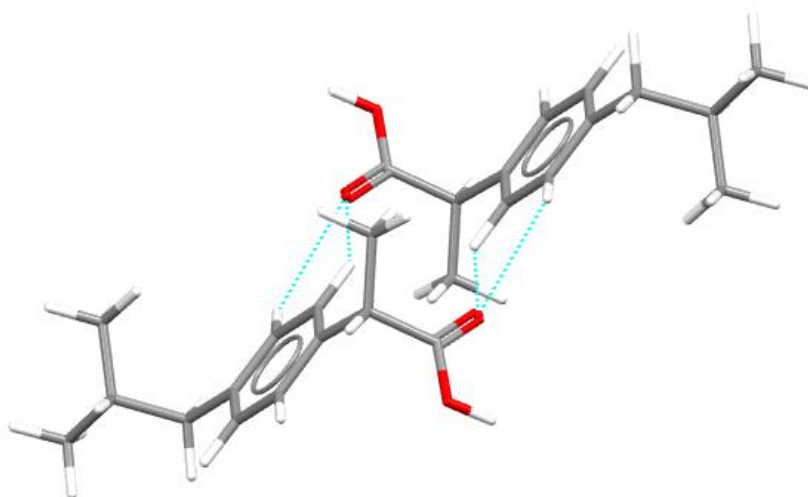


Figure 1.5c: Oxygen-Hydrogen short contacts in Form I

The final short contact was the hydrogen-hydrogen interactions, these only occurred on one end of the molecule, Figure 1.5d, two such interactions occurred for each molecule. One interaction was to a molecule in the same plane, the other to a molecule in a different plane.

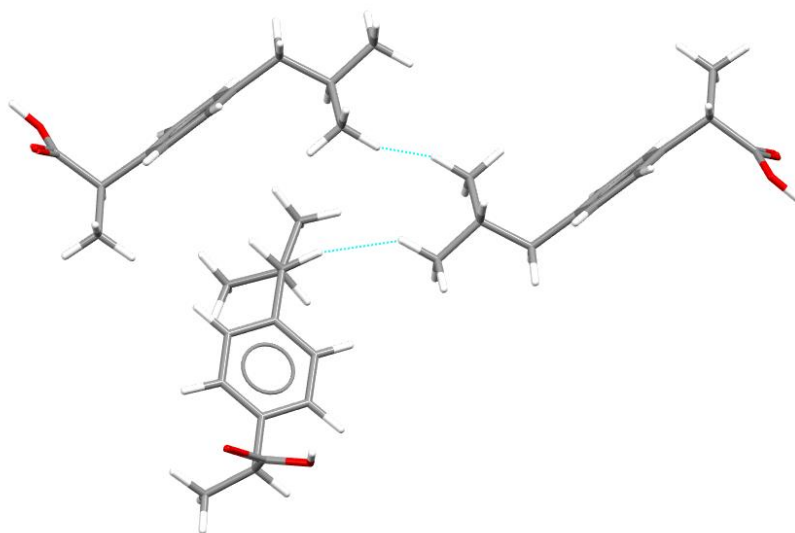


Figure1.5d: Hydrogen-Hydrogen Short Contacts in Form I

Polymorph 2

In polymorph two hydrogen-hydrogen short contacts were dominant; occasionally the neighbouring carbon would also form a short contact to hydrogen. These short contacts were not limited to a single region instead occurred throughout the molecule. All these interactions connected to molecules in a different orientation, Figure 1.5e. Short contacts also occurred between different atoms within the dimer. These were of little significance due to the H bond which occurred in the same location.

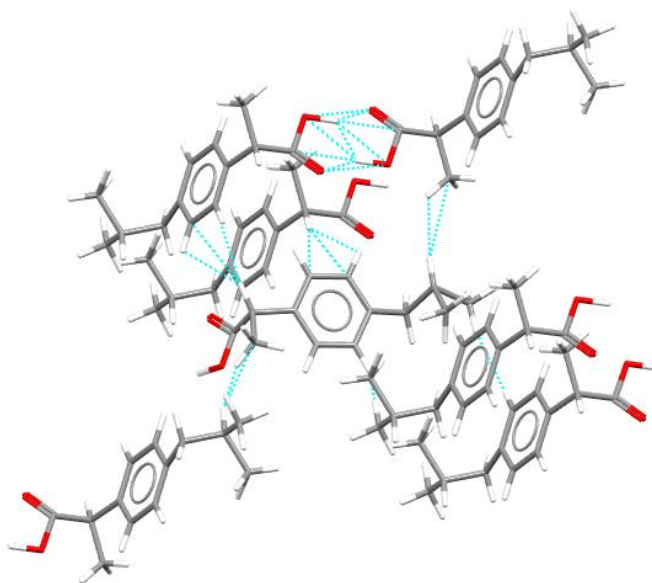


Figure 1.5e: Hydrogen-Hydrogen Short Contacts in Form II

1.5c Packing structure

The packing structure was obtained using the BFDH model since this would give the quickest result for the packing. The relative area of the packing was dependent on the number of short contacts cutting through the plane, the strength of the short contact as well as the angle at which it cuts the plane, with a perpendicular cut being stronger than a parallel cut.

Polymorph 1

An initial study of the relative surface revealed that the $\{100\}$ plane was the largest; the two symmetrical planes accounting for almost 50% of the surface area. The dimers of all the molecules cut through the plane at the same angle despite the two orientations of the molecule (due to the symmetry operation). The molecules were stacked end to end allowing the opposite sides of the molecule, with the methyl groups, to be closest, Figure 1.5f.

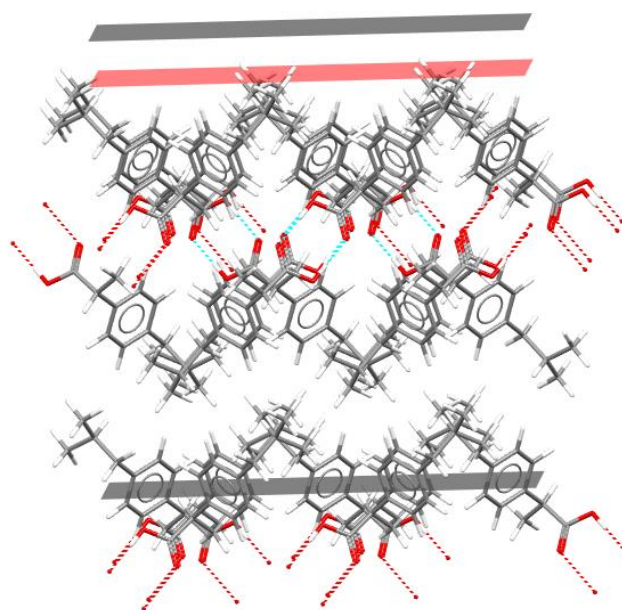


Figure 1.5f: Slice through the $\{100\}$ plane in Form I

The second-largest symmetrical planes were the $\{01-1\}$ planes, which accounted for 20% of the overall surface. One orientation of the molecule cut through the plane at an angle similar to $\{100\}$ whilst the dimer in the other orientation was almost parallel to the plane, resulting in lower energy, Figure 1.5g.

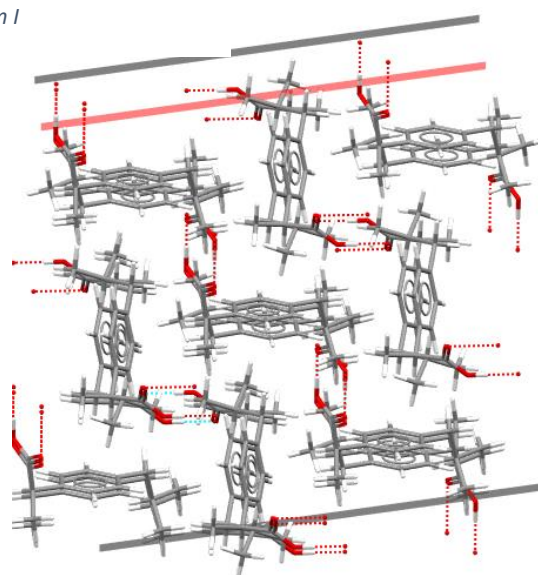


Figure 1.5g: $\{01-1\}$ plane in Form I

The final planes of significance were the {110} planes which accounted for 10% of the total surface area. In this plane, the short contacts dominated the forces that cut through the plane, Figure 1.5h.

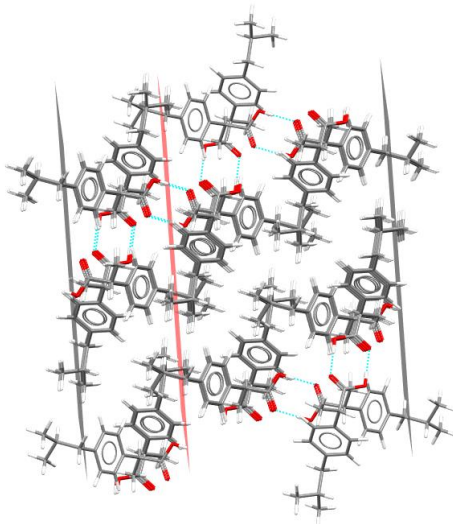


Figure 1.5h: {110} Plane in Form I

Polymorph 2

The largest planes in polymorph two were also the {100} planes, which accounted for 44% of the total surface area. Echoing polymorph one, all the dimers cut through the plane, other ends of the molecules were stacked together, figure 1.5i.

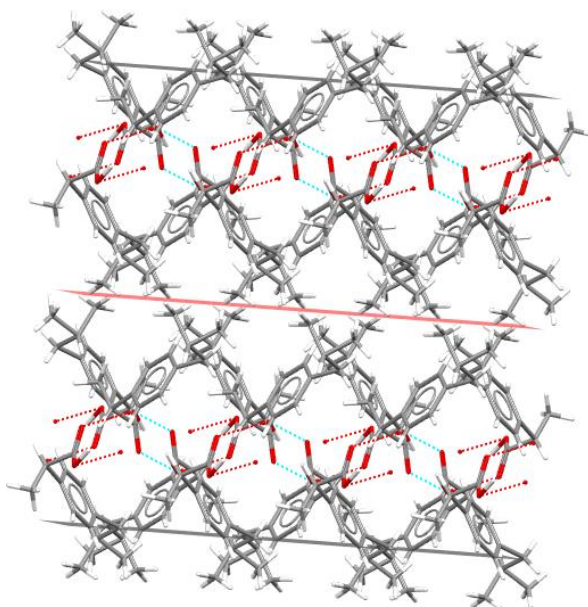


Figure 1.5i: {100} Plane in Form II

The second-largest planes were the {002} planes which were 25% of the total surface area. Unlike the {100} plane, the plane was not composed primarily of dimers, Figure 1.5j. Instead being made up of a combination of both short contacts and dimers.

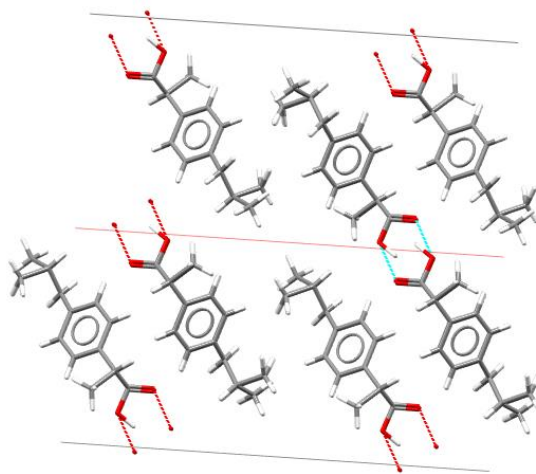


Figure 1.5j: {002} Plane in Form II

The final significant plane was the {011} plane, this plane only accounted for 10% of the total surface area of the crystal and was dominated by short contacts rather than hydrogen bonding; although there were a few hydrogen bonds present in the plane, these were closer to being parallel, Figure 1.5k.

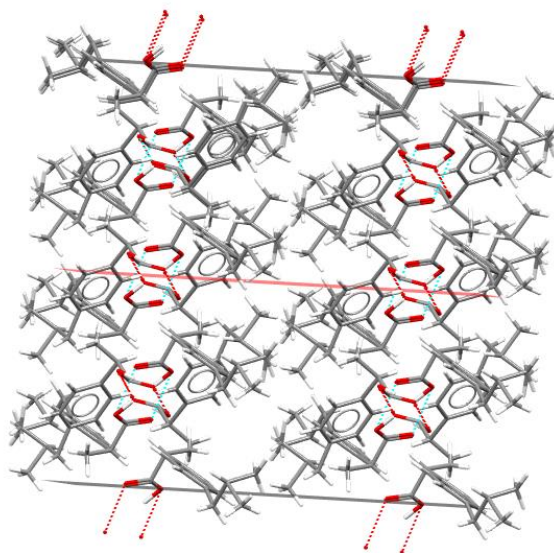


Figure 1.5k: {011} Plane in Form II

1.5 Mercury and VisualHabit

Materials Mercury was a software designed to access and visualise the Cambridge Structural Database (CSD). It was developed by the Cambridge Crystallographic Data Centre (CCDC), as a means of reading the files (Pickering et al., 2017). Other visualisers such as materials studio and LAMMPS were available, Mercury was used because VisualHabit was designed as an add-on for the Mercury software. Mercury is equipped with basic features such as the BFDH model as standard and has the ability to demonstrate the packing and show the Miller planes of the packings. The coordinates of atoms and molecular bonding are also available. Once the files have been loaded and additional data inputted the software can distinguish and label the types of bonding in the molecule, such as whether a carbon atom is aromatic or aliphatic or whether a hydrogen atom is capable of hydrogen bonding

VisualHabit is an addon created in C++, as a modification to the original HABIT program which was developed to determine the lattice energy using attachment energy for a user-defined distance and forcefield (Clydesdale et al., 1996). This distance determines the radial cut off distance, the distance after which no interactions are considered. VisualHabit can show the lattice energy convergence, demonstrating the change in lattice energy as the distance increases up to the radial cut off distance. The lattice energy can be broken down into three main components: Van der Waals forces, electrostatic attraction and hydrogen bonding. The VdW forces and hydrogen bonding can be both attractive and repulsive, giving five components altogether. Values for all these components can be obtained from VisualHabit. These components are dependent on the forcefield that was selected since different forcefields have different parameters and make different assumptions, as shown by table 1.5a. If the number of elements considered was greater than 10 the forcefield was considered to be a general field.

Table 1.5a: Parameters for each forcefield and the elements considered

Potential	Coulombic/ Electrostatic	Van Der Waals Type	Hydrogen bonding	Elements Considered
Dreiding II	Yes	6-12	10-12	General
Dreiding II Mod	Yes	6-12	10-12	General
Momany	Yes	6-exp	None	C, H, N, O
Williams	Yes	6-exp	None	C, H
Gavezzotti	No	6-exp	None	C, H, N, O, Cl, S
Tripos 5.2	Yes	6-12	None	General
Govers 1	Yes	6-exp	None	C, H, N, S
Govers 2	Yes	6-exp	None	C, H, N, S

(Mayo et al., 1990; Momany et al., 1974; Gavezzotti, 1998; Clark et al. 1989; Govers, 1978 and Williams, 1966)

The software also shows the crystal structure and the relative areas of each of the planes as predicted by the attachment energy. The software also shows the d-spacing for the different planes.

1.6 Density Functional Theory

Density functional theory (DFT) is a computational method to determine the minimum energy of a unit cell. DFT obtains a solution using first principles, ie quantum mechanics. DFT was originally developed by Hohenberg and Kohn (1965) and then later modified by Kohn and Sham (1965). Hohenberg and Kohn stated that the total energy of an electron gas was a unique function of the electron density. Kohn and Sham later replaced the many-electron problem with a set of one-electron equations. This total-energy functional for a set can be simplified and written as seen in equation 1.6a

$$E = T + V_{NE} + V_{EE} + V_{XC} \quad (1.6a)$$

Where E is the total energy, T is Kinetic (non-interacting) energy, V_{NE} is the nuclear-electron interaction energy, V_{EE} is the electron-electron repulsion and V_{XC} is the exchange-correlation energy (all in J).

This equation was initially developed on a fictitious system. The kinetic non-interacting energy, T, was the product of the orbital densities of the electron. V_{EE} is the electron density interaction when an electron interacts with itself. Since the electron cannot interact with itself the V_{XC} term was used to account for any errors when combining a non-interacting system with a classical system.

Cambridge Serial Total Energy Package (CASTEP) was originally developed by Payne et al. (1992), was widely used code to electronic structures. However, there were many contributions made by various peoples resulting in the code becoming inefficient when solving larger problems. Therefore, CASTEP was redesigned to work on parallel computers and be more efficient when solving large problems. The DFT function in CASTEP solves the one-electron Kohn-Sham equation using a plane-wave pseudopotential approach.

Since the focus of this paper was the lattice energy the geometry of the unit cell was of greater concern than the electronic structure. The DFT function in CASTEP would allow the unit cell parameters to change along with the atom positions in order to find the minimum energy of the respective unit cell.

1.7 Impact on society

Since ibuprofen is a pharmaceutical, there are ethical implications associated with this field of work. However, the main focus will be the societal impact of carrying out this research rather than the entire field.

The current pharmacological procedure for the creation and approval of a new drug is 10 years and requires around \$2.6billion. The 10 years can be categorised into three distinctive sections; drug discovery and pre-clinical, clinical trials then government approval (PhMRA, 2015). The timeframe for government approval can vary from agency to agency; the Food and Drug Agency (FDA), US agency, may have a different timeframe for approval when compared with the European Medicine Agency (EMA). This research will allow drug discovery and manufacturing portions of the process to be more streamlined.

The crystal morphology has an effect on the effectiveness of a drug (Zimmermann and Baranovic, 2011), therefore this research will enable the stable polymorphs to be found more easily using molecular mechanics, as well as dismissing any other possible polymorph, by

virtue of positive lattice energy. This will reduce the time taken for the initial stage of drug development. Since the morphology also affects the manufacturing, if the morphology is known then designing the manufacturing process is significantly easier, reducing the overall time taken for a drug to enter the market. The time taken for determining a morphology via computational methods is significantly lower than determining the structure through experimental means. The cost and safety considerations are greatly reduced as well, meaning that more resources can be allocated to the other stages of development or the development of new drugs.

Pharmaceutical companies are not obliged to publish any information that may be damaging to their brand or show unforeseen polymorphs after the products have come to the market. Since software that can be used to determine the lattice energies are now commercially available, it will allow individuals to analyse the morphologies of the drugs that are in the market. This will encourage companies to publish more data regarding their findings and discourage them from hiding their damaging findings.

There are common ethical issues associated with the pharmaceutical industry in general, such as the cost of drugs and the availability of drugs. One of the most famous examples of the former was the increase in the HIV drug, Daraprim, in 2015. The price of the drug was increased by 50 times its original value going from \$13.50 for one pill to \$750 for one pill. This increase in price was decided by the then CEO of Turing Pharmaceuticals, Martin Shkreli (Dearden, 2015), who stated that the drug was “woefully underpriced” (Sidahmed, 2016). Which raises the question of the priorities for the pharmaceutical companies, whether it should be profits or a duty of care. It can be argued that since the pharmaceuticals companies are a business, they must first make a profit to enable them to carry on producing drugs. However, the price increase was unnecessary, since a company could increase the price of the most profitable drug by a small amount rather than increasing it by 5000%.

In the UK, the National Institute for Health and Care Excellence (NICE) determines which drugs are available through the NHS. Drugs which are deemed too costly are not available for prescriptions. NICE uses a metric of Quality-Adjusted Life Year (QALY), which considers how long a person will live when given the treatment and the quality of life during that time (Harris, 2005). This means that drugs for conditions common for older patients, such as Alzheimer’s’ disease, are less likely to be approved. The argument can be made that an expensive treatment could be funded if that were to provide lifesaving treatment for a child, instead of an older person.

1.8 Project progress

All the necessary data was collected by the 16th March, when the University was closed, as a result, no sections of the report were abandoned.

2. Literature review

The main areas of focus for this literature review were molecular mechanics, in particular how molecular mechanics had changed, the limitations of molecular mechanics, advancements in molecular. The final area of consideration was the modifications to molecular mechanics to consider solvents.

2.1 History of molecular mechanics

This only the period after the 1960s have covered in the review. The field of molecular mechanics has been growing since the 60s (Williams, 1965; Mayo et al. 1990). Currently, there is a wide range of forcefields which are suited to different functions, ranging from protein packing to the arrangement of inorganic molecules (Lopes et al., 2015; Mayo et al, 1990). However, this portion of the review will focus on the growth of the molecular mechanics for predicting the behaviour of organic molecules.

The early forcefields were limited to aliphatic hydrocarbons and struggled to provide results that mirrored experimental data (Williams, 1966; Engler et al, 1973). Engler et al.'s (1973) evaluation revealed that Allinger's forcefield was able to accurately predict the lattice enthalpies to within several kcal/mol when compared to experimental data. However, the main criticism of Allinger's forcefield was its inability to accurately predict long-chain quaternary or tertiary carbons. However, it was stated that this discrepancy may have been due to the lack of experimental data at the time. Another issue faced at the time was the lack of forcefields to accurately represent other elements such as oxygen or nitrogen, instead being limited to just hydrocarbons (Engler et al. 1973).

In the last forty years, due to improved computational power and a greater understanding of the field significance of these issues have now been reduced. General forcefields, such as the Dreiding or the Universal Force Field (UFF), have increased the number of elements that can be included when carrying out analysis (Mayo et al, 1990; Rappé et al, 1992). The development of forcefields, combined with the development of software, such as HABIT95 allowed for a greater understanding of the crystal morphology. This was further developed by Pickering et al. (2017) when VisualHabit was developed to enable users to view the morphology in Material Mercury.

2.2 Limitations of molecular mechanics

One significant limitation of molecular mechanics is as a result of the assumptions that are made. It is a simple model that uses classical physics where it does not necessarily apply (Boeyens and Comba, 2000). Molecular mechanics also does not consider the effect that the electrons have on the position of the atoms instead focusing entirely on atoms (Hammond, 2019)

Another limitation of molecular mechanics was its inability to accurately predict the crystal morphology when in solvents. This is evident in experiments carried out by Hooper et al. (2017), whose recrystallisation of ibuprofen in four different solvents produced four different crystal habits, shown in Figure 2.2a.

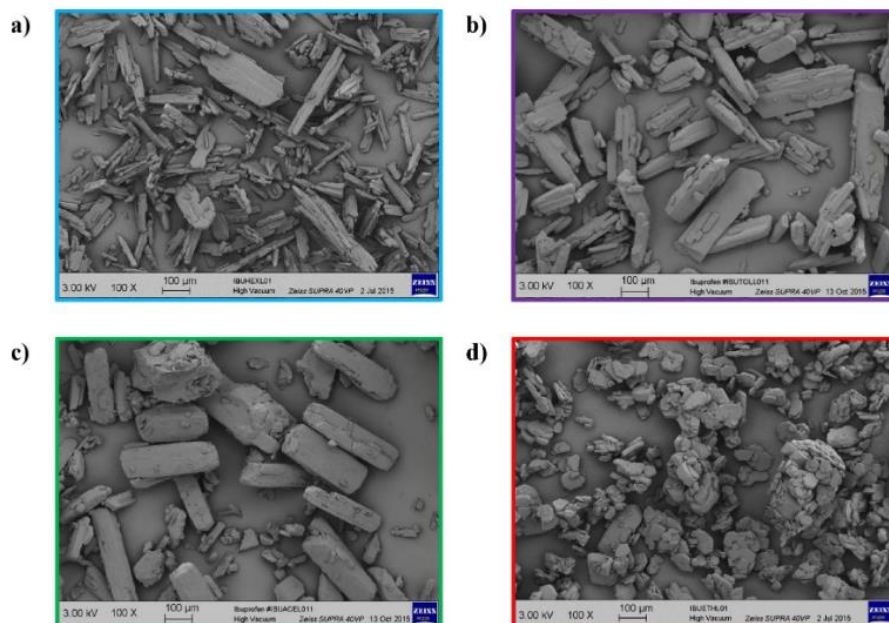


Figure 3.2a: Scanning electron micrograph recrystallised ibuprofen from different solvents a) hexane b) toluene c) acetonitrile d) ethanol (Hooper et al., 2017)

2.3 Molecular mechanics with solvents

Crystal morphology plays a vital part in the process route, needle-like morphologies are prone to blocking filters and pipes and can break during the filtration process (MacLeod and Muller, 2012). Therefore, the shape of the crystal must be predetermined to prevent unfavourable habits forming. The most common method this is to change the solvents until an encouraging structure is formed. If this were to be carried out experimentally it would be time-consuming and not cost-effective. (Aaltonen et al, 2009). Therefore, it would be more ideal to use computational methods to carry this out. The work done by Rosbottom et al (2017) provides a framework to further improve molecular modelling and widen its applications.

3. Aims and Objectives

The main aim of this project was to understand the stability of different polymorphs of ibuprofen. The lattice energy and the crystal morphology were obtained using the computational software VisualHabit. The lattice energy was used as a measure of the crystal stability, a more negative value for a crystal's lattice energy would indicate a crystal that was more stable. The morphology was used to compare the relative growth rates of the various facets of the crystals.

The project had several supplementary objectives; the first was to assess the ability of molecular mechanics to accurately predict the lattice energy of a crystal. The second was to assess the accuracy of different forcefields when predicting the stability of the crystal. An additional objective was to identify the most ideal .cif file that ought to be used when attempting to calculate the lattice energy. The final aim was to compare and assess the ability of DFT to create an accurate molecule.

The foundation of VisualHabit was molecular mechanics (Pickering et al, 2017). The lattice energy generated by VisualHabit was compared with sublimation enthalpy as well as the lattice energy generated by other computational methods.

The wide range of forcefields that were available on VisualHabit were tested to examine which forcefield would find the most comparable result, with the sublimation enthalpy. The various forcefields made assumptions and consider or omit certain factors when considering the lattice energy, such as hydrogen bonding or electrostatic interactions, resulting in a wide range of outputs for the lattice energy. The components of the lattice energy were used as a guide to when the forcefields were studied.

Polymorph one of ibuprofen had 18 different files, each found under different conditions, obtained using various methods and to varying degrees of accuracy. The temperature that the molecules were obtained at varied from 100K to 296K, whilst the pressure ranged from vacuum condition to 4GPa. The majority of the molecules were obtained by the X-ray diffraction (XRD) of a single crystal, whilst the others were found by either the neutron diffraction of a single crystal or the X-ray diffraction of a powder. The initial quality of the molecules was determined using the R factor that was provided with the molecules. These parameters are shown below in Table 3a. The comparison of the lattice energies for these molecules would show which molecule is best suited for calculating the lattice energy.

The DFT minimisation would provide a molecule, which had the minimum energy. The molecule and the solutions would be compared to the files obtained from the CCDC. This comparison would be used to evaluate the capabilities of DFT with regards to producing accurate and comparable data, as well as comparing the accuracy of the existing methods, such as X-Ray and Neutron probe. This would also indicate whether DFT would be necessary, as the minimisation requires significant computing power.

Table 3a: Parameters for all .cif files of polymorph one

<i>cif file</i>	<i>Temperature (K)</i>	<i>Pressure (Gpa)</i>	<i>R factor</i>	<i>Radiation probe</i>	<i>Type</i>
<i>IBPRAC</i>	295	Atmospheric	3.9	X-Ray	Single Crystal
<i>IBPRAC01</i>	100	Atmospheric	5.3	Neutron	Single Crystal
<i>IBPRAC03</i>	295	Atmospheric		X-Ray	Powder
<i>IBRPAC05</i>	296	0	8.33	X-Ray	Single Crystal
<i>IBRPAC06</i>	296	0.23	5.36	X-Ray	Single Crystal
<i>IBRPAC07</i>	296	0.60	8.17	X-Ray	Single Crystal
<i>IBRPAC08</i>	296	0.80	10.66	X-Ray	Single Crystal
<i>IBRPAC09</i>	296	0.88	8.3	X-Ray	Single Crystal
<i>IBRPAC10</i>	296	1.70	9.95	X-Ray	Single Crystal
<i>IBRPAC11</i>	296	1.89	19.04	X-Ray	Single Crystal
<i>IBRPAC12</i>	296	2.32	11.93	X-Ray	Single Crystal
<i>IBRPAC13</i>	296	2.65	11.85	X-Ray	Single Crystal
<i>IBRPAC14</i>	296	3.46	10.03	X-Ray	Single Crystal
<i>IBRPAC15</i>	296	4.00	11.18	X-Ray	Single Crystal
<i>IBRPAC16</i>	100	Atmospheric	4.24	X-Ray	Single Crystal
<i>IBRPAC17</i>	150	Atmospheric	4.51	X-Ray	Single Crystal
<i>IBRPAC18</i>	200	Atmospheric	4.64	X-Ray	Single Crystal
<i>IBRPAC19</i>	250	Atmospheric	4.84	X-Ray	Single Crystal

4. Methodology

The cif files for ibuprofen (IBPRAC-IBPRAC19) were imported from the CCDC website. These were opened using the Mercury visualizer (McConnell, 1974; Shankland et al, 1996; Stone et al, 2009; Derollez et al, 2010; Ostrowska et al, 2015). All the files bar IBPRAC04 were for polymorph one.

4.1 Lattice energy comparison of polymorphs

The lattice energy comparison was used to assess the stability of each polymorph. a more negative lattice energy indicates a more stable structure. It was also used to assess the accuracy of the solution produced by VisualHabit.

The lattice energy was calculated using VisualHabit, a software add-on for the Mercury visualiser. The radial cut off distance was set to 30Å for all calculations, since any distance beyond this would make little difference to the lattice energy, as shown by the lattice energy convergence, figure 4a, there is little increase in the lattice energy after 30Å. The lattice energy was calculated using all the available forcefields, Dreiding II Mod, Dreiding II, Momany, Gavezzotti, Govers 1 and Govers 2. The Williams forcefield could not be used since an error was received since the Williams forcefield will only work for hydrocarbons. These lattice energies were then compared to the sublimation enthalpy from literature since the assumptions made when using VisualHabit are similar to the conditions for calculating the sublimation enthalpy. Forcefields that consistently deviated from the others were not considered for any subsequent comparisons

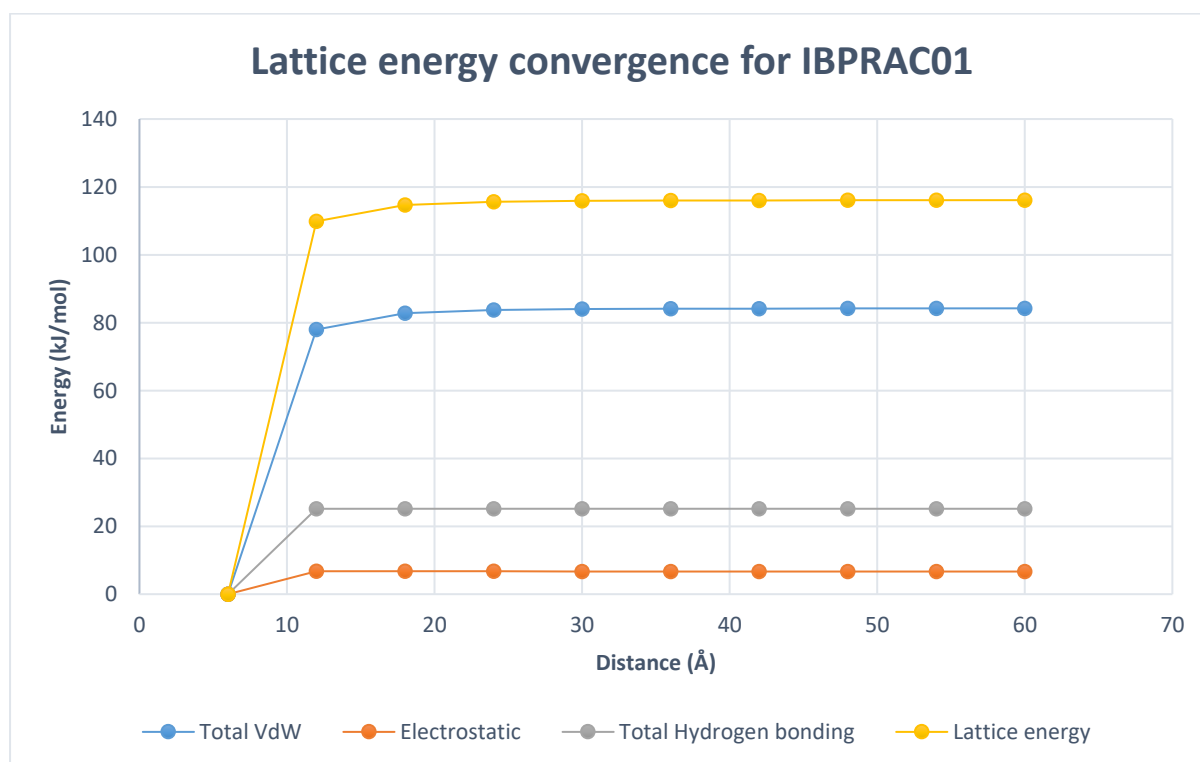


Figure 4.1a: Lattice energy convergence up to 60Å for ibuprofen in a Dreiding II Mod forcefield

4.2 Comparison of Forcefields

Forcefield analysis was carried out using IBPRAC01 because the cell parameters and atom locations were obtained through neutron diffraction rather than X-Ray diffraction. Neutron diffraction is better than using X-ray diffraction at locating the position of the hydrogen atoms. As such, the hydrogen bond lengths are more likely to be accurate when using the neutron diffraction, so values for the intermolecular forces will also be more accurate. The breakdown of the forcefield was obtained by using the list faces function in VisualHabit. The components of the lattice energy, Van der Waals forces, electrostatic attraction and hydrogen bonding, were compared for each of the forcefields to determine the best forcefield.

4.3 Crystal shape

VisualHabit generated crystal habits when it calculated the lattice energy for each forcefield for IBPRAC01 since this would provide the truest reflection of the crystal habit since it was obtained through neutron diffraction of a single crystal. The percentage areas for each of the planes were then compared, to determine the how the crystal would grow, as the relative area of a face is proportional to growth perpendicular to that plane (Hammond, 2015). This was repeated for IBPRAC04, the second polymorph. These crystal shapes were then compared with the crystal that was obtained from the BFDH approach. These crystals are to be compared with pure ibuprofen crystals observed under SEM, to again find the most accurate forcefield.

4.4 Identifying ideal conditions for cif file

The lattice energies of all 18 files of polymorph 1 were calculated using a single forcefield, as these were all were obtained under different conditions such as temperature or pressure or varied in the probe usage such as X-Ray or Neutron diffraction. The lattice energies and cell parameters were compared with the varying conditions.

4.4a Cell parameters and temperature

The cell parameters for IBPRAC16-19 (Ostrowska et al, 2015) were obtained at regular intervals of temperature; ranging 100-250K. This data was then used to estimate the rate at which the cell parameters would change with temperature. The data was extrapolated to obtain the cell parameters at 0K. Cell parameters for α and γ were not observed because they remained at 90° and the crystal remained monoclinic. The extrapolated cell parameters were then compared with the cell parameters obtained from DFT.

4.4b Cell Parameters and pressure

The cell parameters for IBPRAC05-15 were obtained at pressures varying from vacuum to 4GPa. These values for the cell parameters were used to calculate the rate of change of the cell parameter with the pressure. This experiment was carried out to evaluate the best criteria for molecules to calculate the lattice energy

4.4c Short Contacts

There are various types of short contact, including Van der Waals and hydrogen bonding. The number of short contacts affects the final lattice energy of the crystal given that they represent the intermolecular forces between the atoms. The number and type of short contacts were counted for each of the files.

4.4d The effect of chirality on lattice energy

Ibuprofen is a chiral molecule, with the carbon atom shown in Figure 4.4a being the chiral atom. The enantiomers were identified by studying the neighbouring atoms. This revealed that both S and R enantiomers were present in the database. The lattice energies of IBPRAC01 and IBPRAC16 were evaluated since these were obtained under similar circumstances; a temperature of 100K and at atmospheric, and therefore the most comparable.

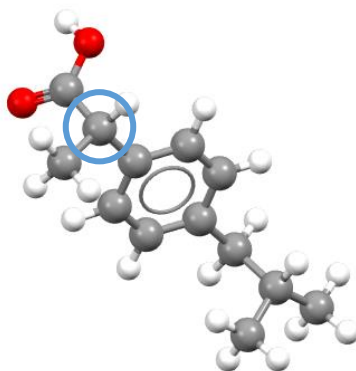


Figure 4.4a: Ibuprofen molecule with chiral centre (blue)

A weighted average was obtained for each enantiomer. There were only 3 files for the S enantiomer, and all were included in the average as there were no anomalous values. Only the molecules IBPRAC16-19 were used for the R enantiomer, since the other molecules had significantly higher R values. These averaged values were then compared to the lattice energy obtained from IBPRAC04 (polymorph 2), to evaluate if the differences in the enantiomers were significant, resulting in polymorph 2 being more stable than a specific enantiomer.

4.5 DFT

The best molecule was identified for polymorph 1 based on the conditions in which the molecule was obtained; outlined in section 4.4. IBPRAC01 was chosen as it was obtained at a temperature of 100K using neutron diffraction. This ensured that the computing time would be reduced. IBPRAC01, along with IBPRAC04 (polymorph 2), were imported into CASTEP. CASTEP was used over other minimisation software since it was free to use. The geometry optimisation convergence parameters are shown in table 4a. This generated DFT 1 and DFT 2 corresponding to polymorph 1 and 2 respectively.

Table 4a: Geometry optimisation convergence parameters

Parameter	Value	Units
Energy	5.0E-06	eV/atom
Max. Force	0.01	eV/Å
Max Stress	0.02	GPa
Max Displacement	5.0E-4	Å
Kinetic energy cut-off	630	eV
k-point mesh density	0.04	Å ⁻¹

4.5a Cell parameter comparison

The molecules produced in the DFT were compared their counterpart. All aspects of the cell parameters were examined, including the lengths of the edges of the unit cell, the angles as well as the crystal structure. These cell parameters were also compared with the data that was obtained through the graphical extrapolation of the cell parameters with varying temperature.

4.5b Molecular overlay

The molecules obtained from DFT were overlaid with the counterpart (IBPRAC01 with DFT1) using the overlay function in Mercury. This would give a root mean square value (RMS); an indication of the similarity of the two, a low RMS would indicate that the molecules were similar. The RMS was calculated depending on the distance between the selected atoms. First only the carbon atoms in the phenyl ring and the carbon in the carboxylic acid group were chosen, the RMS was calculated for both polymorph one and two. The RMS was again calculated overlaying all the atoms bar hydrogen; again, repeated for both polymorphs.

4.5c DFT Lattice energy comparison

The lattice energies for the two DFT molecules were calculated using all applicable forcefields. These values were compared with the previously obtained values in section 4.1 and 2 to assess the precision of DFT. This investigation would indicate as to the necessary precision required to produce an accurate lattice energy.

4.5d Bond analysis

The bond lengths were measured for molecules IBPRAC01 and 16 as well as DFT1. The conditions under which IBPRAC16 was obtained was virtually similar to that of IBPRAC01 varying only in the radiation probe; IBPRAC01 used neutron whilst 16 used X-Ray. This would allow for comparison between the precision of the two probes and theoretical method. Any significant changes to the bond torsion or angle were also examined.

4.6 X-Ray diffraction

X-ray diffraction was carried out using three commercial samples of Tesco caplets. The samples were crushed then placed on a slide and flattened to obtain the prepared sample. The sample was analysed from 10° to 80° in a Bruker B8 under Cu radiation. The peaks that were obtained were then compared with the spectra from literature. The XRD function in Mercury to create a theoretical XRD pattern for IBPRAC01,04 (polymorph 1 and 2) as well as the DFT molecules generated from these. To ensure this function was accurate the theoretical XRD pattern obtained from Mercury was compared with the data obtained from literature (Dudognon et al, 2008). The XRD patterns were compared amongst themselves; IBPRAC01 compared with its counterpart DFT1. These theoretical XRD patterns were then compared with the experimental values obtained from commercial ibuprofen tablet.

5. Results and Analysis

5.1 Lattice energy comparison

The lattice energies generated by VisualHabit is shown in Table 5.1a, along with DFT lattice energies. The molecules IBPRAC8 and IBPRAC11-15 had R factors greater than 10, as such these results were considered anomalous by default, and however, the lattice energies were still calculated. The weighted average and the weighted standard deviations were taken, ignoring the previously mentioned values. This gave an indication towards which forcefields were most similar. A preliminary analysis revealed both Govers forcefields deviated consistently from the other forcefields. This was attributed to the fact that the Govers field does not consider oxygen atoms in its calculations. The Dreiding II forcefield did also deviate from the other forcefields but it was not to the same extent as the Govers fields, therefore it was not emitted from the analysis.

The lattice energies, shown in table 5.1a, show little variance for the values obtained for each cif file in the same forcefield, however, there was a large discrepancy between the forcefield themselves. The values obtained for the Dreiding II Mod, Momany and Gavezzotti forcefields were all similar; with most values ranging from -110 to -130 kJ/mol, once the anomalous results had been ignored. Further reinforced by the similar weighted averages and the low weighted standard deviation among the three forcefields. The results obtained from the Tripos 5.2 field were similar to the previous three fields, but there was a large difference between the lattice energies for the same molecule. For example, the lattice energy obtained for IBPRAC01 from the Dreiding II Mod, Momany and Gavezzotti forcefields ranged from -111 kJ/mol to 128 kJ/mol, whereas the Tripos field gave a value of -98 kJ/mol which was more comparable to the Dreiding II forcefield. Govers 1 and 2 gave values that had a wide range, from -48 kJ/mol to -87 kJ/mol.

The lattice energy obtained for the second polymorph was always more positive than the average lattice energy for the same forcefield, but there was significant variation between the forcefields. Dreiding II Mod and Gavezzotti fields resulted in similar lattice energies, whereas the Momany forcefield gave a positive lattice energy, indicating that the crystal would not be stable. This was also true for the Tripos forcefield, this gave a much more positive value for the lattice energy.

IBPRAC05-15 were taken at higher pressures; as such the lattice energy becomes more positive, this is reflective of the relationship between the distance between atoms and harmonic bond potential (Hammond, 2017), the increased pressure resulting in reduced bond length.

Accuracy comparison

The sublimation enthalpy obtained from literature was -115.8 ± 0.6 kJ/mol (Perlovich et al, 2003), this was comparable to the Dreiding II Mod, Momany and Gavezzotti fields. The Tripos was close to the expected value but there was still a large discrepancy between it and the sublimation enthalpy. The lattice energies produced by the other fields were not concurrent with the sublimation enthalpy as they deviated significantly from the sublimation energy.

Table 5.1a: Cell parameters, R factor and lattice energies for all available molecules of ibuprofen. Molecules with high R factors are shown in red. Positive lattice energies are shown in yellow. Starred molecules were used for weighted average and standard deviation.

		Cell parameters					Probe conditions					Lattice energy (kJ/mol)						
	Enantiomer	a (Å)	b (Å)	c (Å)	V (Å ³)	β (degrees)	Temp (K)	Pressure (Gpa)	R factor	Radiation probe	Type	Dreiding II Mod	Dreiding II	Momany	Gavezzotti	Triplos 5.2	Govers 1	Govers2
Polymorph 1																		
IBPRAC*	S	14.667	7.886	10.73	1241.074	99.362	295	Atmospheric	3.9	X-Ray	Single Crystal	-128.61	-65.82	-111.40	-126.53	-96.63	-51.09	-27.47
IBPRAC01*	S	14.397	7.818	10.506	1182.511	99.700	100	Atmospheric	5.3	Neutron	Single Crystal	-115.86	-69.19	-112.14	-126.59	-98.73	-58.27	-48.51
IBPRAC03*	S	14.671	7.8893	10.7288	1241.81	99.428	295	Atmospheric		X-Ray	Powder	-120.27	-98.55	-108.50	-120.84	-97.66	-78.80	-64.78
IBRPAC05*	R	14.522	7.817	10.619	1205.453	99.540	296	0.00	8.33	X-Ray	Single Crystal	-123.78	-105.75	-112.15	-123.36	-105.71	-89.88	-74.59
IBRPAC06*	R	14.6737	7.895	10.7345	1243.58	99.541	296	0.23	5.36	X-Ray	Single Crystal	-127.72	-114.83	-107.49	-118.89	-101.85	-93.43	-76.56
IBRPAC07*	R	14.309	7.686	10.47	1151.48	99.850	296	0.60	8.17	X-Ray	Single Crystal	-128.38	-113.38	-116.16	-129.56	-113.14	-98.91	-87.38
IBRPAC08	R	14.205	7.6697	10.318	1124.126	100.090	296	0.80	10.66	X-Ray	Single Crystal	-121.07	-101.49	-117.97	-131.86	-114.90	-93.23	-85.47
IBRPAC09*	R	14.196	7.638	10.32	1118.988	100.130	296	0.88	8.3	X-Ray	Single Crystal	-125.33	-109.60	-117.47	-131.91	-116.05	-98.62	-91.30
IBRPAC10*	R	13.977	7.536	10.12	1065.946	100.300	296	1.70	9.95	X-Ray	Single Crystal	-113.68	-95.56	-117.43	-134.11	-118.81	-93.74	-95.36
IBRPAC11	R	13.9958	7.514	10.067	1058.69	100.410	296	1.89	19.04	X-Ray	Single Crystal	-106.38	-85.11	-116.71	-106.38	-117.67	-88.74	-92.06
IBRPAC12	R	13.905	7.4574	10.007	1037.677	100.210	296	2.32	11.93	X-Ray	Single Crystal	-98.42	-80.26	-111.19	-130.46	-116.29	-85.84	-97.21
IBRPAC13	R	13.865	7.1064	9.997	985.0068	100.270	296	2.65	11.85	X-Ray	Single Crystal	-93.98	-73.68	-111.20	-131.05	-116.46	-83.10	-96.42
IBRPAC14	R	13.779	7.324	9.844	993.4308	100.280	296	3.46	10.03	X-Ray	Single Crystal	-64.37	-41.66	-97.69	-123.06	-106.13	-65.96	-91.87
IBRPAC15	R	13.7397	7.285	9.804	981.3188	100.195	296	4.00	11.18	X-Ray	Single Crystal	-48.16	-22.12	-92.34	-119.35	-101.41	-56.67	-87.22
IBRPAC16*	R	14.4847	7.8321	10.4907	1190.124	99.743	100	Atmospheric	4.24	X-Ray	Single Crystal	-129.03	-114.73	-113.22	-125.82	-109.29	-96.93	-83.13
IBRPAC17*	R	14.5144	7.8429	10.5297	1198.648	99.609	150	Atmospheric	4.51	X-Ray	Single Crystal	-129.32	-115.88	-112.20	-124.72	-108.38	-97.36	-83.18
IBRPAC18*	R	14.5609	7.857	10.5867	1211.171	99.563	200	Atmospheric	4.64	X-Ray	Single Crystal	-129.23	-115.98	-110.99	-123.18	-106.59	-96.50	-81.33
IBRPAC19*	R	14.605	7.8721	10.6507	1224.532	99.525	250	Atmospheric	4.84	X-Ray	Single Crystal	-128.63	-115.41	-109.61	-121.40	-104.55	-95.15	-79.06
Weighted average (only *)		14.465	7.797	10.541	1189.610	99.691						-124.99	-102.89	-112.40	-125.58	-106.45	-87.39	-74.39
Weighted standard deviation		0.219	0.118	0.187	55.460	0.289						5.65	18.32	3.28	4.56	7.46	16.88	20.16
DFT 1	S	14.5385	7.7273	10.3025	1157.417	100.950						-95.02	6.57	-92.30	-121.90	-85.52	-20.65	-10.74
Polymorph 2																		
IBPRAC04	S	12.3794	5.8723	17.5615	1276.643	94.873	258	Atmospheric	5.8	X-ray	Powder	-87.50	-68.06	1.63	-80.78	95.93	-39.25	-21.70
DFT2	S	12.6451	5.3507	17.3348	1172.875	94.454						-84.88	39.44	-75.46	-110.27	-72.98	0.21	11.09

5.2 Comparison of Forcefields

The Dreiding II Mod field was derived from the Dreiding II field, therefore they share some features, but they differ in the calculation of the VdW repulsion of the hydrogen bonding atoms. The Dreiding II field divides the repulsion of the hydrogen and oxygen in the hydrogen bond by 100 and the Dreiding II Mod field ignores the repulsion entirely, table 5.2a. The H1 atom was the hydrogen atom involved in hydrogen bonding.

This was most evident in the breakdown of the attachment energy. The breakdown of these attachment energies of IBPRAC01 is shown in Tables 5.2b-d. Both the electrostatic and hydrogen bonding components of the lattice energy being virtually the same. There are slight differences between the four planes, {110}, {11-1}, {10-2} and {002}; which as an effect on the final shape of the crystal. The largest difference occurs in the Van der Waals component. The VdW attraction components for the two force fields were the most similar. These were not the same, but they were comparable. The VdW repulsive force in the Dreiding II field was more positive for all the planes. Only the {100} plane had the same values for all the VdW components, indicating that the repulsion around the carboxylic atoms was not present in this plane.

The Dreiding II Mod was compared with the Momany forcefields since these had similar lattice energies. The attractive and repulsive VdW forces were different, however, the total VdW energies for each were almost identical, differing by less than 2mJ/m^2 for each corresponding plane. The electrostatic attraction for the Momany field was exactly half that of the Dreiding II Mod. The total H bond energies for the two forcefields were very similar, deviating by less than 1mJ/m^2 for each plane.

The Gavezzotti forcefield does not include H bond energy or electrostatic attraction by definition (Filippini and Gavezzotti, 1993), leaving only the VdW energy. This VdW energy was not comparable to the VdW energy of the other forcefields, instead, it was more similar to the total energy of the plane for the other force fields. The Tripos 5.2 field did not consider the H bond energy yet still produced a total energy that was still similar to the other fields.

Table 5.2a: Atom energies for Dreiding II and Dreiding II Mod for a molecule of IBPRAC01

Atom	Element	Dreiding II									Dreiding II Mod							
		VdW Attraction	VdW Repulsion	Total VdW Energy	Electrostatic	H bond Attraction	H bond Repulsion	Total H bond Energy	Total Energy		VdW Attraction	VdW Repulsion	Total VdW Energy	Electrostatic	H bond Attraction	H bond Repulsion	Total H bond Energy	Total Energy
O1	O	-10.273	7.743	-2.53	-2.648	-1.059	0.504	-0.556	-5.734		-10.245	7.715	-2.529	-2.648	-1.059	0.504	-0.556	-5.733
O2	O	-12.202	36.466	24.264	-5.687	-139.099	127.067	-12.032	6.545		-11.41	12.437	1.027	-5.687	-139.099	127.067	-12.032	-16.691
C1	C	-10.097	4.597	-5.5	3.342	0	0	0	-2.159		-10.003	4.287	-5.717	3.342	0	0	0	-2.375
C2	C	-8.61	2.077	-6.533	0.038	0	0	0	-6.495		-8.596	2.075	-6.521	0.038	0	0	0	-6.484
C3	C	-11.55	3.796	-7.754	0.102	0	0	0	-7.653		-11.509	3.769	-7.74	0.102	0	0	0	-7.638
C4	C	-7.879	1.741	-6.139	-0.1	0	0	0	-6.238		-7.871	1.74	-6.131	-0.1	0	0	0	-6.23
C5	C	-9.623	3.243	-6.381	-0.157	0	0	0	-6.537		-9.619	3.243	-6.377	-0.157	0	0	0	-6.533
C6	C	-9.813	5.066	-4.748	-0.128	0	0	0	-4.876		-9.81	5.065	-4.744	-0.128	0	0	0	-4.872
C7	C	-8.208	3.906	-4.302	0.208	0	0	0	-4.094		-8.2	3.905	-4.295	0.208	0	0	0	-4.086
C8	C	-8.927	2.857	-6.07	0.349	0	0	0	-5.72		-8.902	2.847	-6.055	0.349	0	0	0	-5.706
C9	C	-8.811	2.652	-6.158	-0.06	0	0	0	-6.218		-8.789	2.644	-6.144	-0.06	0	0	0	-6.205
C10	C	-7.824	1.958	-5.865	0.278	0	0	0	-5.588		-7.816	1.958	-5.859	0.278	0	0	0	-5.581
C11	C	-7.632	1.298	-6.334	0.24	0	0	0	-6.095		-7.629	1.298	-6.331	0.24	0	0	0	-6.092
C12	C	-10.108	3.167	-6.941	0.344	0	0	0	-6.597		-10.106	3.167	-6.939	0.344	0	0	0	-6.595
C13	C	-10.686	3.367	-7.319	0.375	0	0	0	-6.944		-10.681	3.366	-7.314	0.375	0	0	0	-6.939
H1	H	-1.141	24.476	23.335	-0.558	-140.155	127.571	-12.585	10.192		0	0	0	-0.558	-140.155	127.571	-12.585	-13.142
H2	H	-4.396	5.056	0.66	-0.392	0	0	0	0.268		-4.395	5.056	0.662	-0.392	0	0	0	0.27
H3	H	-2.989	1.072	-1.917	0.056	0	0	0	-1.861		-2.98	1.07	-1.91	0.056	0	0	0	-1.854
H4	H	-4.095	2.72	-1.375	-0.065	0	0	0	-1.44		-4.075	2.702	-1.373	-0.065	0	0	0	-1.438
H5	H	-5.081	4.291	-0.79	-0.176	0	0	0	-0.966		-5.066	4.276	-0.79	-0.176	0	0	0	-0.966
H6	H	-3.403	2.229	-1.174	0.119	0	0	0	-1.055		-3.402	2.229	-1.174	0.119	0	0	0	-1.054
H7	H	-2.992	1.495	-1.497	0.105	0	0	0	-1.391		-2.991	1.495	-1.496	0.105	0	0	0	-1.391
H8	H	-3.109	2.013	-1.096	-0.676	0	0	0	-1.772		-3.096	2.004	-1.092	-0.676	0	0	0	-1.768
H9	H	-3.518	4.003	0.485	0.116	0	0	0	0.601		-3.507	3.996	0.489	0.116	0	0	0	0.605
H10	H	-2.586	0.892	-1.694	-0.693	0	0	0	-2.386		-2.581	0.891	-1.69	-0.693	0	0	0	-2.383
H11	H	-3.364	4.156	0.793	-0.234	0	0	0	0.558		-3.362	4.156	0.794	-0.234	0	0	0	0.56
H12	H	-2.977	1.606	-1.371	-0.024	0	0	0	-1.395		-2.976	1.606	-1.37	-0.024	0	0	0	-1.395
H13	H	-3.664	2.338	-1.326	-0.276	0	0	0	-1.602		-3.664	2.338	-1.325	-0.276	0	0	0	-1.602
H14	H	-3.314	1.93	-1.383	-0.099	0	0	0	-1.482		-3.313	1.93	-1.383	-0.099	0	0	0	-1.482
H15	H	-3.993	4.741	0.748	-0.026	0	0	0	0.721		-3.993	4.741	0.748	-0.026	0	0	0	0.722
H16	H	-3.804	2.032	-1.772	-0.206	0	0	0	-1.978		-3.801	2.031	-1.77	-0.206	0	0	0	-1.976
H17	H	-4.014	3.342	-0.671	-0.038	0	0	0	-0.709		-4.013	3.342	-0.671	-0.038	0	0	0	-0.708
H18	H	-3.373	2.029	-1.344	-0.192	0	0	0	-1.536		-3.371	2.028	-1.343	-0.192	0	0	0	-1.535

Table 5.2b: Breakdown of Dreiding II Field

Dreiding II (mJ/m ²)								
Index	VdW Attraction	VdW Repulsion	Total VdW Energy	Electrostatic	H bond Attraction	H bond Repulsion	Total H bond Energy	Total Energy
{210}	-123.018	103.431	-19.587	-4.918	-210.235	191.356	-18.879	-43.384
{21-1}	-128.843	91.662	-37.181	-3.498	-140.162	127.572	-12.591	-53.27
{111}	-122.973	114.944	-8.029	-6.084	-280.307	255.141	-25.167	-39.279
{110}	-109.834	110.555	0.721	-6.341	-280.308	255.141	-25.167	-30.786
{11-1}	-117.546	99.24	-18.306	-4.699	-210.235	191.356	-18.878	-41.884
{102}	-128.467	88.758	-39.709	-3.656	-140.159	127.571	-12.588	-55.952
{100}	-36.641	19.223	-17.418	-0.025	0	0	0	-17.443
{10-2}	-132.356	107.191	-25.165	-5.112	-210.231	191.356	-18.875	-49.152
{011}	-118.552	112.978	-5.574	-6.085	-280.307	255.141	-25.167	-36.826
{002}	-135.425	107.856	-27.569	-5.077	-210.232	191.356	-18.876	-51.522

Table 5.2c: Breakdown of Dreiding II Mod and Tripos 5.2 fields

Dreiding II Mod (mJ/m ²)										Tripos 5.2 (mJ/m ²)				
Index	VdW Attraction	VdW Repulsion	Total VdW Energy	Electrostatic	H bond Attraction	H bond Repulsion	Total H bond Energy	Total Energy		VdW Attraction	VdW Repulsion	Total VdW Energy	Electrostatic	Total Energy
{210}	-121.301	66.718	-54.582	-4.918	-210.235	191.356	-18.879	-78.379		-110.145	50.152	-59.993	-4.918	-64.911
{21-1}	-127.585	67.139	-60.446	-3.498	-140.162	127.572	-12.591	-76.535		-115.278	48.944	-66.334	-3.498	-69.832
{111}	-120.812	66.053	-54.759	-6.084	-280.307	255.141	-25.167	-86.009		-110.035	50.566	-59.469	-6.084	-65.553
{110}	-103.705	55.263	-48.442	-4.453	-210.235	191.356	-18.878	-71.773		-94.826	42.538	-52.288	-4.453	-56.741
{11-1}	-112.228	59.15	-53.078	-3.38	-140.162	127.572	-12.591	-69.049		-101.071	42.313	-58.758	-3.38	-62.138
{102}	-127.235	64.241	-62.994	-3.656	-140.159	127.571	-12.588	-79.238		-113.974	46.052	-67.922	-3.656	-71.578
{100}	-36.631	19.223	-17.408	-0.025	0	0	0	-17.433		-35.702	18.365	-17.337	-0.025	-17.362
{10-2}	-127.359	66.852	-60.506	-3.688	-140.157	127.571	-12.587	-76.781		-114.718	48.691	-66.027	-3.688	-69.715
{011}	-116.392	64.087	-52.305	-6.085	-280.307	255.141	-25.167	-83.556		-105.819	48.74	-57.079	-6.085	-63.164
{002}	-120.241	61.182	-59.059	-3.686	-140.157	127.571	-12.587	-75.331		-107.18	43.163	-64.017	-3.686	-67.702

Table 5.2d: Break down of Momany and Gavezzotti fields

Momany (mJ/m ²)										Gavezzotti (mJ/m ²)		
Index	VdW Attraction	VdW Repulsion	Total VdW Energy	Electrostatic	H bond Attraction	H bond Repulsion	Total H bond Energy	Total Energy		VdW Attraction	VdW Repulsion	Total Energy
{210}	-107.822	52.413	-55.409	-2.459	-112.186	93.373	-18.813	-76.681		-146.433	59.715	-86.717
{21-1}	-112.524	51.428	-61.096	-1.749	-74.793	62.249	-12.544	-75.389		-140.575	54.108	-86.467
{111}	-107.685	53.195	-54.489	-3.042	-149.58	124.498	-25.083	-82.614		-156.463	64.877	-91.586
{110}	-92.306	44.3	-48.006	-2.226	-112.186	93.373	-18.813	-69.045		-129.131	52.336	-76.795
{11-1}	-99.744	45.509	-54.236	-1.69	-74.793	62.249	-12.544	-68.47		-127.888	49.08	-78.808
{102}	-110.467	48.882	-61.586	-1.828	-74.793	62.249	-12.543	-75.957		-138.495	51.856	-86.639
{100}	-31.26	15.136	-16.124	-0.012	0	0	0	-16.137		-29.745	12.364	-17.382
{10-2}	-111.003	51.094	-59.909	-1.844	-74.793	62.249	-12.544	-74.296		-138.373	53.408	-84.965
{011}	-103.975	51.681	-52.293	-3.042	-149.58	124.498	-25.083	-80.418		-152.883	63.578	-89.304
{002}	-104.617	46.56	-58.057	-1.843	-74.793	62.249	-12.544	-72.443		-132.723	49.823	-82.900

5.3 Crystal Shape

The overall shapes of the crystals generated by both VisualHabit and BFDH approach were compared, as well as the relative areas of the faces. The relative areas are shown in table 5.3a and the crystal shapes are shown in table 5.3b

5.3a Comparison of BFDH models for the two polymorphs

The BFDH model gave an almost identical crystal shape for all the molecules for polymorph one, this was expected as the BFDH approach only considered the spacing between the molecules rather than the intermolecular forces between them. As such the crystal habit obtained by this method is usually not accurate with experimental procedures (Hammond, 2019), the BFDH crystal structure was supplemented by the crystal shape generated through VisualHabit, which was calculated through the attachment energy theory (Hammond, 2017), which had been more accurate when compared to experimental results.

The crystal shape of IBPRAC01 was obtained from the BFDH crystal, Figure 5.3a. The crystal was an octagonal prism with extra facets on the sides. The planes with the largest area were the {100} plane, these were the octagonal faces of the prisms. The three most significant symmetrical planes are shown in table 5.3a. Each symmetrical index had multiple faces, all the faces had the same relative area. The {100} plane was formed as a result of the hydrogen bonds between the carboxylic acid functional groups resulting in a dimer.

Table 5.3a: The three most significant indices for IBPRAC01

Index	Number of faces	Relative area of each face	Distance (Å)
{100}	2	0.248	14.472
{011}	4	0.052	6.324
{110}	4	0.033	6.924

The BFDH crystal for the other molecules of the first polymorph showed the same crystal, albeit they were of different sizes. The crystals produced by the other molecules shared the order of significance for indices. Polymorph two's crystal shape, Figure 6.3b, was more cuboidal than that of polymorph one. The {100} plane remained the most prominent, however, the {002} became the next most important. Both planes were cut through the same intermolecular force, the carboxylic acid dimer. The molecules that formed these places cut through the same interaction but molecules had a different orientation these interactions are at a different orientation to each other.

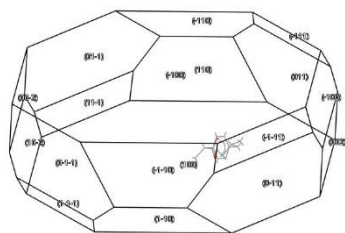


Figure 5.3a: BFDH model for polymorph one

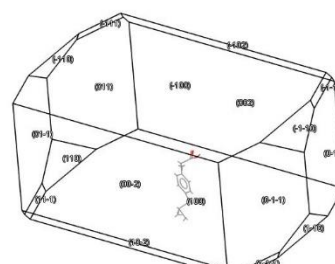


Figure 5.3b: BFDH model for polymorph two

5.3b Comparison of VisualHabit models

Polymorph one

Dreiding forcefields were visually similar. This result was expected since Dreiding II Mod was developed from Dreiding II. Both forcefields were similar to the BFDH model and were octagonal prisms. The crystal shapes for Dreiding II, Dreiding II Mod, Momany, Gavezzotti and Tripos 5.2 were all similar shapes an octagonal prism, which matched the BFDH model., table 5.3b The largest plane was the same for all the crystals and was the {100}, the relative area of these in the three most accurate ones was virtually the same, as seen in table 5.3a. There were variations in the significance of the planes around the prism; the overall structure remained unchanged. The Tripos crystal was similar, but just like its lattice energy there was a noticeable difference but was still similar to the BFDH model.

Polymorph two

The Dreiding forcefields produced analogous crystals for polymorph two, both were cuboidal but had extra facets, similar to the relationship for polymorph one. The Gavezzotti crystal was almost identical to the crystals produced by the Dreiding fields. Both the Momany and Tripos fields gave positive values for the lattice energy, as such their crystals are not stable and could not be compared with the others, since they differed so greatly, as seen in Table 5.3b.

Table 5.3b: Crystal shapes produced from VisualHabit

Forcefield	Polymorph 1 (IBPRAC01)	Polymorph 2 (IBPRAC04)
BFDH		
Dreiding II		
Dreiding II Mod		
Momany		

5.4 Identifying ideal conditions for cif file

5.4a Cell parameters and temperature

Cell parameters, table 5.4a, were plotted as a function of temperature, Figures 5.4a-d. A second-order polynomial was chosen for the equation of the trendline since this gave a higher R^2 value when compared with the exponential or linear trendlines. Therefore, the solution obtained for the cell parameters at 0K would be more accurate; the solution was the y-intercept of the graph.

Table 5.4a: Cell parameters for ibuprofen at different temperatures

Temperature (K)	Cell parameter			
	a (Å)	b (Å)	c (Å)	β (degrees)
100	14.4847	7.8321	10.4907	99.743
150	14.5144	7.8429	10.5297	99.609
200	14.5609	7.857	10.5867	99.563
250	14.605	7.8721	10.6507	99.525

The estimated cell parameters were $a=14.438\text{\AA}$, $b=7.8159\text{\AA}$, $c=10.445\text{\AA}$ and $\beta=100.12^\circ$. The unit cell lengths decreased as expected since there was a decrease temperature, although the β angle increased this was compliant with the expected result. The cosine rule was used to check the length of the a-c diagonal, which also decreased with temperature, verifying that β would increase with a decrease in temperature. These cell parameters were compared to the cell parameters obtained from ab initio, to evaluate the accuracy of both methods.

The change to lattice energies with temperature were also compared and are shown in Table 5.4b and Figure 5.4e. These show that the lattice energy was affected by the temperature, however, this effect was minimal since over the 150K increases the lattice energies only increased by 5kJ/mol. Therefore, it would be ideal to have a lower temperature, however, there were other factors of greater concern.

Table 5.4b: Changes to lattice energy with varying temperature

Temperature (K)	Lattice energy (kJ/mol)				
	Dreiding II Mod	Dreiding II	Momany	Gavezzotti	Tripos 5.2
100	-129.03	-114.73	-113.22	-125.82	-109.29
150	-129.32	-115.88	-112.20	-124.72	-108.38
200	-129.23	-115.98	-110.99	-123.18	-106.59
250	-128.63	-115.41	-109.61	-121.40	-104.55

5.4b Cell parameters and pressure

The change in cell parameters is shown in Table 5.4c were plotted in figure 5.4e-h. The values that did not follow the expected trend, a decrease in unit cell length and increase in β angle, were considered to be anomalous. Graphs were plotted with all the data then the anomalous results were removed, and a new line was plotted on the same graph

Table 5.4c: Change in cell parameters with pressure, with the R factor for each molecule.

Pressure (GPa)	R factor	a (Å)	b (Å)	c (Å)	B (°)
0.00	8.33	14.522	7.817	10.619	99.54
0.23	5.36	14.6737	7.895	10.7345	99.541
0.60	8.17	14.309	7.686	10.47	99.85
0.80	10.66	14.205	7.6697	10.318	100.09
0.88	8.3	14.196	7.638	10.32	100.13
1.70	9.95	13.977	7.536	10.12	100.3
1.89	19.04	13.9958	7.514	10.067	100.41
2.32	11.93	13.905	7.4574	10.007	100.21
2.65	11.85	13.865	7.1064	9.997	100.27
3.46	10.03	13.779	7.324	9.844	100.28
4.00	11.18	13.7397	7.285	9.804	100.195

The unit cell parameters, Table 5.4b, showed a decrease in cell lengths as the pressure was increased. This was expected as the forces exerted on the molecules increased the size of the crystal would decrease. This showed that an ideal molecule to calculate the lattice energy should be taken at low pressures due to the large R factors at the high pressures.

5.4c Short contacts

The total number of short contacts and type of each short contact against pressure is shown in Figure 5.4j. Since the short contacts are affected by pressure, the change in lattice energy against pressure was also observed, Figure 5.4k, only the five forcefields that were similar to the sublimation energy were used for this comparison. The molecules at high pressure had considerably R factors therefore these results are not as reliable.

There were three main types of short contacts between the molecules of ibuprofen, hydrogen bonds, carbon-hydrogen interaction and oxygen-hydrogen interactions. The hydrogen bonds only occurred at the carboxylic acid group, which formed dimers. This was the only site that hydrogen bonding could occur, as such the number of hydrogen bonds remained constant regardless of pressure or temperature. The next most dominate intermolecular force was VdW. The number of VdW remained constant with changing temperature but increased with pressure as the distances between the atoms decreased. The final interaction was between the oxygen atoms and the hydrogen atoms in the phenyl ring. These interactions were similar to hydrogen

bonding but were not a complete hydrogen bond. These were formed as a result of the electron density around the phenyl ring which acts similar to an electronegative atom.

The number of VdW interactions increased with pressure, with new interactions forming after 0.6GPa, namely carbon-oxygen interactions as well as hydrogen-hydrogen interactions. After 3.46GPa there were carbon-carbon interactions formed.

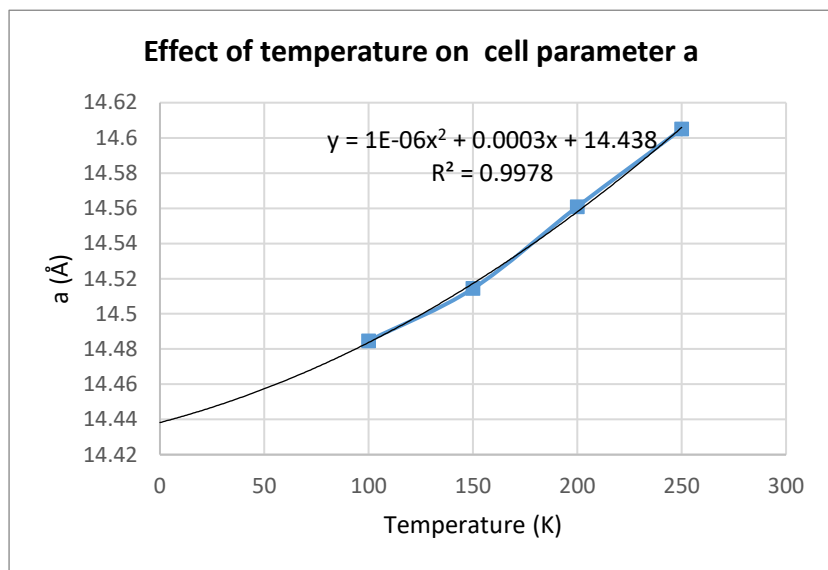


Figure 5.4a: Effect of temperature on cell parameter a

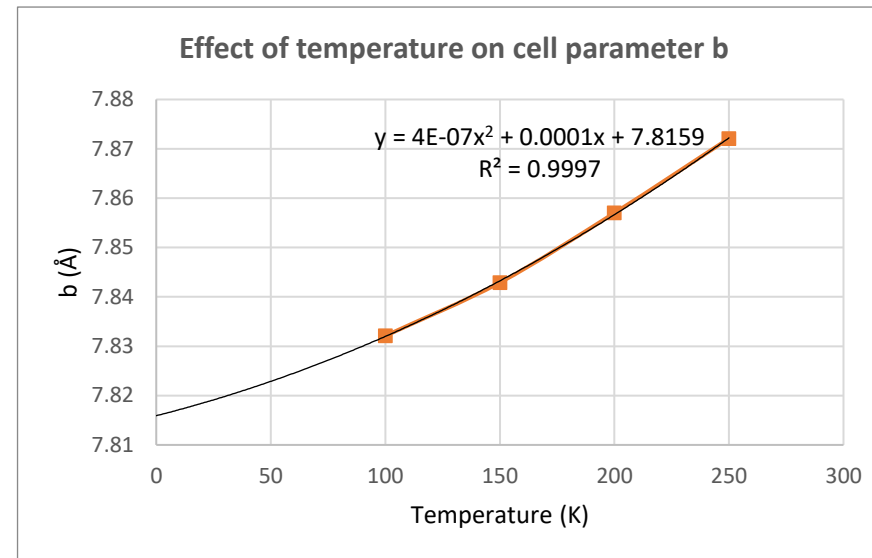


Figure 5.4b: Effect of temperature on cell parameter b

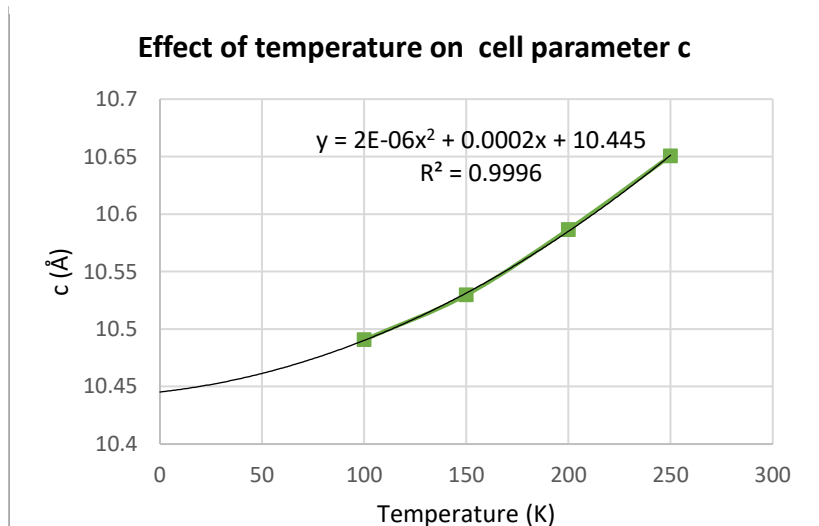


Figure 5.4c: Effect of temperature on cell parameter c

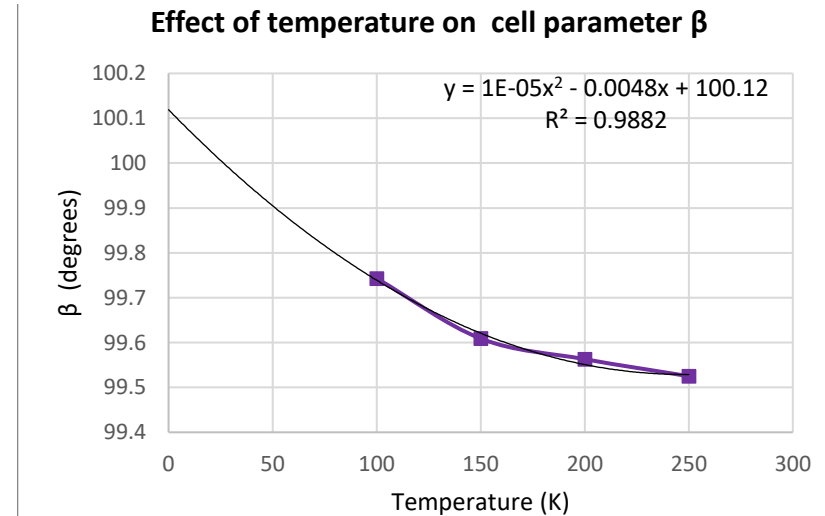


Figure 5.4d: Effect of temperature on cell parameter β

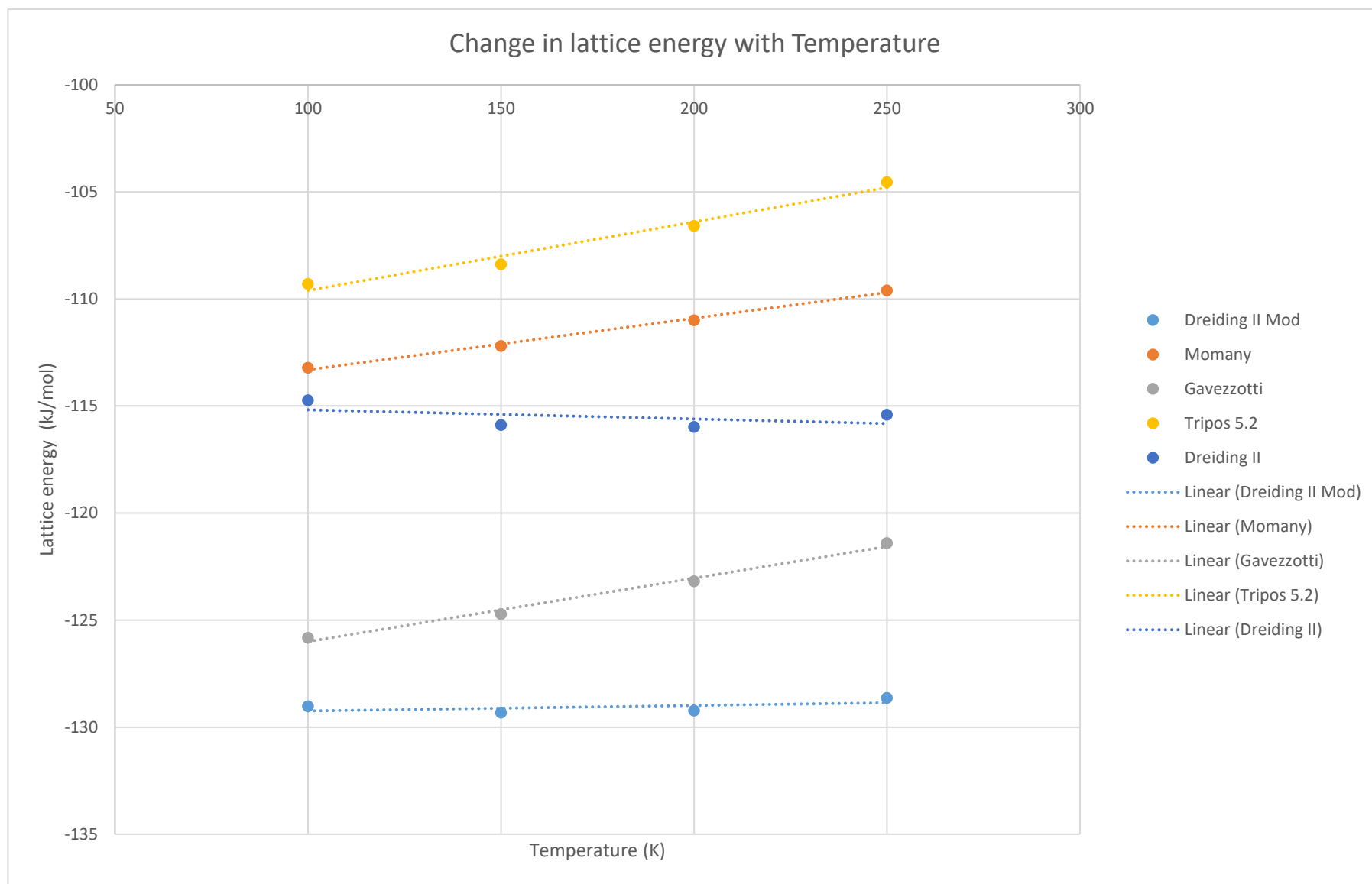


Figure 5.4e: Change in lattice energy with temperature

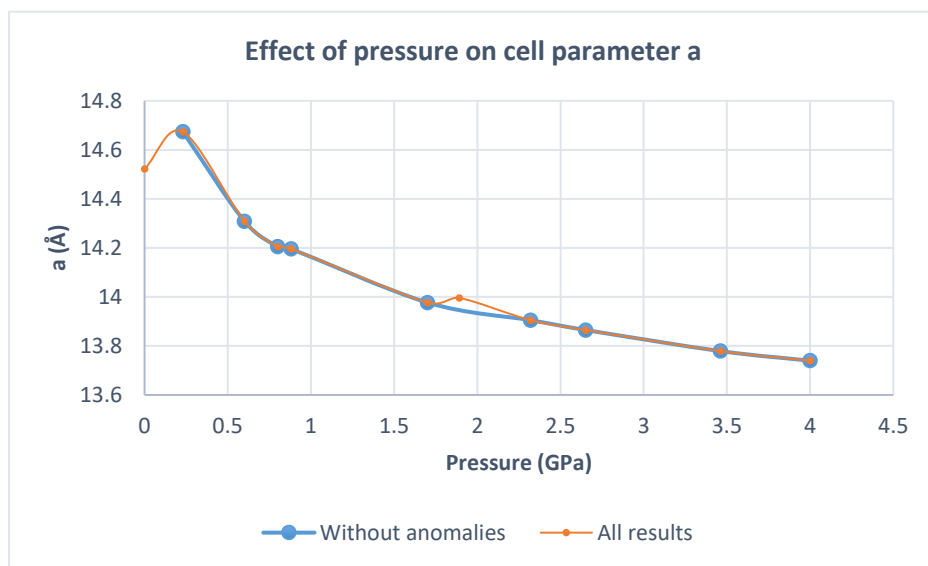


Figure 5.4f: Effect of pressure on cell parameter a

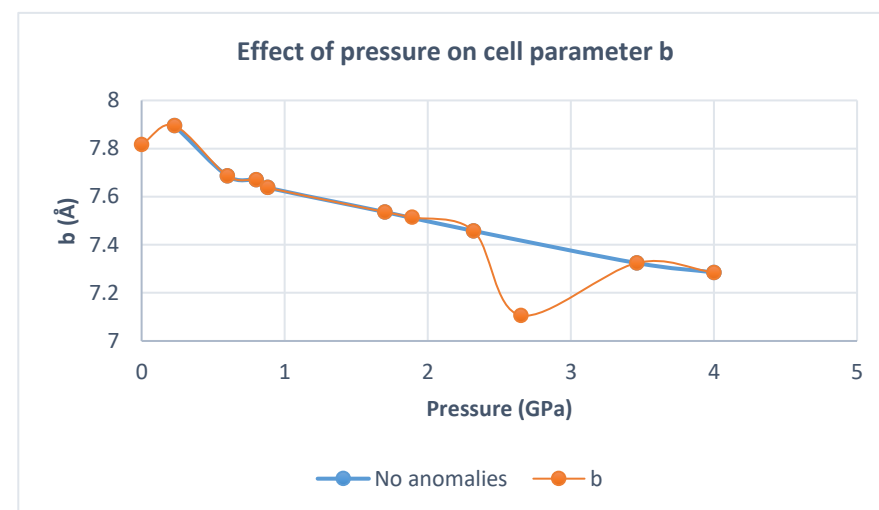


Figure 5.4g Effect of pressure on cell parameter b

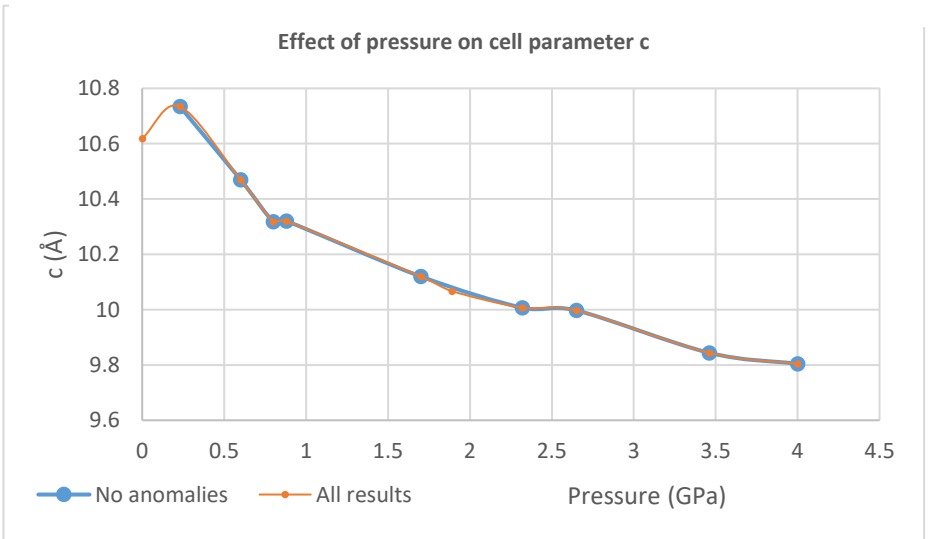


Figure 5.4h: Effect of pressure on cell parameter c

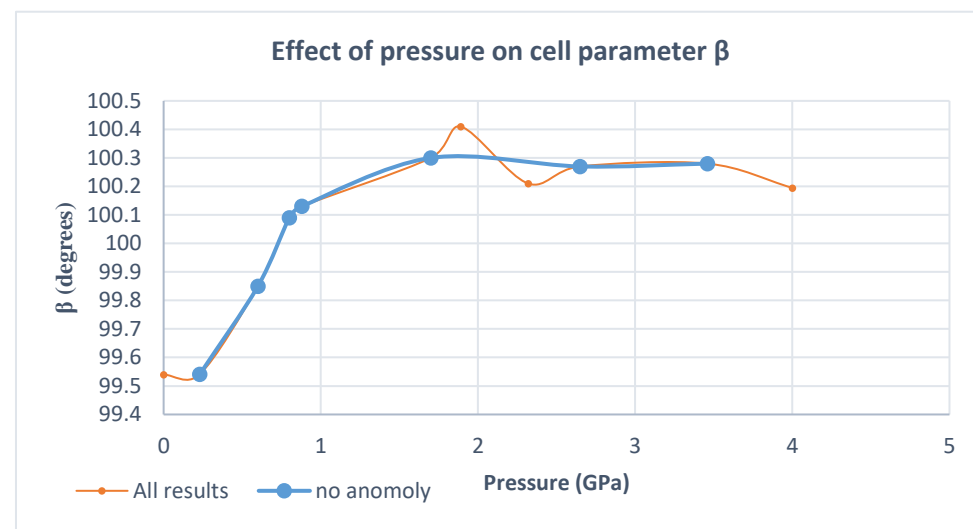


Figure 5.4i: Effect of pressure on cell parameter β

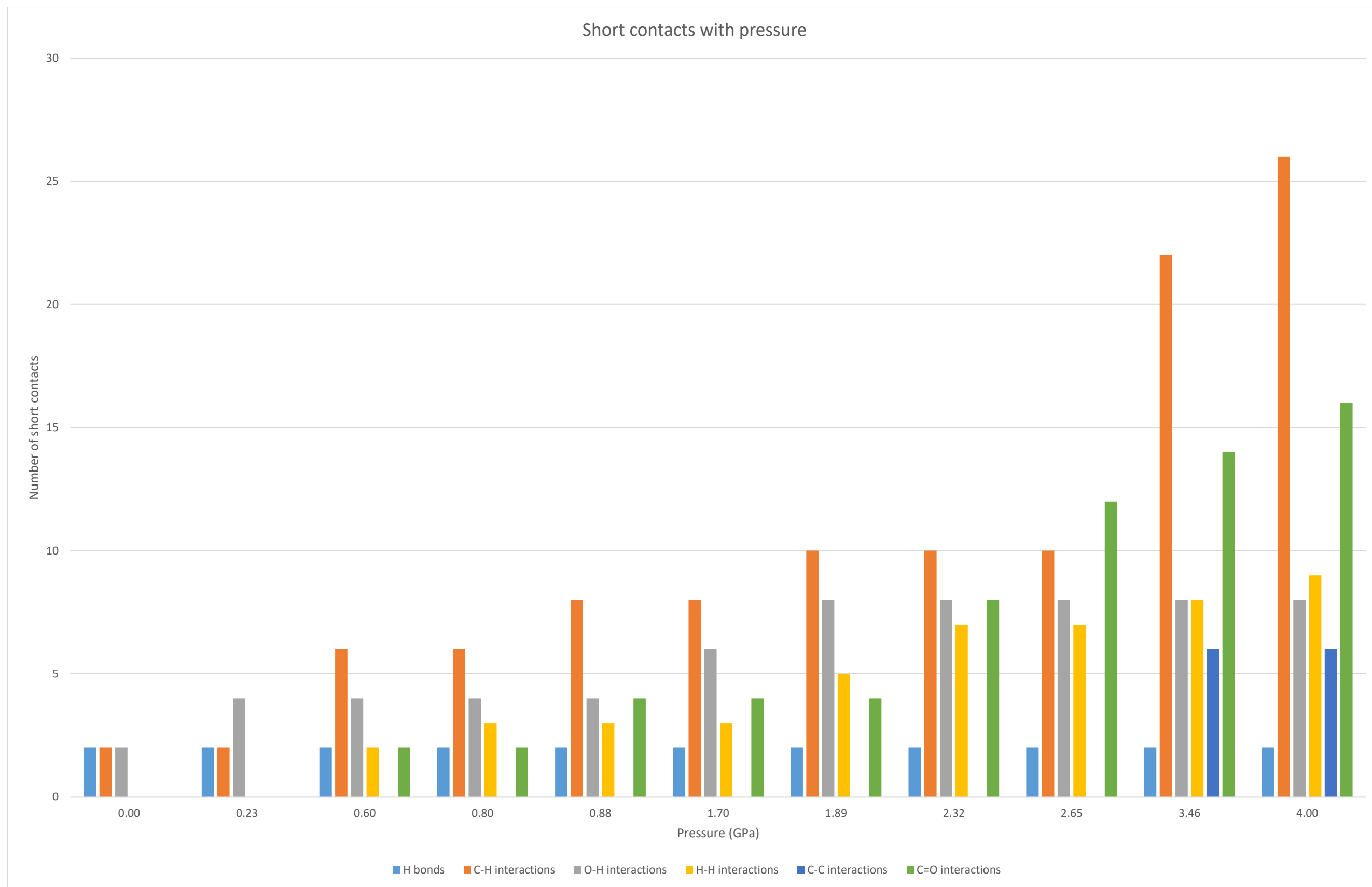


Figure 5.4j: Number of short contacts with pressure

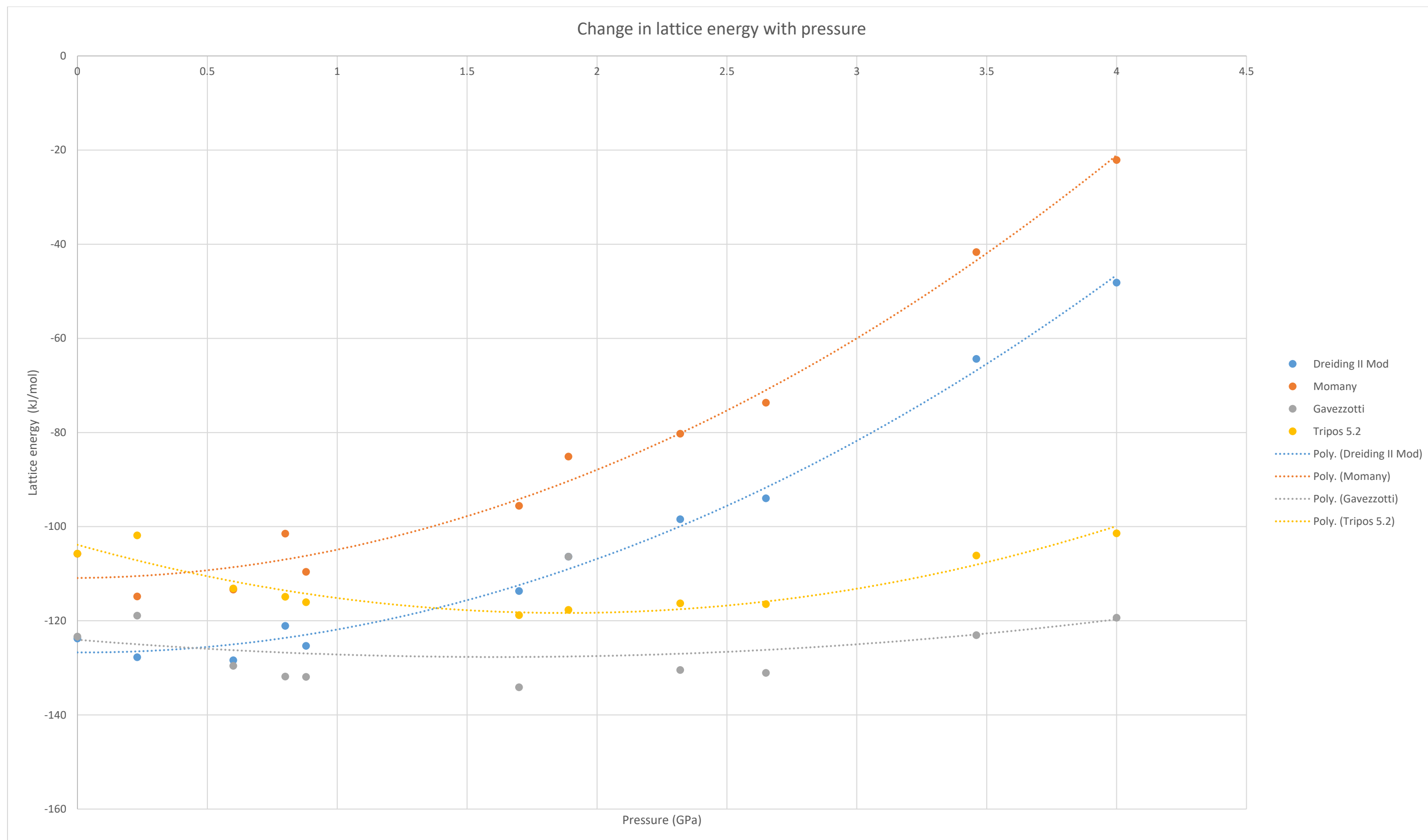


Figure 5.4k: Change in lattice energy with pressure

5.4d The effect of chirality on lattice energy

IBPRAC01 was the S enantiomer whilst IBPRAC16 was the R enantiomer. The lattice energies, shown in Table 5.4d, show there was no discernible difference between the values obtained for the Momany and Gavezzotti fields but produced a slight discrepancy within the Dreiding II, Dreiding II Mod and Tripos fields. Since these were obtained under different probes the carbon-hydrogen bond lengths vary, this change would result in different VdW energies, giving different lattice energies.

Table 5.4d: Lattice energies of both enantiomers of Form I

	Lattice energy (kJ/mol)	
Forcefield	IBPRAC01	IBPRAC16
Dreiding II Mod	-115.86	-129.03
Dreiding II	-69.19	-114.73
Momany	-112.14	-113.22
Gavezzotti	-126.59	-125.82
Tripos 5.2	-98.73	-109.29

The weighted averages for each enantiomer and polymorph 2 are shown in table 5.4e. As before the Momany and Gavezzotti produced nearly identical results for both enantiomers, whilst the Dreiding II Mod and Tripos were comparable but not as close as the other forcefields. The Dreiding II solution differed greatly for the two enantiomers, with a difference of 40kJ/mol. This was likely due to the fact that Dreiding II forcefield calculates the hydrogen bonding interaction in a different manner to Dreiding II Mod. Despite this the lattice energy of both enantiomers was consistently more negative than polymorph 2, indicating that the enantiomer was a factor in determining the stability of two polymorphs, but it was not a significant one. However, this may not be the case for all molecules as some molecules may have multiple chiral centres or the groups branching from the chiral centre may be much larger. The two of the branching chains from the chiral centre for ibuprofen were a hydrogen atom and a carboxylic acid group; two small chains. Larger chains may contribute more to the overall structure of the cell, resulting in a greater difference in the lattice energy of the two enantiomers.

Table 5.4e: Averaged lattice energy of each enantiomer compared with Form II

	Lattice energy (kJ/mol)		
Forcefield	Averaged S	Averaged R	Polymorph 2
Dreiding II Mod	-121.58	-129.052	-87.501
Dreiding II	-77.8513	-115.501	-68.056
Momany	-110.68	-111.504	1.634
Gavezzotti	-124.652	-123.782	-80.776
Tripos 5.2	-97.673	-107.203	95.928

5.5 DFT analysis

5.5a Cell parameter comparison

The cell parameters for DFT 1 molecule, the original molecule and the graphical extrapolation are shown in table 5.5a. All the cell parameters except length a decreased in size resulting in a small cell volume, which was expected since DFT calculates the cell parameters at 0K. The space group and cell structure and space grouped remained the same as expected. Percentage difference was calculated between DFT1 and IBPRAC01 and the graphical extrapolation are shown on the right. The percentage difference between the DFT and graphical extrapolation was smaller than the percentage difference with IBPRAC01, with all percentage differences remaining under 1%. Therefore, it was concluded that the DFT had produced a molecule of good quality and that IBPRAC01 unit cell was close to minimum energy due to the small percentage change between IBPRAC01 and DFT1.

Table 5.5a: Various cell parameters of Form I with percentage differences of DFT with other parameters

Cell parameter	IBPRAC01	Graphical extrapolation (IBPRAC16-19)	DFT1	% Difference of DFT with IBPRAC01	% Difference of DFT with graphical extrapolation
a (Å)	14.397	14.399	14.539	0.97	0.96
b (Å)	7.818	7.8041	7.727	-1.17	-0.99
c (Å)	10.506	10.377	10.303	-1.98	-0.72
V (Å ³)	1182.511	1166.076	1157.417	-2.17	-0.75
α (°)	90	90	90	0.00	0.00
β (°)	99.7	99.855	100.95	1.24	1.08
γ (°)	90	90	90	0.00	0.00

The cell parameters for DFT2 are shown below in table 5.5b. the DFT2 molecule was significantly different from the original molecule, with the largest difference occurring in the unit cell length b, which experienced a change close to 10%. The unit cell structure remained monoclinic as expected since there was not expected to any significant changes in the unit cell structure only minute changes in the lengths and angles.

Table 5.5b: Original cell parameters of Form II with DFT2 cell parameters.

	IBPRAC04	DFT2	% Difference
a (Å)	12.379	12.645	2.10
b (Å)	5.872	5.351	-9.75
c (Å)	17.562	17.335	-1.31
V (Å ³)	1276.643	1172.875	-8.85
α (o)	90	90	0.00
β	94.873	94.454	-0.44
γ	90	90	0.00

5.5b Molecular overlay of polymorphs

The initial molecular overlay of DFT1 with IBPRAC01, using only the phenyl and carboxylic carbons gave an RMS of 0.0239. The final RMS when all the carbon atoms were included was 0.0395, whilst the RMS for the phenyl and carboxylic carbons was 0.029, a small increase indicating that there was little discrepancy in the rest of the molecule.

The initial RMS for DFT2 and IBPRAC04 was significantly higher, with an RMS value of 0.0880, which was consistent with results found in cell parameter comparison. DFT2 had larger percentage change therefore the RMS would be expected to be higher. The RMS increased further to 0.2770 when all the carbon atoms were included. The RMS of the phenyl rings and the carboxylic carbon was 0.1370, showing that most of the discrepancy occurred in the methyl chain of the molecule (the opposite side of the molecule), shown in Figure 5.5a.

Table 5.5c: RMS of the two polymorphs

Atoms overlayed		RMS	
		Polymorph 1	Polymorph 2
Phenyl and carboxylic		0.0239	0.0880
All carbons	Phenyl and Carboxylic	0.0344	0.1370
	Total	0.0395	0.2770

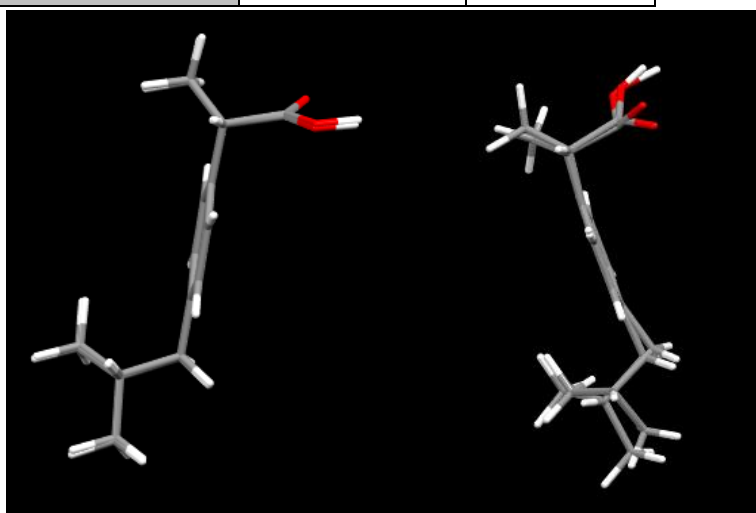


Figure 5.5a: Atom overlay of original molecules with DFT molecule. Form I left, Form II right

An additional discrepancy occurred in the carboxylic acid group (COOH) in DFT2. The hydrogen atom in the COOH group in IBPRAC04 was not in the same plane, however, in DFT2 the hydrogen atom was in the same plane.

5.5c Bond analysis

In DFT the bond length, angle and torsion can change; the focus of this analysis was solely the varying bond lengths in polymorph one; IBPRAC01 the atoms are labelled below in Figure 5.5b. The angles and torsion were not examined unless the changes were noteworthy.

Bond Length

The bond length analysis focused on the various probes of polymorph one; X-Ray, Neutron and DFT. The bond lengths along with the percentage difference between the three are shown in Table 5.5d. The carbon-carbon bond lengths remained the same varying by an average of 1%, the carbon-oxygen bonds varied by a greater amount, 3%. The greatest difference occurred in the length of the carbon-hydrogen bond. The carbon-hydrogen bonds in both DFT and neutron were both comparable varying an average of 1.8% and a maximum of 5%; this was significantly lower than the percentage difference between the DFT and the X-Ray bond lengths where the average was 12% and the maximum was 15%. This increase was expected since the X-Ray probe could not accurately locate the hydrogen atoms and therefore the hydrogen atoms were placed at fixed lengths; since the main purpose of XRD was to determine the crystal structure rather than determine the length of the carbon-hydrogen bonds. Another important change was the length of the carbon-hydrogen bond in the phenyl rings; in both DFT1 and DFT2 the final length of the carbon-hydrogen bond was 1.09Å. The final point of interest was the length of hydrogen in the carboxylic acid group; this bond varied by the greatest amount across all three specimens.

Torsion and bond angle Variation

A noteworthy change in torsion occurred in the carboxylic acid group in polymorph 2. The torsion in IBPRAC04 was 17.35, whilst the torsion in DFT 2.03, a significant change. This change was also evident in the angle of the hydrogen in the dimer, which was originally 138.94° in IBPRAC04 and then 176.80° in DFT2. These changes resulted in a decrease in the length of the hydrogen bond-forming the dimer; the oxygen-oxygen distance decreasing from 2.701Å in IBPRAC04 to 2.570Å in DFT2.

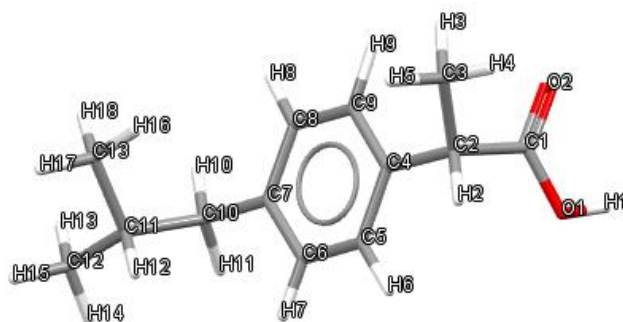


Figure 5.5b: Form I with atoms labelled.

Table 5.5d: Bond lengths of Form I, with % differences (right)

Type of bond	Atoms Bonded		Bond Length (Å)			% difference		
			DFT1	IBPRAC01 (Neutron 100K)	IBPRAC16 (X-Ray 100K)	% Diff DFT Neutron	% Diff DFT Xray	%difference Neutron Xray
C-C	Propanoic acid	C1-C2	1.516	1.504	1.506	-0.79	-0.66	0.13
		C2-C3	1.529	1.5	1.524	-1.90	-0.33	1.60
	Acid to phenyl ring	C2-C4	1.525	1.525	1.523	0.00	-0.13	-0.13
	Phenyl Ring	C4-C5	1.4	1.375	1.386	-1.79	-1.00	0.80
		C5-6	1.394	1.376	1.385	-1.29	-0.65	0.65
		C6-7	1.403	1.392	1.389	-0.78	-1.00	-0.22
		C7-8	1.4	1.381	1.385	-1.36	-1.07	0.29
		C8-9	1.393	1.396	1.384	0.22	-0.65	-0.86
		C4-9	1.399	1.38	1.388	-1.36	-0.79	0.58
	Phenyl to propane	C7-10	1.505	1.493	1.507	-0.80	0.13	0.94
	Propane	C10-11	1.545	1.529	1.531	-1.04	-0.91	0.13
		C11-12	1.53	1.508	1.516	-1.44	-0.92	0.53
		C11-13	1.53	1.519	1.522	-0.72	-0.52	0.20
C-O O-H	COOH	C=O	1.242	1.205	1.219	-2.98	-1.85	1.16
		C-O	1.317	1.306	1.311	-0.84	-0.46	0.38
	O-H	O-H	1.029	0.963	0.82	-6.41	-20.31	-14.85
C-H	C-H propanoic acid	C2-H	1.097	1.091	0.98	-0.55	-10.67	-10.17
		C3-H1	1.096	1.053	0.96	-3.92	-12.41	-8.83
		C3-H2	1.096	1.08	0.96	-1.46	-12.41	-11.11
		C3-H3	1.096	1.073	0.96	-2.10	-12.41	-10.53
	Phenyl Hydrogens	C5-H	1.09	1.077	0.93	-1.19	-14.68	-13.65
		C6-H	1.092	1.065	0.93	-2.47	-14.84	-12.68
		C8-H	1.09	1.041	0.93	-4.50	-14.68	-10.66
		C9-H	1.088	1.104	0.929	1.47	-14.61	-15.85
	Propane Hydrogens	C10-H1	1.101	1.102	0.97	0.09	-11.90	-11.98
		C10-H2	1.101	1.101	0.97	0.00	-11.90	-11.90
		C11-H	1.104	1.086	0.98	-1.63	-11.23	-9.76
		C12-H1	1.099	1.067	0.96	-2.91	-12.65	-10.03
		C12-H2	1.099	1.044	0.96	-5.00	-12.65	-8.05
		C12-H3	1.098	1.1	0.96	0.18	-12.57	-12.73
		C13-H1	1.098	1.061	0.96	-3.37	-12.57	-9.52
		C13-H2	1.099	1.062	0.96	-3.37	-12.65	-9.60
		C13-H3	1.1	1.096	0.96	-0.36	-12.73	-12.41

5.5d DFT Lattice energy comparison

The CASTEP software confirmed the findings of the previous studies, section 5.2, stating that polymorph 2 was less stable than polymorph 1; with polymorph 2 having a lattice energy 18.9 kJ/mol less negative relative to polymorph one. The various lattice energies obtained for DFT 1 and 2 are shown below, along with IBPRAC01, 16 and 04. IBPRAC01 and 04 are the original molecules, whilst IBPRAC16 was of lower quality since it was obtained via X-Ray diffraction, as opposed to neutron diffraction from which IBPRAC01 was obtained; otherwise, both were obtained under similar conditions 100K at atmospheric pressure. This comparison would indicate whether DFT would be necessary to determine the stability of the polymorph.

DFT1 analysis

Table 5.5e shows the lattice energies for the applicable fields as well as the percentage difference of the molecules 01 and 16 with DFT1. Only the Gavezzotti forcefield produced lattice energy, which was comparable to that of the original molecules, varying only by 3%. The Dreiding II Mod, Momany field and Tripos 5.2 fields all produced lattice energies which varied by between 13 -26%. The largest deviation occurred with the Dreiding II field, which gave a positive value for the lattice energy, suggesting that the crystal would not be stable, this was considered to be an anomalous result, since this was the only solution that gave polymorph 1 a positive value for its lattice energy.

Table 5.5e: Various lattice energies of molecules of Form I

Forcefield	Lattice energy (kJ/mol)			Percentage difference of DFT1	
	IBPRAC01	IBPRAC16	DFT1	with IBPRAC01	with IBPRAC16
Dreiding II Mod	-115.861	-129.027	-95.015	-17.99	-26.36
Dreiding II	-69.194	-114.732	6.574	-109.50	-105.73
Momany	-112.144	-113.218	-92.301	-17.69	-18.47
Gavezzotti	-126.588	-125.82	-121.895	-3.71	-3.12
Tripos 5.2	-98.73	-109.292	-85.522	-13.38	-21.75

The analysis of the breakdown of the lattice energies for IBPRAC01 and DFT1, tables 5.5g-k, gave reasons for the change in the total lattice energy. The study of the Dreiding field, tables 5.5g, which changed from negative lattice energy to positive lattice energy, showed that all components of the lattice energy were affected; as expected since the distance between the molecules was decreased. The electrostatic energy experienced a small increase (more negative) in attraction across all planes increasing by an average of 30%. Both the components of the H bond energy, attraction and repulsion, experienced changes; both increased (the attraction became more negative, the repulsion became more positive). This resulted in a decrease of total H bond energy by 20% across all planes. The most significant change occurred in the VdW forces. The attractive forces increased by an average of 13% but the repulsive forces increased by greater factor resulting in the overall VdW force to be positive and therefore repulsive across all planes. One plane of importance was the {100} plane which did not experience any H bond energy in the original molecule, experienced H bond energy in DFT1. There were also significant increases across all other planes, with the greatest increase

occurring in the electrostatic which increased from -0.025mJ/m^2 to -4.035mJ/m^2 , an increase by a factor of 160.

The Dreiding II Mod experienced a similar change, tables 5.5h. The electrostatic forces increased to match the electrostatic values seen in Dreiding II in all fields except in the $\{100\}$ field, where the value increased from -0.025 to -0.044mJ/m^2 . The H bond components experienced near-identical changes which resulted in the strengthening of both attractive and repulsive forces, with the repulsive forces increasing by slightly larger factor across all planes. This caused an overall decrease in the overall H bond energy. The same was observed with the VdW forces, both components strengthen, but the repulsive forces increased by a greater amount.

The Momany forcefield, table 5.5i, experienced similar changes to the Dreiding II Mod field, with increases in both VdW components, but as before the repulsive forces increased by a greater extent than attractive forces, despite this, the overall VdW remained negative. The electrostatic forces increased by the same factor as the Dreiding II Mod. The electrostatic force in the Momany remained half of the electrostatic force in the Dreiding II Mod field. The H bond components experienced identical changes with an increase in both components resulting in the overall weakening of the H bond energy.

The Gavezzotti field, table 5.5j, experienced the smallest change in the overall lattice energy, tables 5.5. Despite the strengthening of both fields the total energy only decreased by 4%. The VdW component in the Tripos field, table 5.5k, followed the same trend as the other fields. Whilst the electrostatic component increased by the same factor as the Momany and Dreiding fields, indicating that these share a similar foundation.

The overall decrease in the lattice energy across all fields was attributed to the VdW force; the VdW force dominated the total energy for each plane. Since the repulsive force increased by a greater factor than the attractive force the total energy of the plane decreased across all planes giving lattice energy that was less negative, suggesting that the stability had decreased. This increase of the repulsive forces showed that the DFT molecule represented a point where the bond length and intermolecular length was less the equilibrium in the Dreiding fields, as the repulsive forces were increasing at a greater rate to the attractive forces, therefore representing a point to the left of minimum in the potential energy functions, as the distance between the atoms was shortening. The changes in the lattice energy were also reflected in the crystal morphology; all the negative lattice energies had a similar morphology, whilst the Dreiding II field, which gave a positive value had a different morphology.

DFT2 analysis

The lattice energies for DFT2, table 5.5f, follow a did not similar trend to the molecules of DFT1. The Gavezzotti field suggested increased stability of DFT2 when compared with IBPRAC04, a trend that was not present in DFT1. Dreiding II Mod showed that both DFT2 and IBPRAC04 would be of similar stabilities, differing by only 3%. The greatest points of interest lie in the other three fields; both the Momany and Tripos fields showed that the lattice energy of IBPRAC04 was positive whilst the lattice energy of DFT2 was negative. The opposite was true for the Dreiding II field, which initially indicated that the lattice energy was negative, returned a positive result for the lattice energy of DFT2.

Table 5.5f: Lattice energies of molecules of Form II

Forcefield	Lattice energy (kJ/mol)		% diff with IBPRAC04
	IBPRAC04	DFT2	
Dreiding II Mod	-87.501	-84.879	-3.00
Dreiding II	-68.056	39.442	-157.96
Momany	1.634	-75.461	-4718.18
Gavezzotti	-80.776	-110.266	36.51
Tripos 5.2	95.928	-72.98	-176.08

The analysis of the lattice energy breakdown of DFT2 revealed details that were not present in the analysis of DFT1. Each molecule, IBPRAC04 and DFT4, had 10 planes; unlike DFT1 not all the planes were shared amongst both molecules. In DFT2 the {202} plane was present whilst {012} was present in IBPRAC04 instead, tables 5.5l-q.

In the Dreiding II field, table 5.5l, the VdW forces strengthen, as per the previous case with DFT1. The repulsive forces grew greater than the attractive forces resulting in the total VdW forces to be positive for all the faces. The repulsive forces grew by 250% whilst the attractive forces only strengthen by 50%; with the greatest increase occurring in the carboxylic acid atoms (COOH). The electrostatic forces also strengthen significantly; increasing by factors up to 140, -0.046mJ/m^2 to -6.026mJ/m^2 . The H bond components also increase significantly, but the total H bond energy only increased by 50%. As before the VdW dominated the lattice energy therefore the total lattice energy was positive despite the changes to the other components.

The attractive VdW forces in the Dreiding II Mod field, table 5.5m, experienced a similar increase as the prior case, increasing by 50%, however, the repulsive forces only increased by 120%. Therefore, the total VdW forces remain negative for the face, becoming 80% of the original value across all the planes. The electrostatic force also increased significantly; however, it did increase as much as the Dreiding II field. The H bond components experienced a similar change as the Dreiding II Mod for DFT1, with all attractive forces increasing by a factor of 3.3, whilst the repulsive forces increased by a factor of 4. The total H bond remained negative increasing by 15% from -8.31mJ/m^2 to -9.54mJ/m^2 .

The Momany field, table 5.5n, originally gave a positive value for the lattice energy of IBPRAC04, this was found to be as a result of the high VdW repulsive force and relatively low VdW attractive forces. There was also some electrostatic repulsion present in IBPRAC04. In DFT2 the VdW attractive forces grew while the repulsive forces decreased. The greatest decrease in repulsion occurred in the atoms involved in hydrogen bonding, namely the oxygen

and hydrogen atoms in the carboxylic acid. The significance of the H bond energy decreased as both increased but the repulsive forces grew by an average of 400%, whilst the attractive forces grew by an average 300%. The total H bond, therefore, decreased to a third of the original value across all planes. The electrostatic forces increased significantly, but the majority of the total energy was due to the VdW forces; making up an average of 85% of the total energy.

The Gavezzotti field, table 5.5p, was composed entirely of VdW forces and did not consider electrostatic or H bond forces. Both VdW components strengthened; the repulsive forces grew by 80%, whilst the attractive forces grew by 70%. However, due to the initial size of the attractive forces, the total energy became more negative; showing increased stability, hence the more negative lattice energy.

The Tripos field, table 5.5q, also initially gave a positive value; mirroring the Momany field, the initial lattice energy had high VdW repulsive forces and relatively low VdW attractive forces. In DFT2, the repulsive forces become half of the original value; this change occurred for the same reason as in the Momany field, where the VdW repulsive force around the carboxylic acid atoms. The VdW attractive forces increased significantly causing the final VdW force to become negative. Although the electrostatic forces increased by factors 40% the VdW dominated the total energy, similar to the previous fields.

Both Gavezzotti and Dreiding II Mod were the two most consistent fields, providing negative values for both IBPRAC04 and DFT2. Since the Gavezzotti field does not consider H bonding, it may not be accurate for molecules where H bonds dominate instead of VdW forces. The change in the other three fields was due to the calculation of the VdW repulsion of the COOH atoms; this repulsion was either overestimated, as in the case of Dreiding II in DFT2 and Momany and Tripos fields for IBPRAC04, appendices A, B and C. As with DFT1 the crystal shapes were reflective of the values. All the negative values produced similar crystal morphologies, but the crystal morphologies of the positive values differed greatly, tables 5.5r and s. Therefore, if only the general crystal morphology was necessary, the field is not of significant importance as long as the lattice energy was negative.

Table 5.5g: Break down of the Dreiding II field for IBPRAC01 and DFT1

Dreiding II	IBPRAC01 (Attachment Energy mJ/m ²)										DFT1 (Attachment Energy mJ/m ²)						
Index	VdW Attraction	VdW Repulsion	Total VdW Energy	Electrost atic	H bond Attraction	H bond Repulsion	Total H bond Energy	Total Energy	Index	VdW Attraction	VdW Repulsion	Total VdW Energy	Electrostat ic	H bond Attraction	H bond Repulsion	Total H bond Energy	
{210}	-123.018	103.431	-19.587	-4.918	-210.235	191.356	-18.879	-43.384	{210}	-137.491	171.93	34.439	-5.923	-242.233	227.133	-15.101	
{21-1}	-128.843	91.662	-37.181	-3.498	-140.162	127.572	-12.591	-53.27	{21-1}	-142.854	145.317	2.463	-4.13	-161.495	151.423	-10.072	
{111}	-122.973	114.944	-8.029	-6.084	-280.307	255.141	-25.167	-39.279	{20-2}	-158.506	199.378	40.872	-7.024	-282.597	264.987	-17.611	
{110}	-109.834	110.555	0.721	-6.341	-280.308	255.141	-25.167	-30.786	{111}	-138.208	196.696	58.488	-7.446	-322.971	302.843	-20.128	
{11-1}	-117.546	99.24	-18.306	-4.699	-210.235	191.356	-18.878	-41.884	{110}	-122.588	189.035	66.447	-7.67	-322.972	302.843	-20.129	
{102}	-128.467	88.758	-39.709	-3.656	-140.159	127.571	-12.588	-55.952	{11-1}	-130.812	164.384	33.573	-5.684	-242.233	227.133	-15.1	
{100}	-36.641	19.223	-17.418	-0.025	0	0	0	-17.443	{100}	-103.057	120.049	16.992	-4.035	-161.487	151.422	-10.066	
{10-2}	-132.356	107.191	-25.165	-5.112	-210.231	191.356	-18.875	-49.152	{10-2}	-147.948	176.083	28.134	-6.119	-242.228	227.132	-15.096	
{011}	-118.552	112.978	-5.574	-6.085	-280.307	255.141	-25.167	-36.826	{011}	-132.949	193.215	60.266	-7.441	-322.971	302.843	-20.128	
{002}	-135.425	107.856	-27.569	-5.077	-210.232	191.356	-18.876	-51.522	{002}	-151.605	177.38	25.775	-6.093	-242.23	227.132	-15.097	

Table 5.5h: Break down of the Dreiding II Mod field for IBPRAC01 and DFT1

Dreiding II Mod	IBPRAC01 (Attachment Energy mJ/m ²)										DFT1 (Attachment Energy mJ/m ²)						
Index	VdW Attraction	VdW Repulsion	Total VdW Energy	Electrostatic	H bond Attraction	H bond Repulsion	Total H bond Energy	Total Energy	Index	VdW Attraction	VdW Repulsion	Total VdW Energy	Electrostatic	H bond Attraction	H bond Repulsion	Total H bond Energy	
{210}	-121.301	66.718	-54.582	-4.918	-210.235	191.356	-18.879	-78.379	{210}	-135.166	93.418	-41.748	-5.923	-242.233	227.133	-15.101	
{21-1}	-127.585	67.139	-60.446	-3.498	-140.162	127.572	-12.591	-76.535	{21-1}	-141.18	92.913	-48.267	-4.13	-161.495	151.423	-10.072	
{111}	-120.812	66.053	-54.759	-6.084	-280.307	255.141	-25.167	-86.009	{20-2}	-154.982	105.942	-49.04	-6.131	-242.228	227.132	-15.096	
{110}	-103.705	55.263	-48.442	-4.453	-210.235	191.356	-18.878	-71.773	{111}	-135.247	92.085	-43.161	-7.446	-322.971	302.843	-20.128	
{11-1}	-112.228	59.15	-53.078	-3.38	-140.162	127.572	-12.591	-69.049	{110}	-115.859	77.256	-38.604	-5.456	-242.233	227.132	-15.1	
{102}	-127.235	64.241	-62.994	-3.656	-140.159	127.571	-12.588	-79.238	{11-1}	-123.55	80.273	-43.278	-4.007	-161.495	151.423	-10.072	
{100}	-36.631	19.223	-17.408	-0.025	0	0	0	-17.433	{100}	-43.38	33.453	-9.927	-0.044	0	0	0	
{10-2}	-127.359	66.852	-60.506	-3.688	-140.157	127.571	-12.587	-76.781	{10-2}	-143.171	95.214	-47.956	-4.32	-161.49	151.422	-10.068	
{011}	-116.392	64.087	-52.305	-6.085	-280.307	255.141	-25.167	-83.556	{011}	-129.988	88.605	-41.383	-7.441	-322.971	302.843	-20.128	
{002}	-120.241	61.182	-59.059	-3.686	-140.157	127.571	-12.587	-75.331	{002}	-134.597	85.461	-49.136	-4.318	-161.49	151.422	-10.068	

Table 5.5i: Break down of the Momany field for IBPRAC01 and DFT1

Momany	IBPRAC01 (Attachment Energy mJ/m ²)										DFT1 (Attachment Energy mJ/m ²)						
Index	VdW Attraction	VdW Repulsion	Total VdW Energy	Electrostatic	H bond Attraction	H bond Repulsion	Total H bond Energy	Total Energy	Index	VdW Attraction	VdW Repulsion	Total VdW Energy	Electrostatic	H bond Attraction	H bond Repulsion	Total H bond Energy	
{210}	-107.822	52.413	-55.409	-2.459	-112.186	93.373	-18.813	-76.681	{210}	-120.772	73.739	-47.033	-2.961	-212.347	200.983	-11.364	
{21-1}	-112.524	51.428	-61.096	-1.749	-74.793	62.249	-12.544	-75.389	{21-1}	-125.179	71.592	-53.588	-2.065	-141.567	133.989	-7.579	
{111}	-107.685	53.195	-54.489	-3.042	-149.58	124.498	-25.083	-82.614	{20-2}	-137.071	82.669	-54.402	-3.066	-212.348	200.983	-11.365	
{110}	-92.306	44.3	-48.006	-2.226	-112.186	93.373	-18.813	-69.045	{111}	-121.076	74.318	-46.759	-3.723	-283.127	267.977	-15.151	
{11-1}	-99.744	45.509	-54.236	-1.69	-74.793	62.249	-12.544	-68.47	{110}	-103.637	62.136	-41.501	-2.728	-212.346	200.983	-11.364	
{102}	-110.467	48.882	-61.586	-1.828	-74.793	62.249	-12.543	-75.957	{11-1}	-110.276	62.125	-48.151	-2.003	-141.567	133.989	-7.579	
{100}	-31.26	15.136	-16.124	-0.012	0	0	0	-16.137	{100}	-37.644	26.549	-11.095	-0.022	0	0	0	
{10-2}	-111.003	51.094	-59.909	-1.844	-74.793	62.249	-12.544	-74.296	{10-2}	-125.359	72.791	-52.568	-2.16	-141.567	133.989	-7.578	
{011}	-103.975	51.681	-52.293	-3.042	-149.58	124.498	-25.083	-80.418	{011}	-116.599	71.602	-44.997	-3.721	-283.127	267.977	-15.151	
{002}	-104.617	46.56	-58.057	-1.843	-74.793	62.249	-12.544	-72.443	{002}	-117.506	64.956	-52.55	-2.159	-141.567	133.989	-7.578	

Table 5.5j: Break down of the Gavezzotti field for IBPRAC01 and DFT1

Gavezzotti	IBPRAC01(Attachment Energy mJ/m ²)					DFT1(Attachment Energy mJ/m ²)		
Index	VdW Attraction	VdW Repulsion	Total Energy		Index	VdW Attraction	VdW Repulsion	Total Energy
{210}	-146.433	59.715	-86.717		{210}	-173.119	90.354	-82.766
{21-1}	-140.575	54.108	-86.467		{21-1}	-162.051	79.171	-82.88
{111}	-156.463	64.877	-91.586		{20-2}	-188.805	97.419	-91.386
{110}	-129.131	52.336	-76.795		{111}	-188.444	100.361	-88.083
{11-1}	-127.888	49.08	-78.808		{110}	-154.196	80.335	-73.861
{102}	-138.495	51.856	-86.639		{11-1}	-147.561	71.341	-76.22
{100}	-29.745	12.364	-17.382		{100}	-35.098	20.227	-14.871
{10-2}	-138.373	53.408	-84.965		{10-2}	-161.721	79.857	-81.864
{011}	-152.883	63.578	-89.304		{011}	-184.197	98.183	-86.014
{002}	-132.723	49.823	-82.9		{002}	-154.929	74.099	-80.83

Table 5.5k: Break down of the Tripos 5.2 field for IBPRAC01 and DFT1

Tripos 5.2	IBPRAC01 (Attachment Energy mJ/m ²)							DFT1(Attachment Energy mJ/m ²)				
Index	VdW Attraction	VdW Repulsion	Total VdW Energy	Electrostatic	Total Energy		Index	VdW Attraction	VdW Repulsion	Total VdW Energy	Electrostatic	Total Energy
{210}	-110.145	50.152	-59.993	-4.918	-64.911		{210}	-125.051	76.992	-48.059	-5.923	-53.982
{21-1}	-115.278	48.944	-66.334	-3.498	-69.832		{21-1}	-130.722	74.467	-56.255	-3.985	-60.24
{111}	-110.035	50.566	-59.469	-6.084	-65.553		{20-2}	-143.859	87.959	-55.9	-7.024	-62.924
{110}	-94.826	42.538	-52.288	-4.453	-56.741		{111}	-125.559	77.751	-47.808	-7.446	-55.254
{11-1}	-101.071	42.313	-58.758	-3.38	-62.138		{110}	-108.023	65.461	-42.562	-5.456	-48.018
{102}	-113.974	46.052	-67.922	-3.656	-71.578		{11-1}	-118.536	69.727	-48.809	-5.684	-54.493
{100}	-35.702	18.365	-17.337	-0.025	-17.362		{100}	-43.378	33.471	-9.907	-0.044	-9.951
{10-2}	-114.718	48.691	-66.027	-3.688	-69.715		{10-2}	-131.022	74.645	-56.377	-4.32	-60.696
{011}	-105.819	48.74	-57.079	-6.085	-63.164		{011}	-120.433	74.376	-46.057	-7.441	-53.498
{002}	-107.18	43.163	-64.017	-3.686	-67.702		{002}	-121.673	64.666	-57.007	-4.318	-61.326

Table 5.5l: Break down of the Dreiding II field for IBPRAC04 and DFT2

Dreiding	IBPRAC04(Attachment Energy mJ/m²)								Dreiding	DFT2(Attachment Energy mJ/m²)							
Index	VdW Attraction	VdW Repulsion	Total VdW Energy	Electrostatic	H bond Attraction	H bond Repulsion	Total H bond Energy	Total Energy	Index	VdW Attraction	VdW Repulsion	Total VdW Energy	Electrostatic	H bond Attraction	H bond Repulsion	Total H bond Energy	Total Energy
{202}									{202}	-139.121	172.44	33.319	-6.026	-216.017	205.415	-10.601	16.692
{20-2}	-99.952	58.71	-41.242	-0.046	-60.392	49.315	-11.077	-52.365	{20-2}	-145.476	193.591	48.115	-6.873	-259.215	246.497	-12.717	28.525
{111}	-83.899	43.066	-40.834	-0.296	-40.263	32.877	-7.386	-48.515	{111}	-119.333	175.654	56.321	-6.764	-259.212	246.497	-12.715	36.842
{110}	-84.08	43.113	-40.967	-0.294	-40.262	32.877	-7.386	-48.647	{110}	-141.42	206.638	65.218	-7.843	-302.414	287.58	-14.834	42.541
{11-1}	-94.462	56.33	-38.131	-0.057	-60.392	49.315	-11.077	-49.265	{11-1}	-150.575	212.84	62.264	-7.758	-302.412	287.579	-14.833	39.673
{102}	-72.94	42.386	-30.554	-0.074	-40.262	32.877	-7.385	-38.013	{102}	-112.649	154.831	42.181	-5.567	-216.009	205.414	-10.595	26.02
{100}	-66.248	39.034	-27.214	-0.03	-40.261	32.877	-7.385	-34.629	{100}	-130.375	183.502	53.128	-6.857	-259.215	246.497	-12.717	33.554
{10-2}	-84.78	52.942	-31.838	0.151	-60.392	49.315	-11.077	-42.764	{10-2}	-124.552	180.097	55.545	-6.408	-259.207	246.496	-12.711	36.426
{011}	-77.222	40.354	-36.868	-0.288	-40.263	32.877	-7.386	-44.541	{011}	-128.527	163.969	35.442	-6.083	-216.02	205.416	-10.604	18.755
{002}	-76.886	50.069	-26.817	0.148	-60.392	49.315	-11.077	-37.746	{002}	-112.912	171.865	58.953	-6.406	-259.207	246.496	-12.711	39.837
{012}	-90.433	55.928	-34.505	0.153	-60.392	49.315	-11.077	-45.429									

Table 5.5m: Break down of the Dreiding II Mod field for IBPRAC04 and DFT2

Dreiding II Mod	IBPRAC04 (Attachment Energy mJ/m²)								Dreiding II Mod	DFT2(Attachment Energy mJ/m²)							
Index	VdW Attraction	VdW Repulsion	Total VdW Energy	Electrostatic	H bond Attraction	H bond Repulsion	Total H bond Energy	Total Energy	Index	VdW Attraction	VdW Repulsion	Total VdW Energy	Electrostatic	H bond Attraction	H bond Repulsion	Total H bond Energy	Total Energy
{202}									{202}	-122.162	82.189	-39.974	-4.735	-172.81	164.332	-8.479	-53.187
{20-2}	-98.675	42.85	-55.825	-0.046	-60.392	49.315	-11.077	-66.948	{20-2}	-142.979	97.855	-45.124	-6.873	-259.215	246.497	-12.717	-64.714
{111}	-83.027	32.491	-50.536	-0.296	-40.263	32.877	-7.386	-58.217	{111}	-123.408	81.834	-41.574	-5.212	-172.821	164.334	-8.487	-55.273
{110}	-83.208	32.538	-50.67	-0.294	-40.262	32.877	-7.386	-58.35	{110}	-123.656	82.353	-41.303	-5.211	-172.821	164.334	-8.487	-55.001
{11-1}	-85.907	34.302	-51.604	-0.167	-40.262	32.877	-7.385	-59.156	{11-1}	-129.279	87.004	-42.274	-5.181	-172.819	164.334	-8.486	-55.941
{102}	-72.064	31.81	-40.254	-0.074	-40.262	32.877	-7.385	-47.714	{102}	-103.534	69.435	-34.099	-4.702	-172.81	164.332	-8.479	-47.279
{100}	-65.396	28.46	-36.936	-0.03	-40.261	32.877	-7.385	-44.35	{100}	-93.998	64	-29.998	-4.579	-172.81	164.332	-8.478	-43.056
{10-2}	-83.519	37.083	-46.436	0.151	-60.392	49.315	-11.077	-57.362	{10-2}	-122.088	84.389	-37.699	-6.408	-259.207	246.496	-12.711	-56.818
{011}	-76.351	29.779	-46.572	-0.288	-40.263	32.877	-7.386	-54.245	{011}	-114.648	75.467	-39.181	-5.19	-172.821	164.334	-8.487	-52.858
{002}	-74.572	33.169	-41.404	0.05	-50.327	41.096	-9.231	-50.585	{002}	-109.07	74.651	-34.42	-5.539	-216.009	205.414	-10.595	-50.553
{012}	-82.384	33.209	-49.175	-0.079	-40.263	32.877	-7.386	-56.639									

Table 5.5n: Break down of the Momany field for IBPRAC04 and DFT2

Momany	IBPRAC04(Attachment Energy mJ/m²)								Momany	DFT2 (Attachment Energy mJ/m²)							
Index	VdW Attraction	VdW Repulsion	Total VdW Energy	Electrostatic	H bond Attraction	H bond Repulsion	Total H bond Energy	Total Energy	Index	VdW Attraction	VdW Repulsion	Total VdW Energy	Electrostatic	H bond Attraction	H bond Repulsion	Total H bond Energy	Total Energy
{202}									{202}	-107.975	65.179	-42.796	-2.367	-167.027	163.365	-3.662	-48.826
{20-2}	-91.009	106.982	15.973	-0.023	-52.241	36.41	-15.831	0.12	{20-2}	-127.49	78.734	-48.756	-3.436	-250.541	245.047	-5.494	-57.686
{111}	-81.999	102.438	20.439	-0.072	-52.239	36.41	-15.829	4.538	{111}	-104.254	65.762	-38.491	-3.382	-250.532	245.046	-5.486	-47.359
{110}	-89.629	118.319	28.69	-0.055	-60.944	42.478	-18.466	10.169	{110}	-108.548	64.235	-44.313	-2.606	-167.029	163.365	-3.664	-50.582
{11-1}	-93.966	121.619	27.653	0.03	-60.946	42.478	-18.468	9.215	{11-1}	-113.991	67.981	-46.009	-2.59	-167.033	163.365	-3.667	-52.267
{102}	-71.62	88.405	16.785	0.013	-43.534	30.342	-13.192	3.606	{102}	-92.21	55.785	-36.424	-2.351	-167.027	163.365	-3.662	-42.438
{100}	-82.86	104.779	21.919	-0.018	-52.241	36.41	-15.831	6.069	{100}	-83.762	51.492	-32.27	-2.29	-167.027	163.365	-3.662	-38.222
{10-2}	-78.678	103.146	24.468	0.075	-52.24	36.41	-15.83	8.713	{10-2}	-110.229	69.933	-40.296	-3.204	-250.539	245.047	-5.492	-48.993
{011}	-77.012	87.192	10.179	-0.08	-43.536	30.342	-13.194	-3.094	{011}	-100.825	59.115	-41.709	-2.595	-167.029	163.365	-3.664	-47.968
{002}	-72.097	101.071	28.974	0.074	-52.24	36.41	-15.83	13.218	{002}	-98.143	61.259	-36.884	-2.769	-208.783	204.206	-4.577	-44.231
{012}	-83.435	105.272	21.837	0.076	-52.243	36.41	-15.833	6.08									

Table 5.5p: Break down of the Gavezzotti field for IBPRAC04 and DFT2

Gavezzotti	IBPRAC04 (Attachment Energy mJ/m²)			Gavezzotti	DFT2 (Attachment Energy mJ/m²)		
Index	VdW Attraction	VdW Repulsion	Total Energy	Index	VdW Attraction	VdW Repulsion	Total Energy
{202}				{202}	-144.316	76.037	-68.278
{20-2}	-115.179	53.441	-61.738	{20-2}	-182.123	98.272	-83.851
{111}	-91.528	37.821	-53.708	{111}	-157.622	87.642	-69.98
{110}	-91.66	37.855	-53.805	{110}	-145.788	75.419	-70.369
{11-1}	-94.302	38.855	-55.447	{11-1}	-151.414	78.311	-73.104
{102}	-82.653	37.43	-45.223	{102}	-129.292	67.964	-61.329
{100}	-76.519	35.568	-40.951	{100}	-120.406	64.695	-55.711
{10-2}	-101.377	50.237	-51.14	{10-2}	-163.383	90.906	-72.477
{011}	-86.11	36.126	-49.985	{011}	-138.538	71.067	-67.471
{002}	-89.37	43.03	-46.339	{002}	-143.274	78.031	-65.243
{012}	-92.199	38.04	-54.159				

Table 5.5q Break down of the Tripos field for IBPRAC04 and DFT2

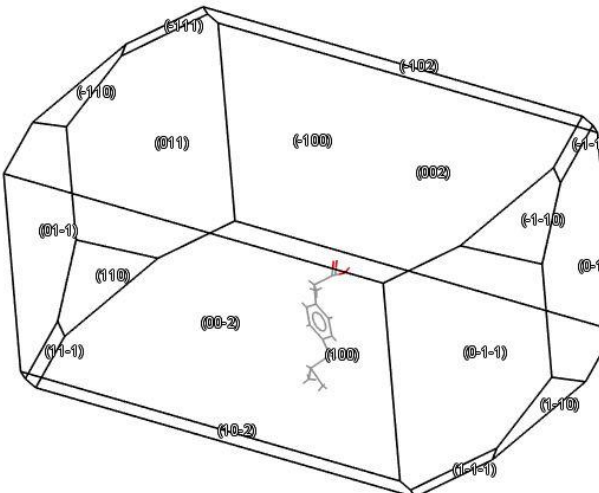
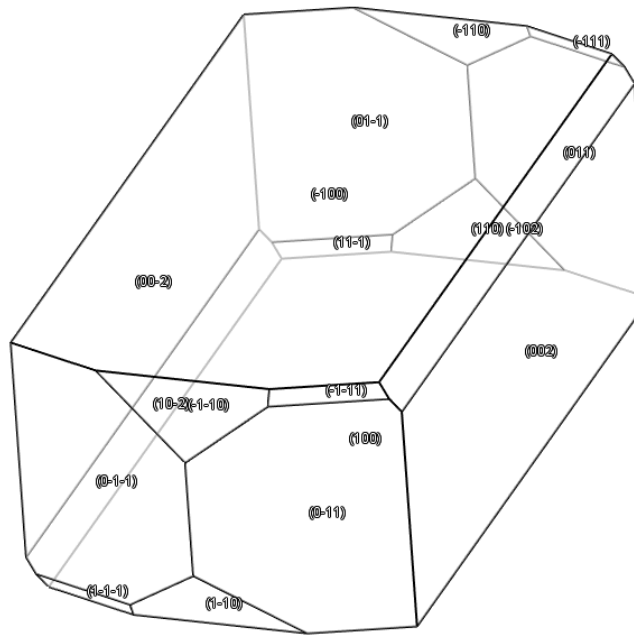
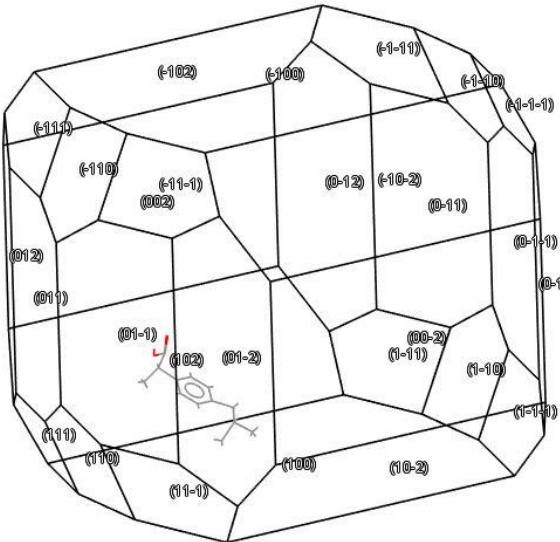
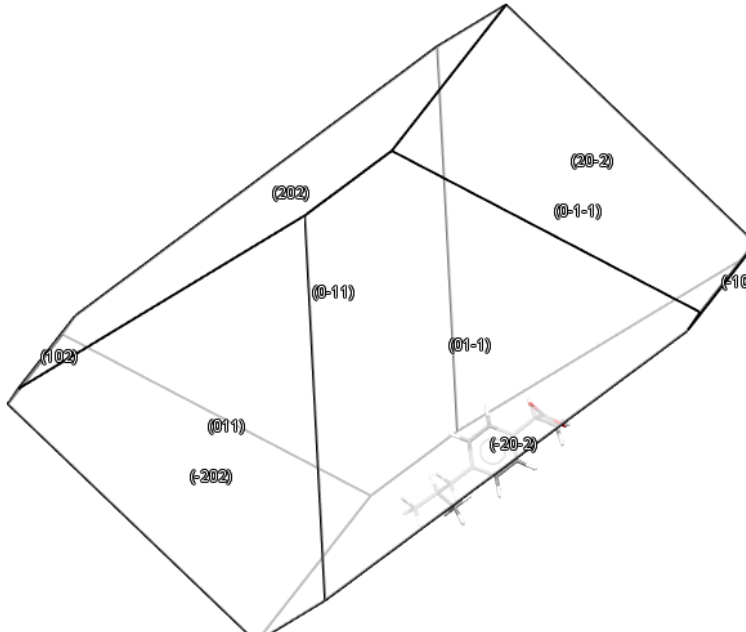
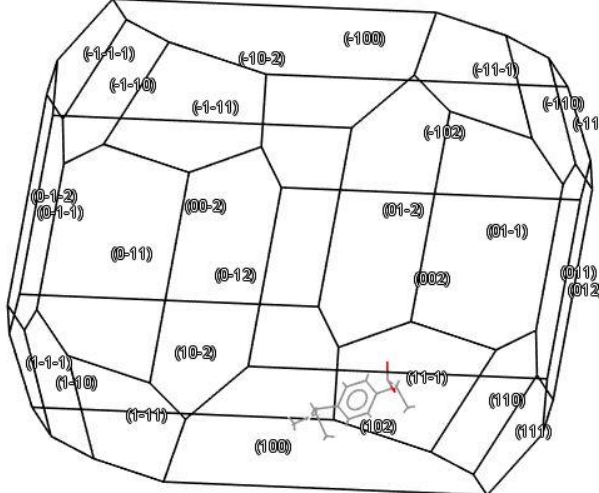
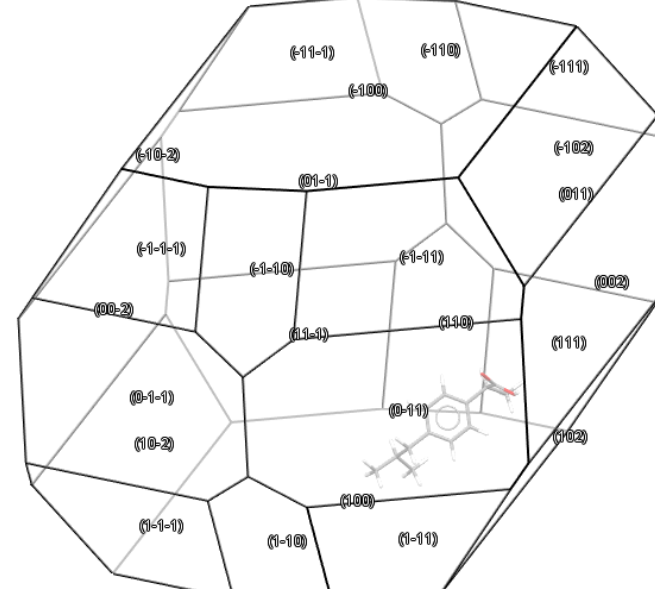
Tripos	IBPRAC04 (Attachment Energy mJ/m²)					Tripos	DFT2 (Attachment Energy mJ/m²)				
Index	VdW Attraction	VdW Repulsion	Total VdW Energy	Electrostatic	Total Energy	Index	VdW Attraction	VdW Repulsion	Total VdW Energy	Electrostatic	Total Energy
{202}						{202}	-115.059	70.717	-44.342	-4.735	-49.076
{20-2}	-94.065	164.824	70.76	-0.046	70.714	{20-2}	-134.017	84.933	-49.083	-6.873	-55.956
{111}	-85.327	160.111	74.784	-0.143	74.641	{111}	-110.515	71.946	-38.569	-6.764	-45.333
{110}	-92.623	185.301	92.678	-0.11	92.569	{110}	-114.711	68.394	-46.317	-5.211	-51.529
{11-1}	-96.937	189.064	92.126	0.06	92.186	{11-1}	-120.222	72.35	-47.872	-5.181	-53.052
{102}	-74.354	137.048	62.694	0.025	62.719	{102}	-97.062	60.268	-36.794	-4.702	-41.496
{100}	-84.911	162.435	77.525	-0.037	77.488	{100}	-87.834	55.449	-32.385	-4.579	-36.965
{10-2}	-81.989	161.296	79.307	0.151	79.458	{10-2}	-116.58	76.623	-39.957	-6.408	-46.365
{011}	-79.347	134.891	55.544	-0.16	55.384	{011}	-105.831	62.371	-43.46	-5.19	-48.65
{002}	-74.535	159.031	84.497	0.148	84.645	{002}	-105.064	69.638	-35.427	-6.406	-41.832
{012}	-86.131	163.424	77.293	0.153	77.446						

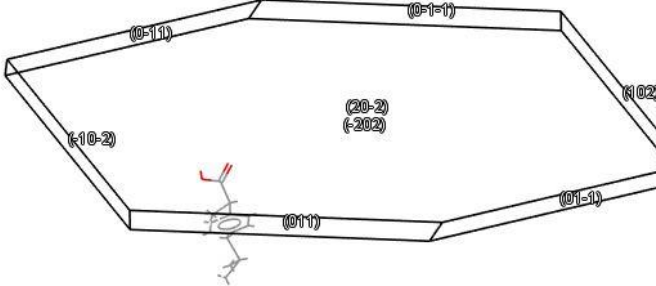
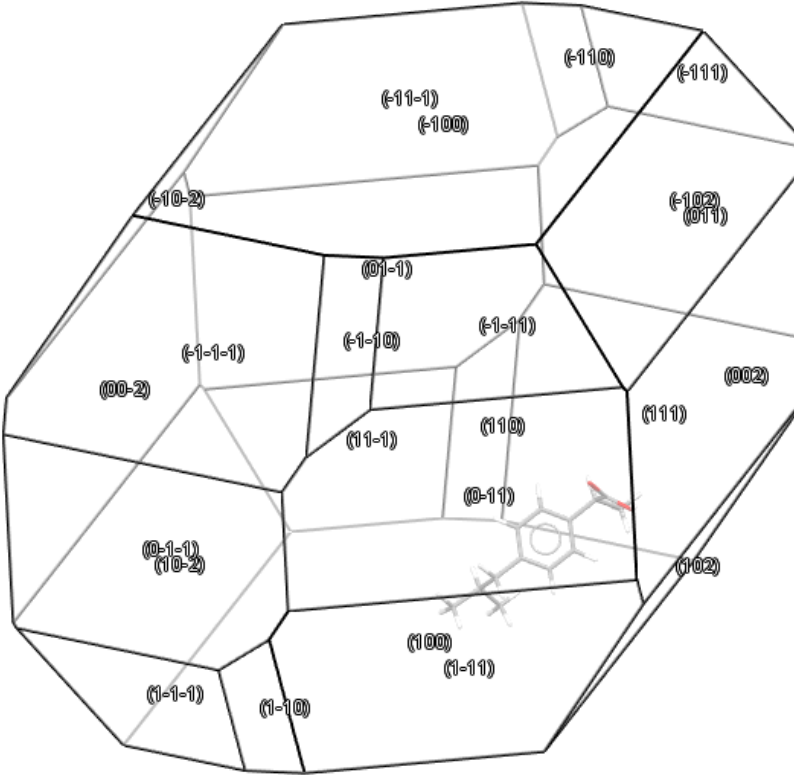
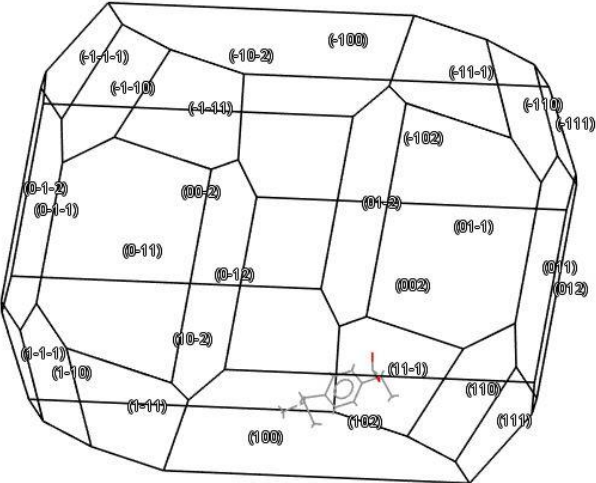
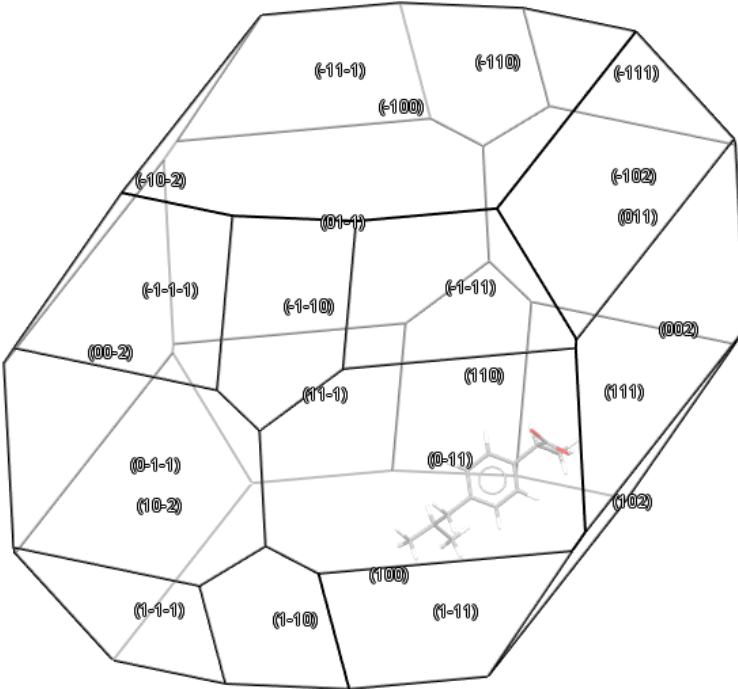
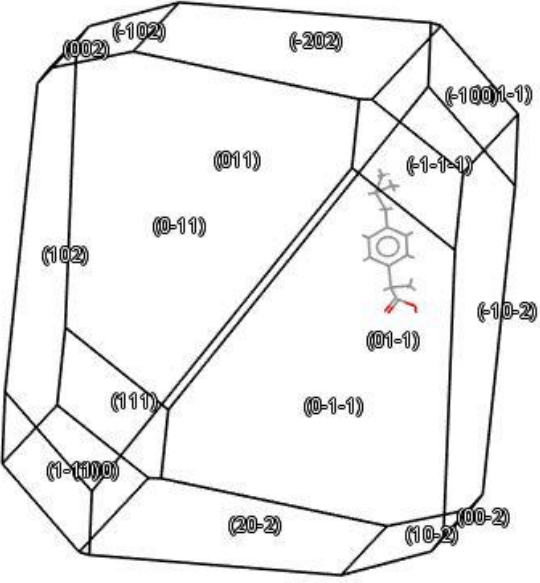
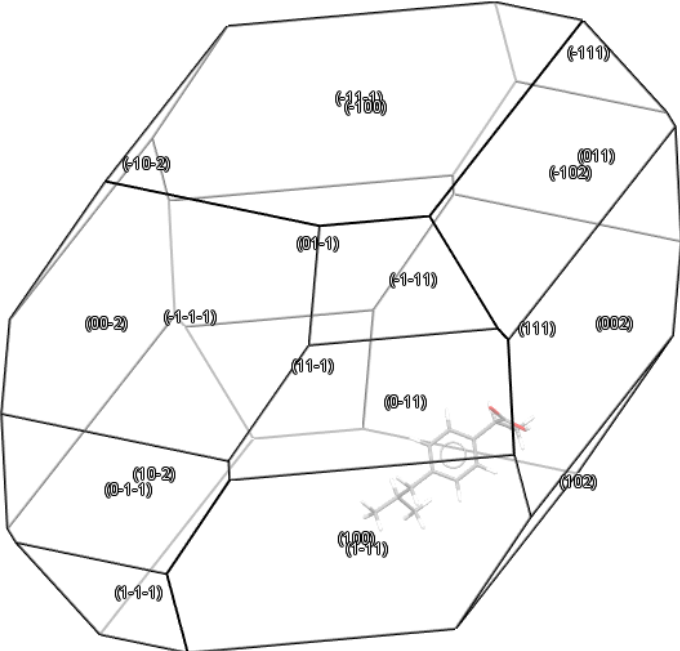
Table 5.5r: Crystal shapes of IBPRAC01 and DFT1

Forcefield d	Polymorph 1 (IBPRAC01)	DFT1
BFDH	<p>A 3D wireframe model of a crystal habit for Polymorph 1 (IBPRAC01) calculated using the BFDH method. The crystal is roughly octahedral with several flat faces. Faces are labeled with Miller indices: (110), (111), (011), (102), (112), (012), (101), (110), (111), (011), (102), (112), (012), (101). A small molecular structure is shown inside the crystal.</p>	<p>A 3D wireframe model of a crystal habit for DFT1 calculated using the BFDH method. The crystal is roughly octahedral with several flat faces. Faces are labeled with Miller indices: (110), (111), (011), (102), (112), (012), (101), (110), (111), (011), (102), (112), (012), (101).</p>
Dreiding II	<p>A 3D wireframe model of a crystal habit for Polymorph 1 (IBPRAC01) calculated using the Dreiding II method. The crystal is roughly octahedral with several flat faces. Faces are labeled with Miller indices: (110), (111), (011), (102), (112), (012), (101), (110), (111), (011), (102), (112), (012), (101). A small molecular structure is shown inside the crystal.</p>	<p>A 3D wireframe model of a crystal habit for DFT1 calculated using the Dreiding II method. The crystal is a long, thin prism. Faces are labeled with Miller indices: (110), (111), (011), (102), (112), (012), (101), (110), (111), (011), (102), (112), (012), (101).</p>
Dreiding II Mod	<p>A 3D wireframe model of a crystal habit for Polymorph 1 (IBPRAC01) calculated using the Dreiding II Mod method. The crystal is roughly octahedral with several flat faces. Faces are labeled with Miller indices: (110), (111), (011), (102), (112), (012), (101), (110), (111), (011), (102), (112), (012), (101). A small molecular structure is shown inside the crystal.</p>	<p>A 3D wireframe model of a crystal habit for DFT1 calculated using the Dreiding II Mod method. The crystal is roughly octahedral with several flat faces. Faces are labeled with Miller indices: (110), (111), (011), (102), (112), (012), (101), (110), (111), (011), (102), (112), (012), (101).</p>

	IBPRAC01	DFT1
Momany		
Gavezzotti		
Tripes 5.2		

Table 5.5s: Crystal shapes of IBPRAC04 and DFT2

Forcefield	Polymorph 2 (IBPRAC04)	DFT2
BFDH		
Dreiding II		
Dreiding II Mod		

Forcefields	IBPRAC04	DFT2
Momany		
Gavezzotti		
Triplos 5.2		

5.5e Polymorph comparison for DFT molecules

CASTEP predicted that form II would have lattice energy which was 18.9kJ/mol higher relative to form I. Table 5.5t shows that this was not the case for any of the five fields that were used in the analysis. Instead, it showed that the two polymorphs had a relative lattice energy difference of 13kJ/mol, ignoring the positive value for Dreiding II. The differences between the two DFT forms was more consistent than the differences between the original molecules, table 5.5u, where the differences varied significantly. Therefore DFT can be used when the relative difference between two forms needs to be quantified since the differences are more consistent across the DFT molecules when compared to the differences in the original molecule.

Table 5.5t: Lattice energies for the two DFT molecules and the difference (positive lattice energies shown in red)

Forcefield	DFT1	DFT2	Difference (Form I -Form II)
Dreiding II Mod	-95.015	-84.879	-10.136
Dreiding II	6.574	39.442	-32.868
Momany	-92.301	-75.461	-16.840
Gavezzotti	-121.895	-110.266	-11.629
Tripos 5.2	-85.522	-72.98	-12.542

Table5.5u: Lattice energies for the two original molecules and the difference (positive lattice energies shown in red)

Forcefield	IBPRAC01	IBPRAC04	Difference
Dreiding II Mod	-115.861	-87.501	-28.36
Dreiding II	-69.194	-68.056	-1.138
Momany	-112.144	1.634	-113.778
Gavezzotti	-126.588	-80.776	-45.812
Tripos 5.2	-98.73	95.928	-194.658

5.6 X-Ray Diffraction

The XRD spectrum, Figure 5.6a, showed many peaks, most of which were too small to identify any material other than ibuprofen. This was because their concentrations were so low. After all, it was not the API.

The XRD spectrum for the commercial tablet was compared against the ICDD database (ICDD, 1984). The peak list provided in the database was compared with the spectrum that was obtained. This revealed that ibuprofen was indeed present in the tablet, as expected. The 2θ angle was found for the faces shown in the crystal morphology and these are shown in Figure 5.6a, along with the highest peaks. However, not all the faces shown in the crystal morphology were observed in the spectrum. Faces $\{111\}$, $\{10-2\}$ and $\{002\}$ did not have values for 2θ in the database. Whereas faces $\{012\}$ and $\{202\}$ were significant peaks in the spectrum but did not appear in the crystal morphology.

5.6a Evaluating Mercury XRD

The XRD plot for IBPRAC04 was superimposed onto the data from the literature, Figure 5.6b. The data was normalised to achieve a maximum value of one; this also allowed for easier comparison. The two plots were virtually identical, with the same peaks at the same intensity in the same position. They only differed in the minimum value; the Mercury plot had a minimum value of zero, whilst the data from the literature had a normalised minimum value of 0.0118. This difference was determined to be insignificant, as the peaks were concordant, therefore the Mercury XRD function was deemed adequate for further analysis.

5.6b XRD analysis of polymorph 1

The initial analysis of polymorph one was conducted using DFT1 reflected the findings of the lattice energy breakdown; there was no change in the planes present. The two XRD patterns, Figure 5.6c, had the same peaks, although the peaks produced by DFT1 were slightly shifted; this was attributed to the overall change in the unit cell of the molecule, which had decreased in volume. However not all peaks were shifted, the $\{210\}$ peak was not shifted instead the intensity decreased slightly.

Two variations of commercial ibuprofen tablets were used, Galpharm Ibuprofen and Tesco fast action. Although there was noise present in both XRD patterns, figure 5.6d, the peaks were easily identifiable. The experimental XRD patterns could not capture the initial peak at 6° since readings were only taken after 10° . There were more peaks present in both the experimental peaks; these were ascribed to the additional ingredients present in both. These additional peaks in the experimental XRDs were also comparable, indicating that they had common ingredients.

5.6c XRD analysis of polymorph 2

As with polymorph one, the XRD analysis reflected the findings of the lattice energy breakdown. There was less similarity between DFT2 and IBPRAC04 than in polymorph one, with only a handful of peaks sharing the same location and intensity, Figure 5.6e. The different peaks were due to different planes present; in DFT2 the $\{202\}$ plane was present whilst $\{012\}$ was present in IBPRAC04 instead. Several peaks in the $25-30^\circ$ appeared to have shifted and increased in intensity. This change was greater than the shift observed in polymorph one since the change in the unit cell was greater in polymorph two than in polymorph one.

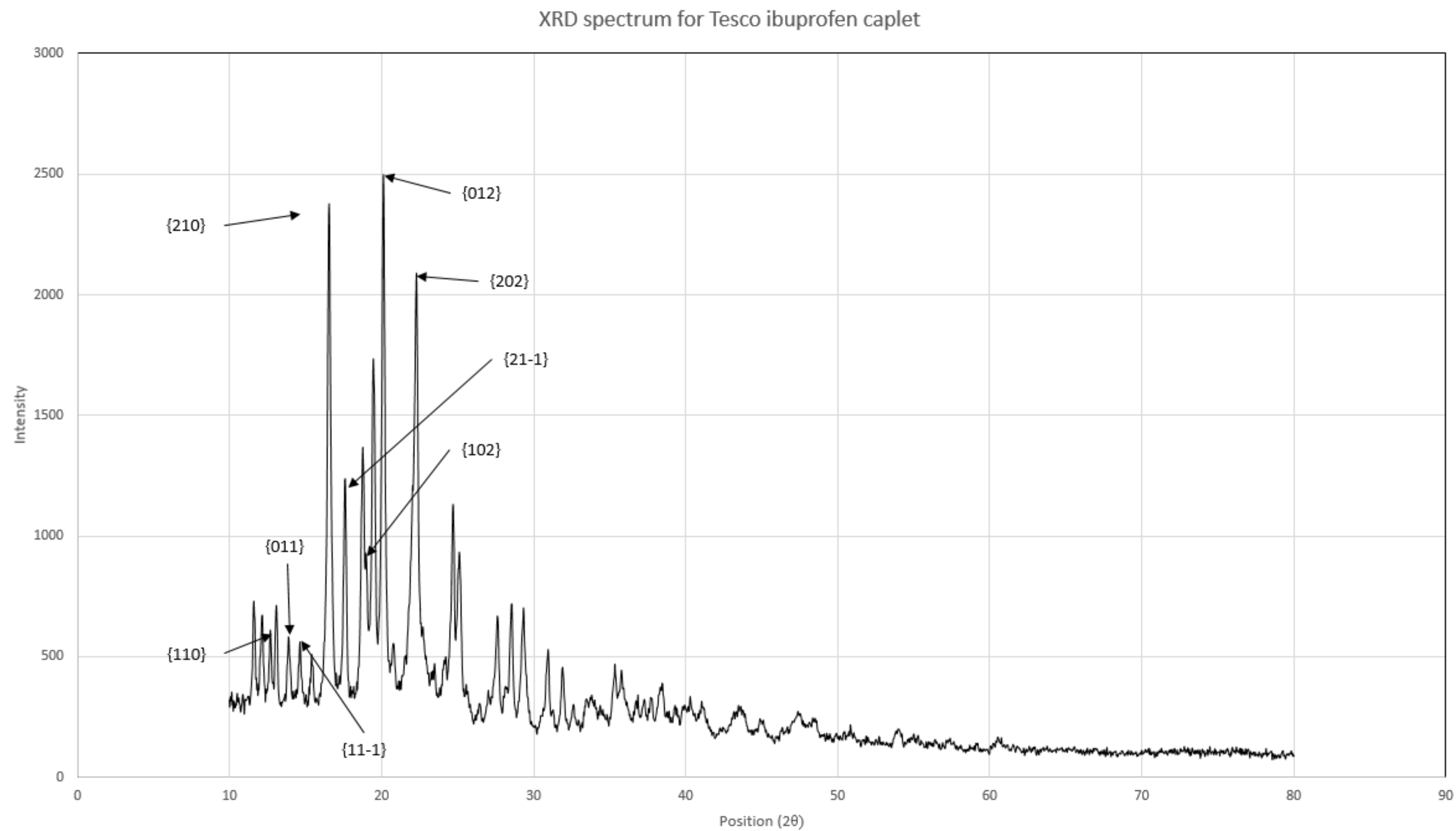


Figure 5.6a: XRD spectrum for Tesco ibuprofen tablet

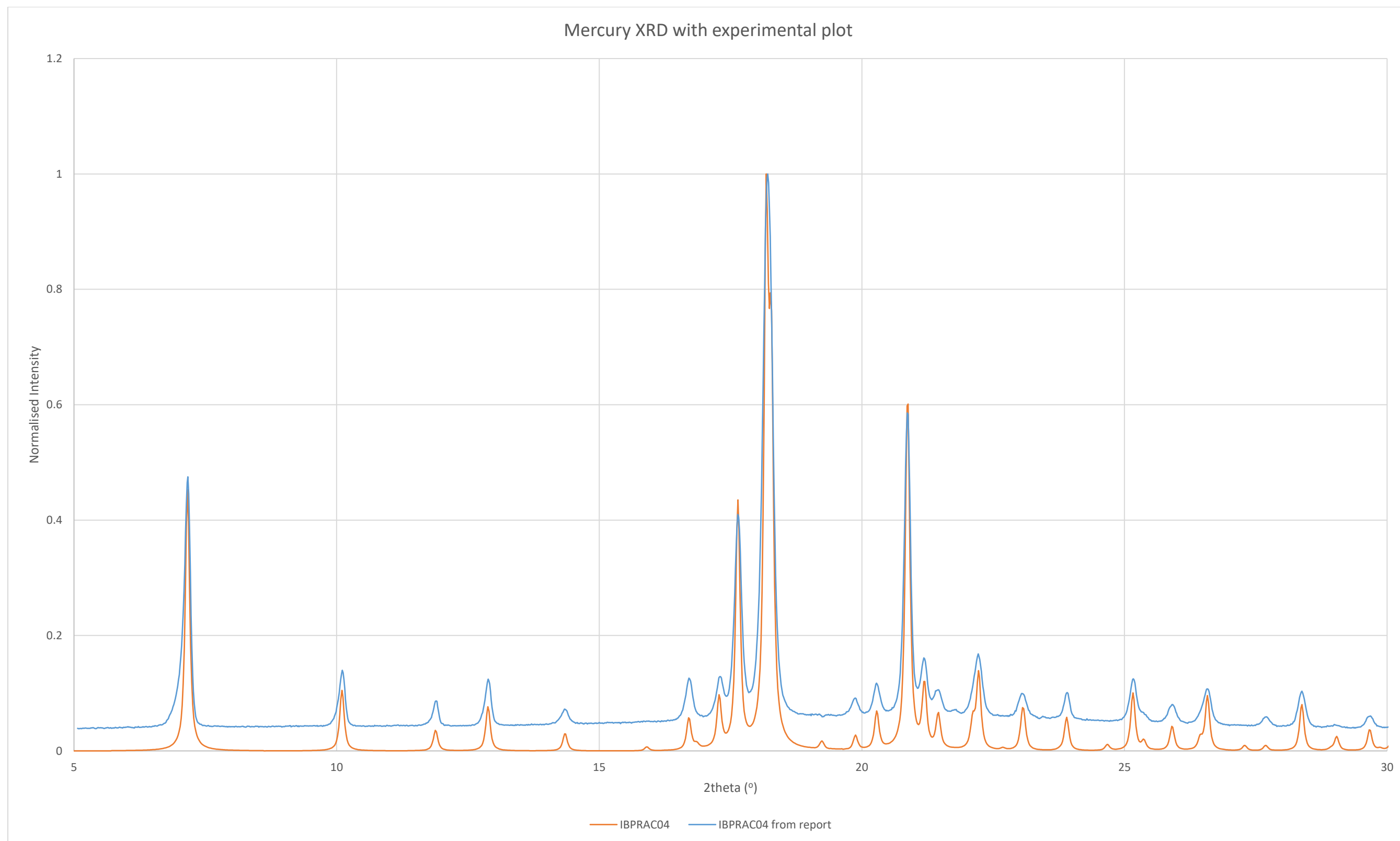


Figure 5.6b: Comparison of Mercury XRD function with raw data form report

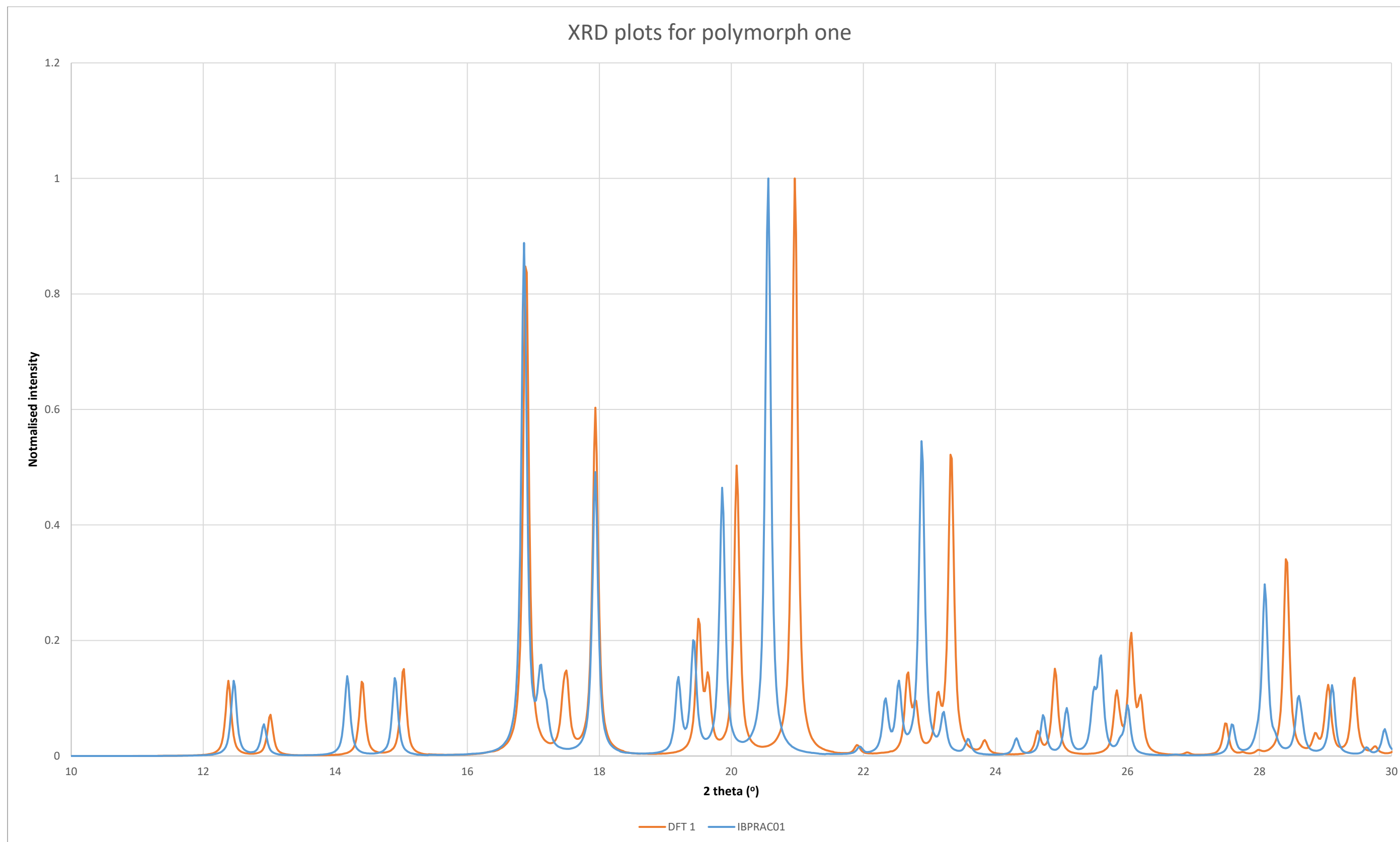


Figure 5.6c: XRD patterns of IBPRAC01 and DFT1 (Obtained from Mercury)

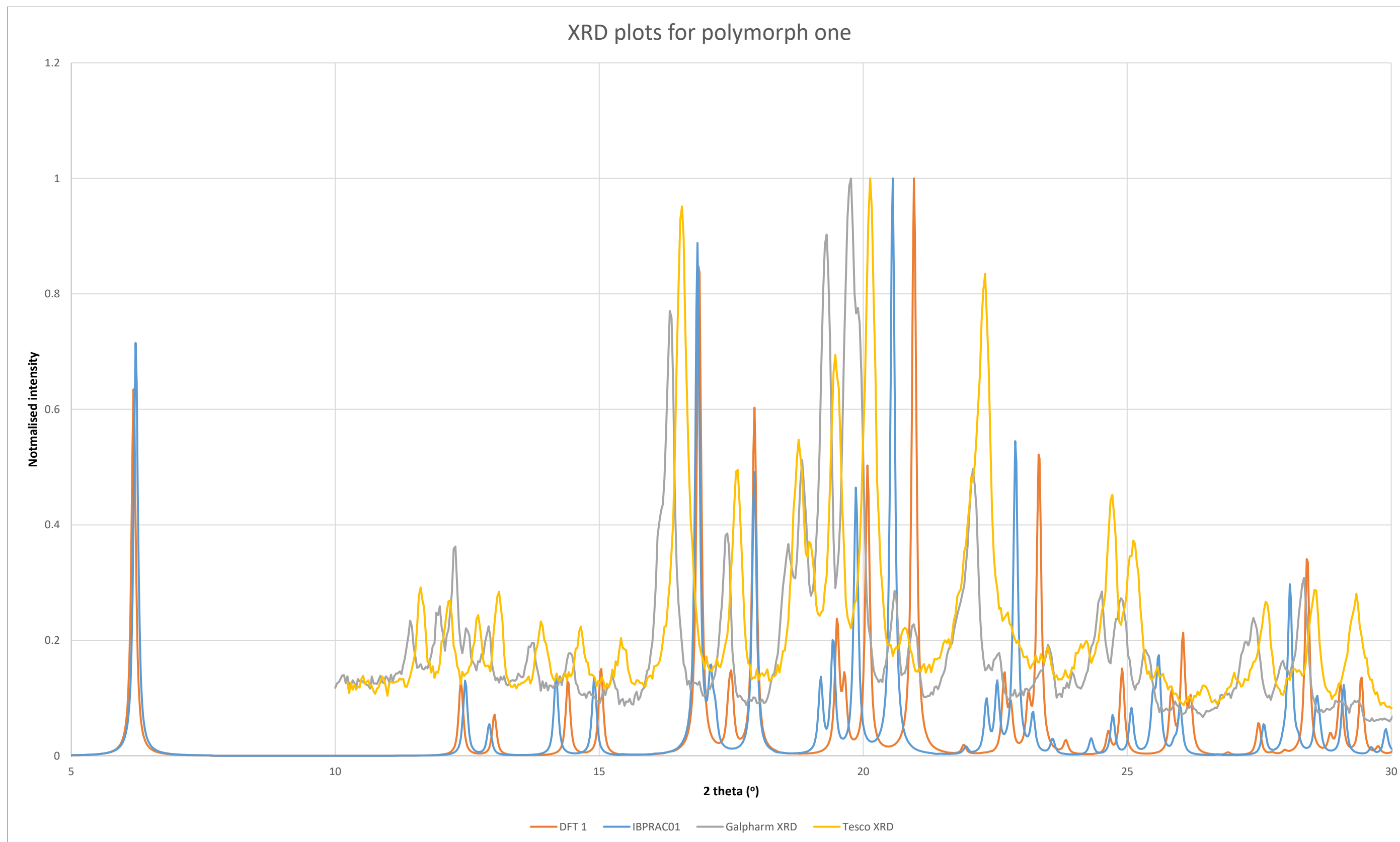


Figure 5.6d: XRD patterns of IBPRAC01 and DFT1 (Obtained from Mercury) and Experimental XRD plots

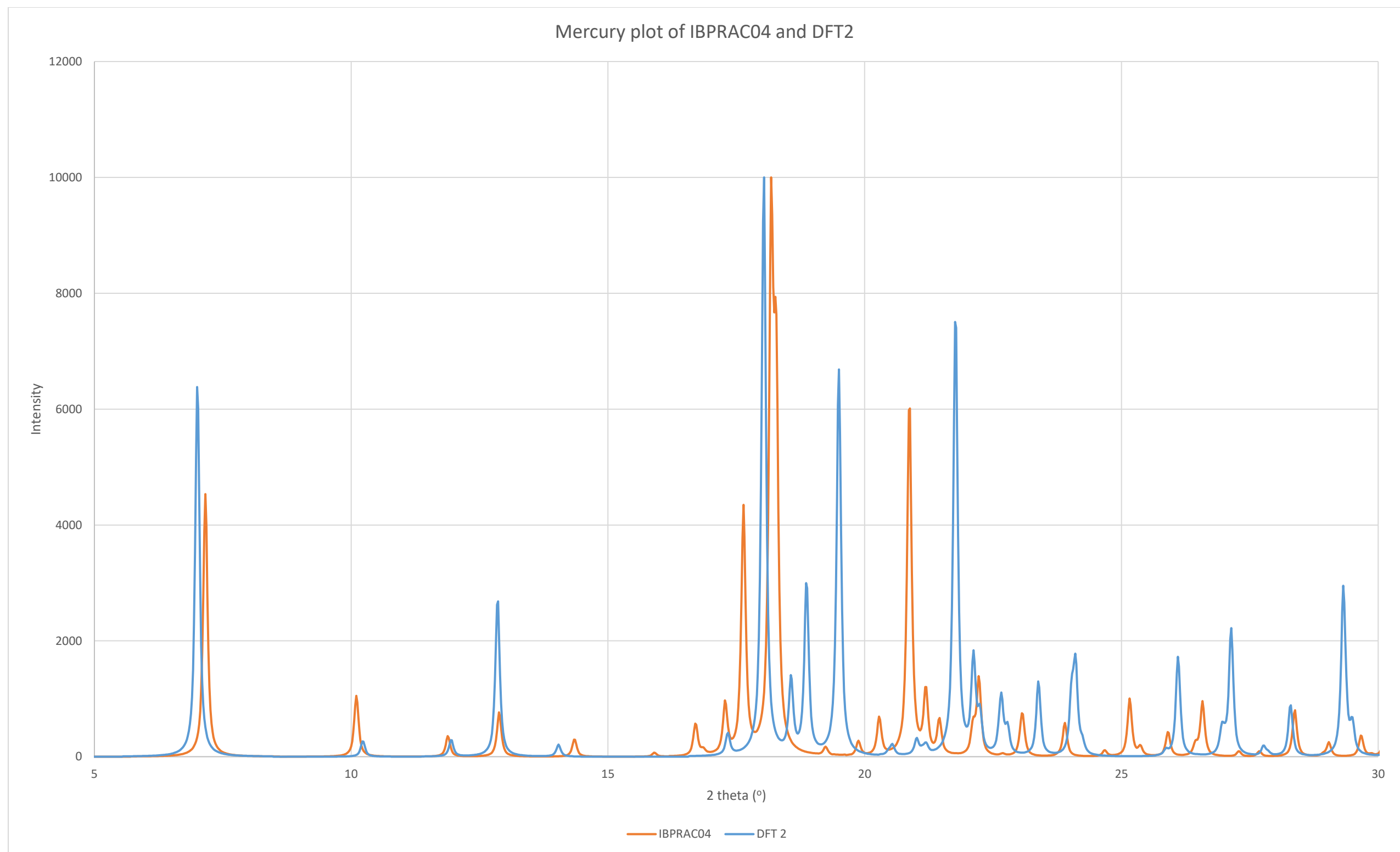


Figure 5.6e: Comparison of XRD plots for form II (

6. Conclusion

The main aim of the report was to use molecular mechanics to predict the stability of the different polymorphs of ibuprofen. The objectives were to evaluate the accuracy of molecular to predict the lattice energy, by comparing the value with sublimation enthalpy, compare the different forcefields and finally to determine the best conditions that a molecule must be obtained under to ensure the best quality of results.

The two polymorphs of ibuprofen had a clear difference in lattice energy, with lattice energy of polymorph one consistently having more negative lattice energy, even when the forcefield was adjusted. The Dreiding II Mod, Momany, Gavezzotti and Tripos 5.2 fields provided lattice energies similar to the sublimation energy for polymorph one. These fields, however, differed significantly for form II; with both Momany and Tripos fields providing positive values for the total lattice energy; found to as a result of the calculation of the Van der Waals repulsive force. There were instances when the lattice energy of polymorph one was more negative but was very close such as the lattice energies generated through the Dreiding II forcefield, which showed a difference of 1kJ/mol between the polymorphs, the breakdown of the forcefield revealed that the Dreiding II overestimated the Van der Waals repulsion when compared with the Dreiding II Mod forcefield. The Govers forcefields produced results that were considerably different and therefore deemed inaccurate. This was shown in the crystal morphologies. The three most accurate forcefields produced similar crystal morphologies. The other forcefields such as Dreiding II and Tripos were similar to the accurate three, they did not have the same degree of unity.

DFT produced accurate molecules with similar lattice energies and crystal shapes to the original crystal. The molecule produced for form I was more similar to the original molecule than the molecule produced for form II, indicating that IBPRAC01, the original molecule for DFT1, was close to the minimum energy for a unit cell. The change to the unit cells was reflected in the XRD plots. The unit cell in form I did not experience much change the peaks followed suit, they were of a similar size and similar location. However, the unit cell for Form II experienced greater change, as a result, there was greater inconsistency in the XRD for Form II. All four fields become consistent when calculating the lattice energy of the DFT molecules; all four fields providing negative lattice energies. Therefore, Dreiding II Mod and Gavezzotti were the most consistent when providing a lattice energy, since they consistently produced comparable values. However, it was noted that Gavezzotti field only considered the VdW energy, therefore it may not be accurate in molecules where the hydrogen bonding is a significant factor. DFT would not be necessary or cost-effective if the sole purpose were to determine which polymorph was more stable since this can be achieved using forcefields. However, DFT is essential if the aim were to quantify the difference between the two molecules since the differences obtained from DFT were more consistent.

The analysis of criteria for the best molecule showed that there are several main criteria for identifying the highest quality material: temperature, pressure, chirality, radiation probe and the type of sample. Low temperature and low pressure were preferable since it would mean that the location of the molecules would be more easily identifiable leading to a more accurate result. The lattice energy was more sensitive to extreme changes in pressure than temperature. The chirality was not a significant issue within the context of ibuprofen due to the small branched chains from the chiral centre; however, this may not be the case when the branched

chains are larger and are a bigger factor when determining the structure. It was preferable to have a neutron probe with single-crystal since this would provide the most accurate location for all the atoms including the hydrogens.

Future work

A combination of experimental and modelling experiments can be carried out to continue from this research. Ibuprofen can be formed in different solvents, eg. Periodic concentrations of ethanol/water. These crystals can then be examined under a scanning electron microscope to examine the crystal morphology. The lattice energies of these crystals can also be calculated to evaluate the effect of the solvent on the lattice energy.

Several modelling experiments can be carried out. These include using other software such as Materials Studio and other forcefields to compare the difference in the values. The second task focuses on the bond lengths, the carbon-hydrogen bond lengths were fixed values in the X-Ray molecules. These bond lengths can be adjusted, to match the length of the carbon-hydrogen bonds in neutron diffraction and increasing the distance by periodic factors ($\pm 10, 20, 50\%$) to measure the effect of the bond lengths on the overall lattice energy. DFT can be used on all the available molecules to assess if there were any local minima for the unit cell.

References

- Aaltonen, J.; Allesø, M.; Mirza, S.; Koradia, V.; Gordon, K. C.; Rantanen, J. 2009 Solid form screening – A review. *Eur. J. Pharm. Biopharm.* **71** (1), 23–37
- Bladon, P., Gorton, J., and Hammond, R.B. 2012. *Molecular modelling computational chemistry demystified*. Cambridge: Royal Society of Chemistry.
- Clark, M., Cramer, R.D. and Vanopdenbosch, N. 1989. Validation of the general-purpose tripos 5.2 force-field. *J Comput Chem* **10**(8):982–1012
- Clark, S.J., Segall, M.D., Pickard, C.J., Hasnip, P.J., Probert, M.I., Refson, K. and Payne, M.C., 2005. First principles methods using CASTEP. *Zeitschrift für Kristallographie-Crystalline Materials*, **220**(5/6), pp.567-570.
- Clydesdale G., Roberts K.J. and Docherty R. 1996. HABIT95 – a program for predicting the morphology of molecular crystals as a function of the growth environment. *J Cryst Growth* **166**(1–4):78–83
- Dearden, L. 2015. Martin Shkreli: Pharmaceuticals CEO who raised HIV drug price by 5,000% 'also hiked cost of pill taken by children with incurable kidney disease'. *Independent*. [Online] 23/09/2015 [Date accessed: 30/11/2019] Available from: <https://www.independent.co.uk/news/people/martin-shkreli-pharmaceuticals-ceo-who-raised-hiv-drug-price-by-5000-also-hiked-cost-of-pill-taken-10513645.html>
- Derollez, P. Dudognon, E. Affouard, F., Danede D, Correia, N.T. and Descamps, M. 2010. Ab initio structure determination of phase II of racemic ibuprofen by X-ray powder diffraction. *Acta Cryst. B.* **66**, 76-80
- Dudognon, E., Danède, F., Descamps, M., & Correia, N. 2008. Evidence for a New Crystalline Phase of Racemic Ibuprofen. *Pharmaceutical Research*, **25**(12), 2853–2858.
- Engler, E. M., Andose, J. D. & Schleyer, P. V. R. 1973. Critical evaluation of molecular mechanics. *Journal of the American Chemical Society*, **95**, 8005-8025
- Evans, A. 2001. Comparative pharmacology of S(+)-ibuprofen and (RS)-ibuprofen. *Clinical Rheumatology*, **20 Suppl 1**, S9–14.
- Franks, M.E., Macpherson, G.R., Figg, W.D. 2004. Thalidomide. *The Lancet*. **363**(9423) pp 1802-1811.
- Gangolli S. 2005. ibuprofen. In *Dictionary of Substances and Their Effects* (DOSE, 3rd Electronic Edition, pp. 1–1).
- Gavezzotti, A. 1998 The crystal packing of organic molecules: challenge and fascination below 1000 Da. *Crystallogr Rev* **7**(1):5–121
- Hammond, R.B. 2019. *Molecular Mechanics*. Lecture notes distributed in CAPE5320 Multiscale modelling and simulations. 07/10/19 School of Chemical and Process Engineering
- Hammond, R.B. 2017. Modelling Route Map: From Molecule Through the Solution State to Crystals. In: Roberts, K.J., Docherty, R., and Tamura, R. *Engineering Crystallography: From*

Molecule to Crystal to Functional Form. NATO Science for Peace and Security Series A: Chemistry and Biology. pp71-108

Harris, J. 2005. It's not NICE to discriminate. *Journal of Medical Ethics*. **31** (7), 373–375

Hooper, D., Clarke, F., Docherty, R., Mitchell, J., & Snowden, M. 2017. Effects of crystal habit on the sticking propensity of ibuprofen—A case study. *International Journal of Pharmaceutics*, *531*(1), 266–275

ICDD. 1984. Ibuprofen.

J.F.McConnell, 1974. *Crystal Structure Communications*. **3**(73)

Karamertzanis, P. G. & Pantelides, P. C. 2005. Ab initio crystal structure prediction—I. Rigid molecules. *Journal of computational chemistry*, *26*, 304-324

Kohn, W. and Sham, L.J., 1965. Self-consistent equations including exchange and correlation effects. *Physical review*, *140*(4A), p.A1133.

Kohn, W. and Sham, L.J., 1965. Self-consistent equations including exchange and correlation effects. *Physical review*, *140*(4A), p.A1133

Lopes, P.E., Guvench, O. and MacKerell, A.D., 2015. Current status of protein force fields for molecular dynamics simulations. In *Molecular modeling of proteins* (pp. 47-71). Humana Press, New York, NY.

MacLeod, C. S.; Muller, F. L. 2012 On the Fracture of Pharmaceutical Needle-Shaped Crystals during Pressure Filtration: Case Studies and Mechanistic Understanding. *Org. Process Res. Dev.* **16** (3), 425– 434.

Mayo S.L., Olafson B.D., Goddard W.A. 1990. Dreiding – a generic force-field for molecular simulations. *J Phys Chem* **94**(26):8897–8909

Momany F.A., Carruth L.M., McGuire R.F., Scheraga H.A. (1974) Intermolecular potentials from crystal data .3. Determination of empirical potentials and application to packing configurations and lattice energies in crystals of hydrocarbons, carboxylic-acids, amines, and amides. *J Phys Chem* **78**(16):1595–1620

National Toxicology Program, Institute of Environmental Health Sciences, National Institutes of Health (NTP). 1992. National Toxicology Program Chemical Repository Database. Research Triangle Park, North Carolina: NTP

O'Neil, M.J. (ed.). 2001. *The Merck Index - An Encyclopedia of Chemicals, Drugs, and Biologicals*. 13th Edition, Whitehouse Station, NJ: Merck and Co., Inc., p. 876

Osol, A. (ed.). 1981. Remington's Pharmaceutical Sciences. 16th ed. Easton, Pennsylvania: Mack Publishing Co, p. 1057

Ostrowska, K., Kropidłowska, M. and Katrusiak, A., 2015. High-pressure crystallization and structural transformations in compressed R, S-ibuprofen. *Crystal Growth & Design*, *15*(3), pp.1512-1517.

- Payne, M.C., Teter, M.P., Allan, D.C., Arias, T.A. and Joannopoulos, A.J., 1992. Iterative minimization techniques for ab initio total-energy calculations: molecular dynamics and conjugate gradients. *Reviews of modern physics*, **64**(4), p.1045.
- PhMRA. 2015. *Biopharmaceutical research and development: The process behind new medicine*. [Online] [Accessed on 08/12/19] Available from: http://phrma-docs.phrma.org/sites/default/files/pdf/rd_brochure_022307.pdf
- Pickering J., Hammond R.B., Ramachandran V., Soufian M., Roberts K.J. 2017. Synthonic Engineering Modelling Tools for Product and Process Design. In: Roberts K., Docherty R., Tamura R. (eds) *Engineering Crystallography: From Molecule to Crystal to Functional Form*. NATO Science for Peace and Security Series A: Chemistry and Biology. Springer, Dordrecht
- Pickering J., Hammond, R.B., Ramachandran, V., Soufina, M. and Roberts, K.J. 2017. Synthonic Engineering Modelling Tools for Product and Process Design. In: Roberts, K.J., Docherty, R., and Tamura, R. *Engineering Crystallography: From Molecule to Crystal to Functional Form*. NATO Science for Peace and Security Series A: Chemistry and Biology. Pp 155-176
- Rappé, A.K., Casewit, C.J., Colwell, K.S., Goddard III, W.A. and Skiff, W.M., 1992. UFF, a full periodic table force field for molecular mechanics and molecular dynamics simulations. *Journal of the American chemical society*, **114**(25), pp.10024-10035.
- Rosbottom, I. and Roberts K. J. 2017. Crystal Growth and Morphology of Molecular Crystals. In: Roberts, K.J., Docherty, R., and Tamura, R. *Engineering Crystallography: From Molecule to Crystal to Functional Form*. NATO Science for Peace and Security Series A: Chemistry and Biology. Pp109-131
- Rosbottom, I., Ma, C.Y., Turner, T.D., O'Connell, R.A., Loughrey, J., Sadiq, G., Davey, R.J. and Roberts, K.J., 2017. Influence of solvent composition on the crystal morphology and structure of p-Aminobenzoic acid crystallized from mixed ethanol and nitromethane solutions. *Crystal Growth & Design*, **17**(8), pp.4151-4161.
- Shankland, N., Florence, A.J., Cox, P.J., Sheen, D.B., Love, S.W., Stewart, N.S. and Wilson C.C. 1996 CCDC 128796: Experimental Crystal Structure Determination
- Sidahmed, M. 2016. Martin Shkreli: I'm not upset about HIV drug hike; it was 'woefully underpriced'. *The Guardian*. [Online] 28/10/2016 [Date accessed: 30/11/2019] Available from: <https://www.theguardian.com/business/2016/oct/28/martin-shkreli-daraprim-hiv-drug-price-hike-interview>
- Williams, D.E .1966. Nonbonded potential parameters derived from crystalline aromatic hydrocarbons. *J Chem Phys* **45**(10):3770
- Yalkowsky, S.H. and Dannenfelser, R.M. 1992. The Aquasol Database of aqueous solubility. Ver 5. Tucson, AZ: University of Arizona, College of pharmacy.

Zimmermann, B. and Baranovic, G. 2011. Thermal analysis pf paracetamol polymorphs by FT-IR spectroscopies. *Journal of Pharmaceutical and Biomedical Analysis* **54** (2011) 295–302

.

Appendix

Appendix A: Atom energies for a single molecule of IBPRAC04 and DFT2 Mod in the Dreiding II field (Hydrogen bonding atoms shown in red)

Atom	Element	IBPRAC04 Dreiding II								DFT2 Dreiding II							
		VdW Attraction	VdW Repulsion	Total VdW Energy	Electros tatic	H bond Attraction	H bond Repulsio n	Total H bond Energy	Total Energy	VdW Attraction	VdW Repulsion	Total VdW Energy	Electrostat ic	H bond Attraction	H bond Repulsion	Total H bond Energy	Total Energy
C1	C	-9.913	4.225	-5.688	8.077	0	0	0	2.389	-13.228	6.76	-6.469	6.388	0	0	0	-0.081
C2	C	-6.905	1.345	-5.56	0.827	0	0	0	-4.733	-8.371	1.504	-6.867	0.483	0	0	0	-6.383
C3	C	-9.234	3.782	-5.453	-0.305	0	0	0	-5.757	-13.993	6.836	-7.157	0.047	0	0	0	-7.109
C4	C	-5.595	0.519	-5.076	-0.399	0	0	0	-5.475	-7.222	1.34	-5.883	-0.285	0	0	0	-6.167
C5	C	-5.819	1.025	-4.794	-0.431	0	0	0	-5.225	-9.481	8.761	-0.72	-0.302	0	0	0	-1.023
C6	C	-6.287	1.66	-4.627	-0.169	0	0	0	-4.796	-9.325	6.738	-2.587	-0.07	0	0	0	-2.657
C7	C	-5.458	0.54	-4.918	0.054	0	0	0	-4.864	-6.943	1.078	-5.865	0.165	0	0	0	-5.701
C8	C	-9.567	5.393	-4.174	-0.238	0	0	0	-4.412	-10.374	4.167	-6.207	-0.107	0	0	0	-6.314
C9	C	-9.016	3.978	-5.037	-0.722	0	0	0	-5.759	-9.868	3.414	-6.454	-0.569	0	0	0	-7.024
C10	C	-6.381	1.039	-5.342	0.272	0	0	0	-5.069	-7.442	1.259	-6.183	0.318	0	0	0	-5.865
C11	C	-5.737	1.11	-4.627	0.474	0	0	0	-4.153	-7.121	1.696	-5.425	0.407	0	0	0	-5.018
C12	C	-6.656	1.268	-5.388	0.63	0	0	0	-4.758	-10.011	3.973	-6.038	0.487	0	0	0	-5.551
C13	C	-6.71	1.411	-5.299	0.314	0	0	0	-4.985	-10.08	5.16	-4.92	0.254	0	0	0	-4.666
O1	O	-10.81	8.995	-1.815	-11.414	-12.541	7.035	-5.506	-18.736	-15.548	16.987	1.439	-3.577	-2.256	1.122	-1.134	-3.272
O2	O	-13.514	28.422	14.908	-7.462	-67.98	58.719	-9.262	-1.816	-18.277	143.313	125.037	-11.99	-343.344	327.538	-15.806	97.241
H1	H	-1.654	22	20.347	11.321	-80.521	65.753	-14.768	16.9	-3.178	127.575	124.398	-6.133	-345.6	328.659	-16.94	101.325
H2	H	-3.481	4.874	1.393	0.502	0	0	0	1.896	-3.524	3.85	0.326	0.22	0	0	0	0.547
H3	H	-4.312	8.613	4.302	0.183	0	0	0	4.485	-5.046	3.308	-1.738	0.015	0	0	0	-1.722
H4	H	-2.039	0.378	-1.661	0.087	0	0	0	-1.574	-6.03	11.663	5.633	-0.003	0	0	0	5.63
H5	H	-2.949	0.925	-2.024	0.064	0	0	0	-1.959	-6.134	11.786	5.652	-0.216	0	0	0	5.436
H6	H	-1.734	0.337	-1.397	0.375	0	0	0	-1.022	-3.027	1.485	-1.542	0.213	0	0	0	-1.329
H7	H	-2.569	2.173	-0.395	0.03	0	0	0	-0.365	-4.026	5.786	1.76	-0.091	0	0	0	1.67
H8	H	-4.389	4.828	0.439	-0.175	0	0	0	0.264	-5.484	7.067	1.583	-0.322	0	0	0	1.261
H9	H	-3.537	2.554	-0.983	0.932	0	0	0	-0.052	-3.947	2.361	-1.586	0.697	0	0	0	-0.889
H10	H	-2.579	1.498	-1.08	-0.607	0	0	0	-1.687	-2.873	1.059	-1.815	-0.642	0	0	0	-2.456
H11	H	-1.975	0.501	-1.475	-0.3	0	0	0	-1.775	-2.867	1.573	-1.293	-0.407	0	0	0	-1.7
H12	H	-2.861	5.16	2.3	-0.473	0	0	0	1.826	-2.973	4.816	1.843	-0.389	0	0	0	1.454
H13	H	-2.585	2.192	-0.394	-0.153	0	0	0	-0.546	-3.814	3.699	-0.116	-0.131	0	0	0	-0.246
H14	H	-1.835	0.343	-1.492	-0.183	0	0	0	-1.675	-3.581	3.255	-0.326	-0.092	0	0	0	-0.418
H15	H	-1.856	0.275	-1.581	-0.362	0	0	0	-1.943	-3.248	1.781	-1.466	-0.288	0	0	0	-1.755
H16	H	-2.064	0.566	-1.498	-0.087	0	0	0	-1.585	-3.809	4.285	0.476	-0.023	0	0	0	0.453
H17	H	-2.097	0.692	-1.406	-0.126	0	0	0	-1.531	-3.849	3.624	-0.225	-0.16	0	0	0	-0.384
H18	H	-2.286	0.983	-1.303	-0.044	0	0	0	-1.347	-3.411	3.365	-0.047	-0.04	0	0	0	-0.087

Appendix B: Atom energies for a single molecule of IBPRAC04 and DFT2 Mod in the Momany field (Hydrogen bonding atoms shown in red)

Atom	Element	IBPRAC04 Momany									DFT2 Momany							
		VdW Attraction	VdW Repulsion	Total VdW Energy	Electrostatic	H bond Attraction	H bond Repulsion	Total H bond Energy	Total Energy		VdW Attraction	VdW Repulsion	Total VdW Energy	Electrostatic	H bond Attraction	H bond Repulsion	Total H bond Energy	Total Energy
C1	C	-13.477	15.491	2.014	4.038	0	0	0	6.053		-13.228	6.76	-6.469	6.388	0	0	0	-0.081
C2	C	-4.726	0.949	-3.777	0.413	0	0	0	-3.363		-8.371	1.504	-6.867	0.483	0	0	0	-6.383
C3	C	-6.3	2.93	-3.37	-0.152	0	0	0	-3.522		-13.993	6.836	-7.157	0.047	0	0	0	-7.109
C4	C	-3.758	0.268	-3.49	-0.199	0	0	0	-3.69		-7.222	1.34	-5.883	-0.285	0	0	0	-6.167
C5	C	-3.936	0.565	-3.371	-0.216	0	0	0	-3.587		-9.481	8.761	-0.72	-0.302	0	0	0	-1.023
C6	C	-4.244	0.913	-3.332	-0.084	0	0	0	-3.416		-9.325	6.738	-2.587	-0.07	0	0	0	-2.657
C7	C	-3.705	0.288	-3.416	0.027	0	0	0	-3.389		-6.943	1.078	-5.865	0.165	0	0	0	-5.701
C8	C	-6.763	2.958	-3.805	-0.119	0	0	0	-3.924		-10.374	4.167	-6.207	-0.107	0	0	0	-6.314
C9	C	-6.182	2.14	-4.041	-0.361	0	0	0	-4.402		-9.868	3.414	-6.454	-0.569	0	0	0	-7.024
C10	C	-4.338	0.76	-3.578	0.136	0	0	0	-3.442		-7.442	1.259	-6.183	0.318	0	0	0	-5.865
C11	C	-3.921	0.86	-3.061	0.237	0	0	0	-2.824		-7.121	1.696	-5.425	0.407	0	0	0	-5.018
C12	C	-4.455	0.925	-3.53	0.315	0	0	0	-3.215		-10.011	3.973	-6.038	0.487	0	0	0	-5.551
C13	C	-4.464	1.039	-3.425	0.157	0	0	0	-3.268		-10.08	5.16	-4.92	0.254	0	0	0	-4.666
O1	O	-8.577	5.223	-3.355	-5.707	-3.066	1.297	-1.77	-10.832		-15.548	16.987	1.439	-3.577	-2.256	1.122	-1.134	-3.272
O2	O	-12.438	6.682	-5.755	-3.731	-66.583	47.25	-19.333	-28.819		-18.277	143.313	125.037	-11.99	-343.344	327.538	-15.806	97.241
H1	H	-17.72	191.078	173.358	5.661	-69.649	48.546	-21.103	157.916		-3.178	127.575	124.398	-6.133	-345.6	328.659	-16.94	101.325
H2	H	-3.615	3.268	-0.347	0.251	0	0	0	-0.095		-3.524	3.85	0.326	0.22	0	0	0	0.547
H3	H	-4.889	7.013	2.123	0.092	0	0	0	2.215		-5.046	3.308	-1.738	0.015	0	0	0	-1.722
H4	H	-2.134	0.292	-1.842	0.043	0	0	0	-1.799		-6.03	11.663	5.633	-0.003	0	0	0	5.63
H5	H	-3.138	0.672	-2.466	0.032	0	0	0	-2.434		-6.134	11.786	5.652	-0.216	0	0	0	5.436
H6	H	-1.866	0.274	-1.592	0.188	0	0	0	-1.404		-3.027	1.485	-1.542	0.213	0	0	0	-1.329
H7	H	-2.831	1.781	-1.05	0.015	0	0	0	-1.035		-4.026	5.786	1.76	-0.091	0	0	0	1.67
H8	H	-5.06	3.86	-1.2	-0.088	0	0	0	-1.288		-5.484	7.067	1.583	-0.322	0	0	0	1.261
H9	H	-3.825	2.021	-1.804	0.466	0	0	0	-1.338		-3.947	2.361	-1.586	0.697	0	0	0	-0.889
H10	H	-2.876	1.087	-1.789	-0.303	0	0	0	-2.092		-2.873	1.059	-1.815	-0.642	0	0	0	-2.456
H11	H	-2.044	0.378	-1.666	-0.15	0	0	0	-1.816		-2.867	1.573	-1.293	-0.407	0	0	0	-1.7
H12	H	-3.234	4.185	0.952	-0.237	0	0	0	0.715		-2.973	4.816	1.843	-0.389	0	0	0	1.454
H13	H	-2.716	1.563	-1.153	-0.076	0	0	0	-1.229		-3.814	3.699	-0.116	-0.131	0	0	0	-0.246
H14	H	-1.953	0.268	-1.685	-0.091	0	0	0	-1.777		-3.581	3.255	-0.326	-0.092	0	0	0	-0.418
H15	H	-1.971	0.21	-1.761	-0.181	0	0	0	-1.942		-3.248	1.781	-1.466	-0.288	0	0	0	-1.755
H16	H	-2.199	0.442	-1.758	-0.043	0	0	0	-1.801		-3.809	4.285	0.476	-0.023	0	0	0	0.453
H17	H	-2.187	0.502	-1.685	-0.063	0	0	0	-1.748		-3.849	3.624	-0.225	-0.16	0	0	0	-0.384
H18	H	-2.472	0.777	-1.695	-0.022	0	0	0	-1.717		-3.411	3.365	-0.047	-0.04	0	0	0	-0.087

Appendix C: Atom energies for a single molecule of IBPRAC04 and DFT2 Mod in the Tripos 5.2 field (Hydrogen bonding atoms shown in red)

Atom	Element	IBPRAC04 Tripos 5.2						DFT2 Tripos 5.2				
		VdW Attraction	VdW Repulsion	Total VdW Energy	Electrostatic	Total Energy		VdW Attraction	VdW Repulsion	Total VdW Energy	Electrostatic	Total Energy
C1	C	-9.033	9.716	0.683	8.077	8.76		-10.931	9.099	-1.831	6.388	4.556
C2	C	-4.473	0.47	-4.003	0.827	-3.176		-5.455	0.541	-4.914	0.483	-4.431
C3	C	-6.122	1.573	-4.549	-0.305	-4.854		-9.072	2.337	-6.735	0.047	-6.688
C4	C	-3.581	0.177	-3.404	-0.399	-3.802		-4.713	0.511	-4.201	-0.285	-4.486
C5	C	-3.873	0.406	-3.467	-0.431	-3.898		-6.626	4.07	-2.557	-0.302	-2.859
C6	C	-4.208	0.678	-3.529	-0.169	-3.698		-6.454	3.043	-3.411	-0.07	-3.481
C7	C	-3.447	0.171	-3.276	0.054	-3.222		-4.447	0.376	-4.071	0.165	-3.907
C8	C	-6.206	2.188	-4.018	-0.238	-4.256		-6.803	1.66	-5.143	-0.107	-5.25
C9	C	-5.867	1.67	-4.197	-0.722	-4.919		-6.483	1.386	-5.097	-0.569	-5.667
C10	C	-3.94	0.294	-3.645	0.272	-3.373		-4.69	0.387	-4.302	0.318	-3.984
C11	C	-3.73	0.41	-3.32	0.474	-2.847		-4.747	0.685	-4.062	0.407	-3.656
C12	C	-4.351	0.454	-3.897	0.63	-3.267		-6.797	1.534	-5.263	0.487	-4.776
C13	C	-4.43	0.531	-3.899	0.314	-3.585		-6.846	2.17	-4.677	0.254	-4.423
O1	O	-7.261	2.73	-4.531	-11.414	-15.945		-10.701	6.017	-4.685	-3.577	-8.261
O2	O	-9.947	5.543	-4.405	-7.462	-11.866		-14.634	19.543	4.909	-11.99	-7.081
H1	H	-23.066	350.486	327.42	11.321	338.741		-13.443	27.289	13.846	-6.133	7.713
H2	H	-4.345	4.145	-0.2	0.502	0.303		-4.553	3.858	-0.695	0.22	-0.475
H3	H	-6.069	10.386	4.317	0.183	4.5		-6.658	3.14	-3.518	0.015	-3.502
H4	H	-2.597	0.33	-2.267	0.087	-2.181		-8.26	12.807	4.547	-0.003	4.544
H5	H	-3.67	0.745	-2.925	0.064	-2.86		-6.934	6.597	-0.337	-0.216	-0.553
H6	H	-2.291	0.331	-1.961	0.375	-1.585		-4.144	1.55	-2.593	0.213	-2.381
H7	H	-3.552	2.372	-1.18	0.03	-1.15		-5.623	5.894	0.271	-0.091	0.181
H8	H	-5.563	4.646	-0.918	-0.175	-1.093		-7.077	7.021	-0.056	-0.322	-0.378
H9	H	-4.485	2.712	-1.774	0.932	-0.842		-4.954	2.159	-2.794	0.697	-2.097
H10	H	-2.981	0.952	-2.029	-0.607	-2.636		-3.478	0.767	-2.711	-0.642	-3.353
H11	H	-2.462	0.451	-2.011	-0.3	-2.311		-3.631	1.511	-2.121	-0.407	-2.527
H12	H	-3.896	5.717	1.821	-0.473	1.348		-4.153	5.714	1.562	-0.389	1.173
H13	H	-3.351	2.101	-1.25	-0.153	-1.403		-5.208	3.814	-1.395	-0.131	-1.525
H14	H	-2.398	0.33	-2.068	-0.183	-2.25		-4.973	3.592	-1.382	-0.092	-1.473
H15	H	-2.344	0.231	-2.113	-0.362	-2.476		-4.312	1.665	-2.647	-0.288	-2.935
H16	H	-2.722	0.567	-2.155	-0.087	-2.242		-5.327	5.004	-0.323	-0.023	-0.346
H17	H	-2.692	0.65	-2.042	-0.126	-2.167		-4.946	3.284	-1.662	-0.16	-1.822
H18	H	-3.081	1.054	-2.026	-0.044	-2.07		-4.806	3.94	-0.866	-0.04	-0.906